

Linear and Nonlinear Kelvin Waves/Tropical Instability Waves in the Shallow-Water System

by

Cheng Zhou

A dissertation submitted in partial fulfillment
of the requirements for the degree of
Doctor of Philosophy
(Atmospheric and Space Sciences and Scientific Computing)
in The University of Michigan
2010

Doctoral Committee:

Professor John P. Boyd, Chair
Professor Richard B. Rood
Professor Robert Krasny
Assistant Professor Xianglei Huang

© Cheng Zhou 2010
All Rights Reserved

To Liang and Peipei

ACKNOWLEDGEMENTS

I have been extremely fortunate to have Prof. John P. Boyd as my advisor. His extensive expertise and broad knowledge made great contribution to my entire research. Talking with him is not only helpful, but also inspiring. I really appreciate his insightful ideas, mathematical expertise, encouragement.

Then I gratefully acknowledge Dr. Rood, Dr. Krasny and Dr. Huang for serving on my dissertation committee. Their expert suggestions and comments strongly improved this thesis.

In addition, I want to say thank you my classmates, colleagues, and whoever I may forget to mention here.

Last but not least, I want to thank my dear wife, Liang Zhao, and my daughter, Liana Yipei Zhou. This thesis could not have been done without you.

TABLE OF CONTENTS

DEDICATION	ii
ACKNOWLEDGEMENTS	iii
LIST OF FIGURES	vii
LIST OF TABLES	xiii
ABSTRACT	xiv
CHAPTER	
I. Introduction	1
1.1 Purposes	1
1.2 Shallow Water Equations(SWEs)	2
1.3 Linear Kelvin waves on sphere	3
1.4 Nonlinear Kelvin waves on sphere	7
1.5 Nonlinear Kelvin waves on the equatorial beta-plane	9
1.6 Tropic instability waves	10
1.7 Outline	13
II. Uniform Asymptotics for the Linear Kelvin Wave in Spherical Geometry	15
2.1 A New Asymptotic Approximation	15
2.1.1 Derivation	15
2.1.2 Results	20
2.2 Results and Numerical Plots of Errors	21
2.3 Summary	22
III. Kelvin Waves in the Nonlinear Shallow Water Equations on the Sphere: Nonlinear Traveling Waves and the Corner Wave Bifurcation	24

3.1	Nonlinear Kelvin wave on sphere by perturbation theory . . .	25
3.1.1	Introduction	25
3.1.2	Nonlinear shallow Water Equations on the Sphere .	25
3.1.3	Traveling waves by perturbative double expansion .	27
3.2	Kepler mapping/Galerkin method/Newton continuation method	30
3.2.1	Kepler mapping	30
3.2.2	Galerkin method	31
3.2.3	Newton continuation method	34
3.2.4	Resolution Check	37
3.3	Spatial Structure of the Corner Wave	38
3.4	Variations of Phase Speed and Corner Height	43
3.5	Limitations of Theory	45
3.6	Summary and Conclusions	47
 IV. Kelvin Waves in the Presence of a Jet on the Equatorial β-plane		50
4.1	Model	50
4.1.1	The equatorial beta-plane approximation	50
4.1.2	Nonlinear Shallow Water Equations on the Equatorial β -Plane	51
4.1.3	The background jet	54
4.1.4	Mapping in longitude and latitude	55
4.1.5	Galerkin method	56
4.1.6	Newton continuation method	59
4.2	Modified linear Kelvin waves in the presence of a jet	62
4.2.1	Wave structure	62
4.2.2	Phase speed	67
4.3	Nonlinear Traveling Kelvin waves	68
4.3.1	Results of westward jets	68
4.3.2	Results of eastward jets	76
4.4	Conclusion and Discussion	79
 V. Nonlinear Shallow Water Tropical Instability Waves on the Equatorial β-plane: Genesis of Two Distinct Types of Waves		81
5.1	Model	81
5.2	Nonlinear Evolution	82
5.2.1	Free nonlinear evolution	82
5.2.2	Sensitivity of the late emerging Yanai wave to the zonal mean	86
5.2.3	Forced nonlinear evolution	87
5.3	Summary and Discussion	88
 VI. Conclusion and Discussion		90

6.1	Linear Kelvin waves	90
6.2	Nonlinear Kelvin waves	91
6.3	Nonlinear tropical instability waves	92
	APPENDIX	93
	BIBLIOGRAPHY	99

LIST OF FIGURES

Figure

1.1	<p>The Kelvin wave lives in a two-dimensional parameter space where the horizontal axis is the square root of Lamb’s parameter ϵ and the vertical axis is the zonal wavenumber s. When s and ϵ are both small, the Kelvin wave fills the entire globe from pole to pole. When $r = \sqrt{s^2 + \epsilon}$ is large compared to one, the Kelvin wave is equatorially-trapped, proportional to $\exp(-(1/2)r\mu^2)$ where μ is the sine of latitude. The horizontal axis is $\sqrt{\epsilon}$ rather than ϵ itself so that r is just distance from the origin in this map of the parameter space. When ϵ is large and much greater than s^2, the Kelvin wave is well-approximated by the equatorial beta-plane. When $s \gg \sqrt{\epsilon}$ (and not necessarily large), the velocity potential $\chi \approx \exp(is\lambda) P_s^s(\mu)$ where P_s^s is the usual associated Legendre function and the frequency $\sigma \approx \sqrt{s(s+1)}/\sqrt{\epsilon}$. The regions of validity of these two regimes are marked by the dashed lines. The new asymptotic approximation derived in Chapter 2 fills the gap between these two previously-known limits.</p>	6
1.2	<p>Tropical instability waves (TIW) seen in SST from the Tropical Rainfall Measuring Mission (TRMM) Microwave Imager (TMI). TMI imagery courtesy of Remote Sensing Systems (http://www.ssmi.com/). Cold area, called cold tongue, forms each year around June. Soon after it forms, its south and north boundaries(between the cold water(blue) and warm water(red)) are subjected to cusp shape deformation which propagate to the west with a wavelength of about 1000 km and a period of about 15~45 days. These oscillations are associated with the Tropical Instability Waves.</p>	12
2.1	<p>Schematic of the approximation of the exact pair of equations (middle inside the dotted rectangle) by the terms at the top and bottom of the diagram; this simplified pair of equations is then solved exactly.</p>	17

2.2 The latitudinal structure of u or ϕ (which are identical) for the lowest ten zonal wavenumbers s for $\epsilon = 0$ [barotropic waves]. $u = (1 - \mu^2)^{s/2}$. The widest curve is $s = 1$ and the waves become more and more narrow as s increases. The dotted curves are guidelines that show that the half-width of the wave is within the tropics ($|\text{latitude}| \leq 30^\circ$) for $s \geq 5$ 18

2.3 The thick black curve is the exact Kelvin mode for $s = 5$ and $\epsilon = 5$. The red curve is the improved new asymptotic approximation, $\phi \approx (1 - \mu^2)^{s/2} \exp(-(1/2) \{ \sqrt{\epsilon + s^2} - s \} \mu^2)$ which is graphically indistinguishable from the Kelvin wave. The dashed curve is the new asymptotic approximation without the $(1 - \mu^2)$ factor, $\phi \approx \exp(-(1/2) \sqrt{\epsilon + s^2} \mu^2)$. The dotted curve is the classical equatorial beta-plane approximation, $\phi \approx \exp(-(1/2) \sqrt{\epsilon} \mu^2)$ 21

2.4 $\text{Log}_{10}(\text{errors})$ in the new asymptotic approximation to the Kelvin wave for the frequency (upper left) and the three unknowns (remaining three panels). The frequency error is the error in $\sigma/(s/\sqrt{\epsilon})$, which is close to one for all s and ϵ . The eigenfunctions are normalized by scaling the height to have a maximum of one, so the errors are both the absolute and relative errors in this variable. u and v were scaled by dividing the absolute errors by the global maximum of each velocity, and plotting these scaled variables. 23

3.1 Normalized absolute values of Fourier coefficients of ϕ . ϕ is the solution of the corner wave of $s = 1$ and $\epsilon = 1$ case. m and n are coefficient degree in longitudinal and latitudinal directions respectively. The solid line has a slope proportional to K^{-4} , confirming the predicted fourth order rate of convergence when the Kepler change-of-coordinate is used. The rate of convergence is good enough to show that the solution of the corner wave is reliable. 38

3.2	Traveling Kelvin wave solutions with $s = 1$ and $\epsilon = 1$. Left: equatorial section of ϕ for $\phi_{00} = 0.1705, 0.1755, 0.1805, 0.1855$ and 0.1905 , respectively. $\phi(x, \theta = \pi/2)$ steepens with the increasing ϕ_{00} . When $\phi_{00} = 0.1905$, $\phi(x, \pi/2)$ is the corner wave, discontinuous in its first derivative at the crest. Right: A zoom in plot of $\phi(x, \pi/2)$ with $\phi_{00} = 0.1755, 0.1805, 0.1855, 0.1905, 0.1955, 0.2005$. The heavy curve is for $\phi_{00} = 0.1905$. Note that this graph includes two values of ϕ_{00} larger than that of the corner wave (dashed); these are unphysical as indicated by their unphysical oscillations near $x = 0$. The interval in longitude is from 0 to 0.1, which is about 1.6% of the total width. (Note that the plot is in the physical longitudinal coordinate x ; the circles on each curve show the points of the grid, which is evenly spaced in z , but very heavily concentrated in x near $x = 0$.) This graph shows that the corner wave is easily distinguished by eye from near-corner waves with a zoom plot.	39
3.3	ϕ of the corner wave for $s = 1$ and $\epsilon = 1$ on sphere; left and right differ only in viewing angle. The peak value of ϕ_{00} is 0.1905 . The comparison shows that only the longitudinal derivative is discontinuous at the peak.	40
3.4	Profile of ϕ along the equator (solid) and the profile of ϕ at $x = 0$ as a function of latitude (dashed) for the corner wave for $s = 1$ for two different values of Lamb's parameter. [Left: $\epsilon = 1$. Right: $\epsilon = 30$.] The horizontal axis does doubly duty, being longitude for $\phi(x, \text{latitude} = 0)$ and latitude for $\phi(x = 0, \text{latitude})$. In both panels, the longitudinal derivative (solid) is clearly discontinuous at the crest whereas the north-south derivative shows not the slightest hint of non-smoothness.	41
3.5	Normalized $\phi(x, \theta = \pi/2)$ [longitudinal section at the equator] of the corner wave solution of $s = 1$ and $\epsilon = 0.01, 1, 5, 30$. The profiles of $\phi(x, \theta = \pi/2)$ are scaled by their corresponding maxima, ϕ_{00} . The shape of ϕ at the equator becomes narrower and narrower as ϵ increases.	42
3.6	The derivative of ϕ of the corner wave solution of $s = 1$ and $\epsilon = 0.01$ case with respect to the longitude x . Left: ϕ_x at latitudes $0, \frac{\pi}{64}, \frac{\pi}{32}, \frac{\pi}{16}, \frac{\pi}{8}, \frac{\pi}{4}$, plotted on the full global domain. Right: same, but a zoom plot with a much smaller range.	43
3.7	h_{00} of the corner waves of different ϵ for $s = 1$ [upper thick curve with diamonds] and $s = 2$ [lower thick curve with circles]. The dashed line on this log-log plot shows that h_{00} decays asymptotically proportional to $1/\sqrt{\epsilon}$ as $\epsilon \rightarrow \infty$	44

4.1	Surface height ϕ (contours) and $u - v$ velocity fields (vectors) of the modified linear Kelvin waves with $k = 1, 4$ and $U_0 = \pm 0.25$. Values of ϕ, u, v have been normalized by $\phi(x = 0, y = 0)$. Solid contour lines are positive ϕ with a contour interval of 0.2 units. Dotted lines are negative ϕ and the zero contour is omitted. The maximum velocity vectors in each panel are specified in the bottom right corner. The x axis is the product of the nondimensionalized longitude and the wavenumber k	64
4.2	Eigenfunctions corresponding to the modified Kelvin waves in the presence of a westward jet for $U_0 = -0.25$ (top panel), $U_0 = -0.5$ (middle panel) and $U_0 = -1.0$ (bottom panel), $k = 0.25$ (left column), and for $k = 1$ (middle column), $k = 4$ (right column).	65
4.3	Eigenfunctions corresponding to the modified Kelvin waves in the presence of a eastward jet for $U_0 = 0.25$ (top panel), $U_0 = 0.5$ (middle panel) and $U_0 = 1.0$ (bottom panel), $k = 0.1$ (left column), and for $k = 1$ (middle column), $k = 4$ (right column).	66
4.4	Phase speeds of free Kelvin modes for various wavenumber k and U_0	67
4.5	Surface height ϕ (contours) and $u - v$ velocity fields (vectors) of the nonlinear traveling Kelvin waves with amplitude $\phi_{00}=0.02$ (left) and 0.113 (right) for $k = 1$ and $U_0 = -0.25$. When $\phi_{00}=0.113$, it is the corner wave. Solid contour lines are positive ϕ . Dotted lines are negative ϕ and the zero contour is omitted. Contour intervals are 0.002 for left graph and 0.01 for the right graph. The maximum velocity vectors in each panel are specified in the bottom right corner.	68

4.6	Traveling Kelvin wave solutions with $U_0 = -0.25$ and $k=1$. (Upper left) Equatorial section of ϕ for $\phi_{00}=0.01, 0.03, 0.05,$ and $0.113,$ respectively; $\phi(x, y = 0)$ steepens with the increasing ϕ_{00} . When $\phi_{00}=0.113,$ $\phi(x, y = 0)$ is the corner wave, discontinuous in its first derivative at the crest. (Upper right) A zoom in plot of $\phi(x, y = 0)$ with $\phi_{00}=0.106, 0.108, 0.11, 0.111, 0.112, 0.113, 0.114.$ The heavy curve is for $\phi_{00}=0.113.$ Note that this graph includes one dotted curve with the value of $\phi_{00}(0.114)$ larger than that of the corner wave; this is unphysical as indicated by its unphysical oscillations near $x=0.$ The interval in longitude is from 0 to 0.016, which is about 0.25% of the total one wavelength. (Note that the plot is in the physical longitudinal coordinate $x;$ the circles on each curve show the points of the grid, which is evenly spaced in z but very heavily concentrated in x near $x=0.$) This graph shows that the corner wave is easily distinguished by the eye from near-corner waves in a zoom in plot. (Lower left) Equatorial section of u for $\phi_{00}=0.01, 0.03, 0.05,$ and $0.113,$ respectively. $u(x, y = 0)$ exhibits the same behavior as $\phi(x, y = 0)$ and is also discontinuous for $\phi_{00}=0.113.$ (Lower right) v along $y = 1$ for $\phi_{00}=0.01, 0.03, 0.05,$ and $0.113,$ respectively. $v(x, y = 1)$ is continuous for all $\phi_{00}.$	71
4.7	Longitudinal sections of ϕ (left) and ϕ_x (right) along different latitudes at the corner wave limit for $U_0 = -0.25$ and $k = 1.$	72
4.8	Latitudinal sections of ϕ along $x=0$ divided by ϕ_{00} of the modified linear Kelvin wave and nonlinear traveling Kelvin waves for $\phi_{00}=0.02, 0.05, 0.08,$ and 0.113 with $U_0 = -0.25$ and $k=1.$ $\phi(x = 0, y)$ steepens with the increasing $\phi_{00}.$ At the corner wave limit when $\phi_{00}=0.113,$ $\phi(x = 0, y)$ is still continuous in latitude.	72
4.9	(left) Longitudinal sections of $\phi, \phi(x, y = 0),$ at the corner wave limit along the equator with $U_0=-0.25$ and $k=0.25, 1$ and $4.$ The x axis is the product of longitude and the wavenumber $k.$ $\phi(x, y = 0)$ has been normalized in a way such that the base is 0 and tip is 1. The dashed line is the normalized $\cos(x).$ (right) Latitudinal sections of $\phi, \phi(x = 0, y),$ at the corner wave limit along $x = 0$ with $U_0=-0.25$ and $k=0.25, 1$ and $4.$ $\phi(x = 0, y)$ has been normalized by $\phi_{00}.$	73
4.10	Latitudinal sections of u along $x=0$ divided by $u(x = 0, y = 0)$ for $U_0 = -0.5$ (left) and $U_0 = -1.0$ (right) and $k=1.$ The curves correspond to normalized $u(x = 0, y)$ of the modified linear Kelvin wave(thin solid line) to the corner Kelvin wave(thick solid line) from right to left.	74

4.11	Surface height ϕ (contours) and $u - v$ velocity fields (vectors) of the nonlinear traveling Kelvin waves with amplitude $\phi_{00}=0.02$ (left) and 0.04 (right) for $k = 1$ and $U_0 = 0.25$. Solid contour lines are positive ϕ . Dotted lines are negative ϕ and the zero contour is omitted. Contour interval is 0.002. The maximum velocity vectors in each panel are specified in the bottom right corner.	76
4.12	Latitudinal sections of ϕ along $x=0$ divided by ϕ_{00} of the modified linear Kelvin wave and nonlinear traveling Kelvin waves for $\phi_{00}=0.01, 0.02, 0.03,$ and 0.04 with $U_0 = 0.25$ and $k = 1$. Unlike the westward jets' cases, $\phi(x = 0, y)$ expands in latitude with the increasing ϕ_{00}	77
4.13	Phase speeds of the modified linear Kelvin waves and first 3 symmetric eastward inertial gravity waves (EIGW) for $U_0=-0.25$ (left) and $U_0=0.25$ (right). The horizontal dashed horizontal line is a guide line showing the phase speed of the Kelvin wave with $k = 1$	78
5.1	Zonal mean velocity (left column), zonal deviation h' and $u' - v'$ (middle column), and h and $u - v$ (right column) on a moving coordinate following a positive h' center near $5^\circ N$ on day 175 (top panel), 200 (2nd panel), 225 (3rd panel) and 450 (bottom panel).	84
5.2	Time-longitude plots of v along the equator and $5^\circ N$. Before the most unstable wave reaches to its fully nonlinear stage around day 200, the periods are 29 days at both the equator and $5^\circ N$. After day 250, the periods are 20 days at the equator and about 36 days at $5^\circ N$	85
5.3	(a) Phase speed and periods of the free modes with a wavelength of 995 km when increasing the background zonal mean from 0 to 100% of the zonal mean on day 450. Blue dashed line denotes where the phase speed equals to the minimum value of the zonal mean. Neutral modes in the shaded area are continuous. (b) The free Yanai wave with a wavelength of 995 km wave, linearized about the zonal mean on day 450.	85
5.4	(left)Zonal mean velocity without nudging terms($\tau = \infty$) and with forcing terms($\tau=60$ days) for $U_{max} = 1.0 \text{ ms}^{-1}$; (middle)Zonal deviation h' and $u' - v'$ on day 450 without nudging terms; (right)Zonal deviation h' and $u' - v'$ on day 450 with nudging terms($\tau=60$ days).	87

LIST OF TABLES

Table

1.1	Lamb's Parameter	5
3.1	Relative coarse-fine differences in the L_∞ norm	37
3.2	Parameters in the corner wave limit for s=1 case	43
3.3	Parameters in the corner wave limit for s=2 case	44
4.1	Phase speeds of modified linear Kelvin waves, phase speeds and ϕ_{00} of nonlinear traveling Kelvin waves at corner wave limits for various U_0 and wavenumber k	75
5.1	Periods of TIWs centered about $5^\circ N$ and late emerging Yanai waves near the equator for $U_{max} = 0.7 \text{ ms}^{-1}$ after the nonlinear adjustment with various relaxation times. The period of TIWs during the linear stage is 29 days over the domain.	88

ABSTRACT

This thesis has three major purposes. First, we will derive an new asymptotic approximation for the linear Kelvin wave on sphere which fills the gap between two limits which have known asymptotic solutions. The second major purpose is to study how the nonlinearity changes the properties, like spatial structure and phase speed, of the steadily translating(traveling) nonlinear Kelvin waves either on the sphere or on the equatorial-beta plane. The third major purpose is to study the origin of two different kinds of westward propagating Tropical Instability Waves observed in the equatorial Pacific ocean.

The Kelvin wave is the slowest eastward propagating eigenmode of Laplace's Tidal Equation. It is widely observed in both the ocean and the atmosphere. On the sphere, in the absence of mean currents, the Kelvin wave depends on two parameters: the zonal wavenumber s [always an integer] and Lamb's parameter ϵ which is a nondimensional reciprocal depth of the fluid. First, for the linear Kelvin wave we derive an asymptotic approximation valid in the limit $\sqrt{s^2 + \epsilon} \gg 1$, which generalizes the usual "equatorial wave" limit that $\epsilon \rightarrow \infty$ for fixed s and we also show that the width of the Kelvin wave is $\{\epsilon + s^2\}^{-1/4}$ rather than $\epsilon^{-1/4}$ as in the classical equatorial beta-plane approximation.

The nonlinear traveling Kelvin wave on the sphere depends on three parameters: the zonal wavenumber s , Lamb's parameter ϵ and the wave amplitude. For fixed wavenumber s , we derive the asymptotic solution of the traveling Kelvin wave in the limit when both ϵ and amplitude are small with a perturbation method. As

the perturbation method fails when either ϵ or the wave amplitude is big, we use a numerical method which combines coordinate mapping, Galerkin method, Newton iteration and continuation method. We show that for sufficiently small amplitude, there are Kelvin traveling waves (cnoidal waves); as the amplitude increases, the branch of traveling waves terminates in a so-called “corner wave” with a discontinuous first derivative in longitude only. Corner waves give maximum wave amplitude of steadily translating nonlinear Kelvin waves. All waves larger than the corner wave evolve to fronts and break. As the dispersion weakens with increasing ϵ (“Lamb’s parameter”), the amplitude of the corner wave decreases rapidly and the longitudinal profile of the corner wave narrows dramatically.

On the equatorial beta-plane, we study the linear and nonlinear traveling Kelvin waves in the presence of a jet. The jet has the form of $U = U_0 e^{-3y^2}$, where y is nondimensional latitude (in the equatorial ocean, nondimensional unit y is about 300 km and unit U_0 is about 2 m/s). We show that the linear Kelvin waves have much more complicated structures than the Kelvin wave with a rest background. Phase speed decreases as wavenumber increases regardless whether the jet is eastward or westward. For sufficiently small amplitude, again there are nonlinear Kelvin traveling waves (cnoidal waves). As the amplitude increases, the waves narrow in longitude; in latitude, the waves narrow for a westward jet but widen for an eastward jet; phase speeds also increase to the east. However, the phase speeds are largely determined by the linear Kelvin waves’ dynamics; nonlinearity only increases the phase speeds by several percent. For a westward jet, the traveling waves also terminate in a corner wave and have the same singularity as that of the corner Kelvin waves on the sphere without mean currents. For an eastward jet, calculation of nonlinear Kelvin waves with large amplitude is numerically impossible due to the resonance with waves of higher wavenumbers.

Tropical Instability Waves (TIWs) are prominent intraseasonal oscillations in both

the equatorial Pacific and Atlantic oceans. We study how the nonlinearity of the TIWs affects the development of the instabilities through both linear stability analysis and numerical simulation. In the early stage of TIWs, unstable wave centered near $5^{\circ}N$ with a wavelength about 1000 km and a period about one month which are consistent with the stability analysis, dominate the whole domain. However neutral Yanai waves with periods of about 15-22 days emerge near the equator when the unstable TIWs grow into fully nonlinear vortices and begin to rotate, which stabilizes the mean states substantially. Meanwhile the original TIWs centered near $5^{\circ}N$ are slowed down and weakened. The strength of these Yanai waves is sensitive to the instability of the initial mean flow and the external forcing. The external forcing terms are found to be important for the TIWs centered near $5^{\circ}N$ to retain their dominance from $3^{\circ}N$ to $7^{\circ}N$ and also be able to suppress the late emerging Yanai waves if strong enough.

CHAPTER I

Introduction

1.1 Purposes

This thesis has three major purposes. First, we will derive an new asymptotic approximation for the linear Kelvin wave on sphere which will fill the gap between two limits which have known asymptotic solutions. The second major purpose is to study how the nonlinearity changes the properties, like spatial structure and phase speed, of the steadily translating(traveling) nonlinear Kelvin waves. Solitary/traveling waves are the result of balance between nonlinearity and dispersion. The nonlinearity comes from the wave-wave interaction terms in the nonlinear equations and the dispersion could come from either the spherical geometry or the background mean flow. We will study two different kinds of nonlinear traveling Kelvin waves, Kelvin waves on sphere without a background mean whose dispersion comes from the spherical geometry and Kelvin waves on the equatorial beta-plane with a background mean whose dispersion comes from the background mean. The third major purpose is to study the origin of two different kinds of Tropical Instability Waves(TIW's). Tropical instability waves are westward propagating oscillation observed in both the equatorial Pacific ocean and Atlantic ocean. We will compare the nonlinearity development of these instability waves with the result from linear stability analysis and show how the nonlinearity gives rise to two different types of TIWs. All these works will be based on the shallow-water

model either on the spherical coordinate or on the equatorial beta-plane.

1.2 Shallow Water Equations(SWEs)

Laplace showed more than two centuries ago that the free oscillations of a layer of homogeneous fluid and uniform depth on a rotating, spherical earth are governed by a trio of nonlinear partial differential equations which are usually called the “Laplace Tidal Equations” or the “nonlinear shallow water equations”. The nonlinear shallow water equations in spherical coordinates over a flat sea bottom are

$$\frac{\partial u'}{\partial t'} + \frac{u'}{a \sin(\theta)} \frac{\partial u'}{\partial \lambda} - \frac{v'}{a} \frac{\partial u'}{\partial \theta} - \left(2\Omega \cos(\theta) + \frac{u' \cot(\theta)}{a} \right) v' + \frac{g}{a \sin(\theta)} \frac{\partial h'}{\partial \lambda} = 0 \quad (1.1)$$

$$\frac{\partial v'}{\partial t'} + \frac{u'}{a \sin(\theta)} \frac{\partial v'}{\partial \lambda} - \frac{v'}{a} \frac{\partial v'}{\partial \theta} + \left(2\Omega \cos(\theta) + \frac{u' \cot(\theta)}{a} \right) u' - \frac{g}{a} \frac{\partial h'}{\partial \theta} = 0 \quad (1.2)$$

$$\frac{\partial h'}{\partial t'} + \frac{u'}{a \sin(\theta)} \frac{\partial h'}{\partial \lambda} - \frac{v'}{a} \frac{\partial h'}{\partial \theta} + \frac{h'}{a \sin(\theta)} \left(\frac{\partial u'}{\partial \lambda} - \sin(\theta) \frac{\partial v'}{\partial \theta} - v' \cos(\theta) \right) = 0 \quad (1.3)$$

where θ is colatitude($\pi/2$ minus latitude), λ is longitude, t' is the dimensional time, u' is the dimensional eastward velocity, v' is the dimensional northward velocity, h' is the total depth of the fluid, and a is the radius of the planet. (Note that following the usual geophysical convention, $v' = -a D\theta/Dt$ where D/Dt is the total derivative because colatitude θ is increasing southward.) In Chapter IV, we will show that this set of equations can be simplified when applying the equatorial beta-plane approximation.

This set of equations also describes the baroclinic mode of a two-layer model in the limit that the lower layer depth is infinite, in which case motion is confined to the upper layer, a so-called “one-and-a-half-layer” model (*Gill*, 1982). This is a decent first approximation to the ocean, especially in the tropics. The only modification is that the actual mean depth is replaced by the “equivalent depth”, which is the product of the mean depth with the fractional density difference between the two layers (*Pedlosky*, 1987). As explained in *Chapman and Lindzen* (1970), *Majda* (2003)

and *Marshall and Boyd* (1987), the shallow water equations can also be profitably employed for continuously-stratified (rather than homogeneous) fluids if the depth is interpreted as the “equivalent depth” of a given baroclinic mode of a continuously stratified fluid as first observed by G. I. Taylor more than seventy years ago; the main effect of continuous stratification is to slightly weaken the nonlinearity because of coupling between different vertical modes.

1.3 Linear Kelvin waves on sphere

When shallow water wave equations are linearized about a state of rest, the tidal equations can be written (*Longuet-Higgins*, 1968),

$$\sigma U - \mu \tilde{V} - s\phi = 0 \quad (1.4)$$

$$\mu U - \sigma \tilde{V} + (1 - \mu^2)\phi_\mu = 0 \quad (1.5)$$

$$sU - (1 - \mu^2)\tilde{V}_\mu - \epsilon \sigma(1 - \mu^2)\phi = 0 \quad (1.6)$$

where $\mu = \cos(\theta)$, θ is colatitude, λ is longitude, ϕ is the height and σ the nondimensional frequency. All variables have been nondimensionalized using a as the length scale, 2Ω as the time scale and H as the depth scale. U and \tilde{V} are the nondimensional “Margules-Robert” velocities:

$$U = \frac{1}{2\Omega} \frac{d\lambda}{dt} \sqrt{1 - \mu^2}; \quad \tilde{V} = -i \frac{1}{2\Omega} \frac{d\theta}{dt} \sqrt{1 - \mu^2} \quad (1.7)$$

These three equations have four unknowns (U , \tilde{V} , ϕ and σ) and two free parameters (wavenumber s and Lamb’s parameter ϵ). The zonal wavenumber s is always a positive integer (The case of $s = 0$ is a nonpropagating mode which is not relevant to

our analysis). Lamb’s parameter ϵ is a nondimensional mean depth which is explicitly

$$\epsilon = \frac{4\Omega^2 a^2}{gH} \quad (1.8)$$

where Ω is the angular frequency of the earth’s rotation in radians per second, a is the radius of the planet, g is the gravitational constant, which is 9.8 m/s^2 for earth, and H is the mean depth of the fluid. The eigenmodes which are commonly called “Hough”¹ functions represent many types of motion of the atmosphere and the ocean, including Rossby waves(or Rossby-Howitz waves on the sphere), inertial gravity waves, mixed Rossby-gravity waves(or Yanai waves preferred by oceanographers) and Kelvin waves.

The slowest eastward-travelling wave has been given the special name of the “Kelvin wave” because of many striking similarities to the coastally-trapped waves analyzed by Lord Kelvin in the nineteenth century (*Thomson*, 1880). The Kelvin wave has enormous practical importance as reviewed in sources as diverse as *Chapman and Lindzen* (1970), *Majda* (2003) and *Andrews et al.* (1987). A Kelvin wave is the main oceanic component of the coupled ocean/atmosphere oscillation known as ENSO (El Niño-Southern Oscillation) which relates torrential rains in California with the drought known as “The Great Dry” in Australia. Kelvin waves are important in the troposphere and the middle atmosphere, and are primary drivers of the semiannual oscillation in the tropical upper stratosphere and the Quasi-Biennial Oscillation in the tropical lower stratosphere in Lindzen and Holton’s theory(in recent years however gravity waves have come to be seen as a major contributor). Kelvin waves are also important in Martian atmospheric dynamics (*Zurek*, 1976). Because the Kelvin wave is the lowest mode of the atmosphere, it is the most strongly excited wave from any sort of broadband forcing.

Longuet-Higgins (1968) carried out a magisterial study of the Hough functions in

¹“Hough” is pronounced “Huf” in honor of Sydney Samuel Hough, F. R. S., (1870-1922), for Hough (1897, 1898).

Table 1.1: Lamb’s Parameter

ϵ	Description	Source
0.012	External mode: Venus	Lindzen (1970)
6.5	External mode: Mars	Zurek (1976)
12.0	External mode: Earth (7.5 km equivalent depth)	Lindzen (1970)
2.6	Jupiter: simulate Galileo data	Williams (1996)
21.5	Jupiter	Williams (1996)
43.0	Jupiter	Williams (1996)
260	Jupiter	Williams (1996)
2600	Jupiter	Williams and Wilson (1988)
87,000	ocean: first baroclinic mode (1 meter equivalent depth)	Moore & Philander (1977)
> 100,000	ocean: higher baroclinic modes	Moore & Philander (1977)

general and the Kelvin wave in particular nearly forty years ago. Even so, there are some gaps in the theory which we fill.

Since the set of linearized shallow-water equations has two free parameters, the Kelvin wave also depends on these parameters. The zonal wavenumber s is always a positive integer. Lamb’s parameter ϵ is which is a nondimensional reciprocal depth of the fluid. When SWEs are employed for a thick layer of fluid which has large depth H , ϵ is very small. When SWEs are employed for continuously-stratified (rather than homogeneous) fluids, the depth H is interpreted as the “equivalent depth” of a given baroclinic mode. In this case, H could be very small and ϵ could be very large. Thus, to describe all possible varieties of Kelvin waves in a three-dimensional stratified ocean or atmosphere, one needs to solve Laplace’s Tidal Equations for a very wide range of ϵ ranging from very small (for the “barotropic” or nearly-barotropic waves) to very large (for high order baroclinic modes) as illustrated in Table 1.1.

When s and ϵ are both small, the Kelvin wave fills the entire globe from pole to pole. When ϵ is getting large, the Kelvin wave is becoming equatorially-trapped. In the limit $\epsilon \rightarrow \infty$, Kelvin waves are completely equatorially-trapped. The usual derivation assumes that s is fixed as this limit is taken. Figure 1.1 shows that when $s \gg \sqrt{\epsilon}$ (and not necessarily large), the velocity potential $\chi \approx \exp(is\lambda) P_s^s(\mu)$ where P_s^s is the usual associated Legendre function and the frequency $\sigma \approx \sqrt{s(s+1)}/\sqrt{\epsilon}$. When $r = \sqrt{s^2 + \epsilon}$ is large compared to one, the Kelvin wave is equatorially-trapped,

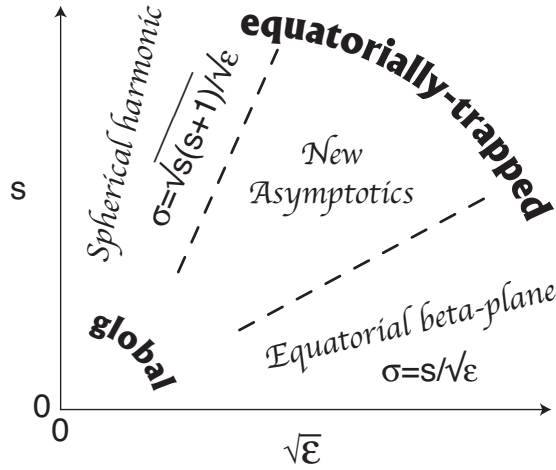


Figure 1.1: The Kelvin wave lives in a two-dimensional parameter space where the horizontal axis is the square root of Lamb's parameter ϵ and the vertical axis is the zonal wavenumber s . When s and ϵ are both small, the Kelvin wave fills the entire globe from pole to pole. When $r = \sqrt{s^2 + \epsilon}$ is large compared to one, the Kelvin wave is equatorially-trapped, proportional to $\exp(-(1/2)r\mu^2)$ where μ is the sine of latitude. The horizontal axis is $\sqrt{\epsilon}$ rather than ϵ itself so that r is just distance from the origin in this map of the parameter space. When ϵ is large and much greater than s^2 , the Kelvin wave is well-approximated by the equatorial beta-plane. When $s \gg \sqrt{\epsilon}$ (and not necessarily large), the velocity potential $\chi \approx \exp(is\lambda) P_s^s(\mu)$ where P_s^s is the usual associated Legendre function and the frequency $\sigma \approx \sqrt{s(s+1)}/\sqrt{\epsilon}$. The regions of validity of these two regimes are marked by the dashed lines. The new asymptotic approximation derived in Chapter 2 fills the gap between these two previously-known limits.

proportional to $\exp(-(1/2)r\mu^2)$ where μ is the sine of latitude. So in these two limits, there are known solutions. But there is gap between these two limits. In this thesis, we will derive an asymptotic solution which fills the gap. Especially, we will show that the structure and speed of the Kelvin wave are significantly modified when s is large. Our approximation is uniformly valid for large s and/or ϵ regardless of the size of the smaller parameter. The new approximation turns to be surprisingly accurate outside its formal range of validity in the region where both s and ϵ are small.

Twenty years ago, *Boyd* (1985) showed that for *Rossby* waves, the parameter that controls the width of an equatorially-trapped wave is not ϵ , but rather

$$\epsilon_{eff} \equiv \epsilon + s^2, \tag{1.9}$$

Furthermore, even in the barotropic limit ($\epsilon = 0$), a Rossby wave of large zonal wavenumber s and low latitudinal mode number is confined to low latitudes. The new asymptotic approximation shows that the same is true for the Kelvin wave.

1.4 Nonlinear Kelvin waves on sphere

The nonlinear self-interaction of Kelvin waves has been studied by *Boyd* (1980, 1984, 1991, 1998), *Chen and Boyd* (2002), *Marshall and Boyd* (1987), *Ripa* (1982, 1985), *Long and Chang* (1990), *Fedorov and Melville* (2000), *Greatbatch* (1985), *Majda et al.* (1999), *Le Sommer et al.* (2004), *Milewski and Tabak* (1999). In spite of these work, there are still significant gaps in both linear and nonlinear theory. Some of the linear gaps have recently been filled by *Boyd* (2005d) and *Boyd and Zhou* (2008b). But for the nonlinear Kelvin waves, there are still many unsolved problems. For example, are there any steadily translating (traveling) nonlinear Kelvin waves? If any, how does the nonlinearity change the spatial structure and phase speed? When in the presence of a background mean, how does it change the spatial structure and

phase speed? As for the first question, since solitary/traveling waves are the result of balance between nonlinearity and dispersion, the nonlinearity comes from the wave-wave interaction terms in the nonlinear equations and the dispersion could come from either the spherical geometry or the background mean flow, so it is possible to get traveling nonlinear Kelvin waves.

In Chapter III, we will show how to get such traveling waves. We extend the nonlinear shallow water equations theory in a couple of ways. First, instead of using the equatorial beta-plane, which corresponds to the limit of a very thin ocean, we explicitly include the effects of the earth's sphericity and finite depth (i. e., finite "Lamb's parameter".) In the equatorial beta-plane approximation, traveling waves can be modeled by applying the method of multiple scales to derive the Korteweg-deVries (KdV) equation (with mean currents) or the inviscid Burgers equation (neglecting mean currents) and then invoking the known analytic traveling waves of these models. On the sphere, it is impossible to derive an analytic solution. However, a mixture of perturbation theory (for small amplitude) and a continuation/Fourier-Galerkin/Newton iteration algorithm (for larger amplitude) allows us to describe the nonlinear Kelvin wave on the sphere.

The nonlinear Kelvin wave exhibits, with increasing amplitude, the so-called Cnoidal/Corner/Breaking (CCB) Scenario. That is, for small amplitude, nonlinear Kelvin waves are steadily-traveling periodic waves similar to the cnoidal waves of the Korteweg-deVries equation. The branch of solutions terminates in a wave of finite amplitude which is a "corner wave" in the sense that there is a slope discontinuity at the crest (*Boyd* (2003, 2006)). For waves whose initial amplitude is higher than that of the corner wave, the wave rapidly steepens to an infinite slope ("wave-breaking").

Much is known about the CCB Scenario as reviewed in *Boyd* (2005b), *Boyd* (2003), *Boyd* (2005c) and *Grimshaw et al.* (1998). Pioneering work was done by *Stokes* (1847), *Ostrovsky* (1978) and *Shrira* (1981, 1986). Near-corner waves are de-

scribed through matched asymptotic expansions in *Longuet-Higgins and Fox* (1996) and *Boyd* (2005a). Although we shall not compute initial-value solutions here, the statement that large amplitude Kelvin waves break is demonstrated in *Boyd* (2006), *Boyd* (2005b) and *Chen and Boyd* (2002).

Kelvin breaking has been discussed elsewhere (*Boyd* (1980, 1998); *Chen and Boyd* (2002); *Fedorov and Melville* (2000); *Le Sommer et al.* (2004)). Here, we will attempt to describe the traveling waves up to and including the corner wave. This poses a severe numerical challenge because in the corner wave limit, the wave will have a discontinuous x -derivative at the peak of the wave. The convergence rate of Fourier coefficients of functions with a slope discontinuity is only $O(K^{-2})$, where K is the degree of Fourier coefficients. By employing the Kepler mapping developed in *Boyd* (2006), the convergence rate can be improved to $O(K^{-4})$.

1.5 Nonlinear Kelvin waves on the equatorial beta-plane

Linear Kelvin waves on the equatorial beta-plane in the presence of a zonal shear flow or jet have been studied by *McPhaden and Knox* (1979) and *Philander* (1979) three decades ago. However, the nonlinearity has been left out when obtaining these steadily traveling waves. Unlike the Kelvin wave on the sphere, Kelvin waves on the equatorial beta-plane without mean currents are nondispersive. It has been shown that an inviscid Burger's equation can be derived by applying the method of multiple scales and finite Kelvin waves always evolve to fronts and break (*Boyd*, 1980). Without the dispersive mean flow terms, such traveling wave solutions do not exist since the nonlinear traveling solution is the result of the perfect balance between dispersion and nonlinearity. By adding a background jet, we can introduce the necessary dispersion terms. Such jets are an observed feature of the tropical ocean and atmosphere.

1.6 Tropic instability waves

Tropical Instability Waves (TIWs) are westward propagating oscillations observed in both equatorial Pacific and Atlantic oceans. Each year around June, an cold area called cold tongue with sea surface temperature less than $25^{\circ}C$ appears in the east equatorial Pacific ocean in response to the intensified winds and a shallowing of the thermocline. Soon after the cold tongue forms, its north boundary(North Equatorial Front)and also south boundary undergo westward oscillations which are called Tropical Instability Waves. Around March next year when cold tongue weakens and disappears, TIWs also weaken and disappear. They were first detected in satellite infrared images as cusplike deformations of the North Equatorial Front in the Pacific ocean by *Legeckis* (1977). Subsequent measurements observed TIWs with various wavelengths and periods, in ranges of 600-2000 km and 16-40 days, respectively (*Qiao and Weisberg*, 1995). They are stronger during the warm phase of ENSO cycle and weaker during the cold phase. In strong La Niña years, TIWs can extend as far as $160^{\circ}E$ in Pacific ocean. They play an important role in mixing and cross equator transport of sea water. Figure 1.2 shows the evolution of TIWs in Pacific Ocean observed in SST images from June 1,1998 to August 30, 1998.

Even though the TIWs in Figure 1.2 appear to be just one instability wave propagating westward at first glance, previous studies have shown that TIWs generally fall into two categories(see Figure 11 in *Kennan and Flament* (2000) for an example). The first has periods around 15-23 days, is most prominent in meridional velocity, and has been observed within a few degrees of the equator(*Halpern et al.*, 1988; *Qiao and Weisberg*, 1995; *Flament et al.*, 1996; *Kennan and Flament*, 2000; *Lyman et al.*, 2007). The second has periods around one month and has been observed in sea surface height, thermocline depth, velocity, and subsurface temperature centered about $5^{\circ}N$ (*Miller et al.*, 1985; *Flament et al.*, 1996; *Kennan and Flament*, 2000; *Lyman et al.*, 2005, 2007; *Shinoda et al.*, 2009). *Flament et al.* (1996) and *Kennan and Fla-*

ment (2000) observed two drastically different propagation speeds of TIWs at the same time, 0.8 ms^{-1} along the equator and 0.3 ms^{-1} along $4.5^\circ N$. They suggested they were two distinct phenomena. Lyman *et al.* (2007) also observed two different types of TIWs: unstable Rossby waves at a period of about 33 days characterized by subsurface temperature at $5^\circ N$ and Yanai waves at a period of about 17 days characterized by fluctuations in meridional velocity at the equator and in subsurface temperature at $2^\circ N$ and $2^\circ S$.

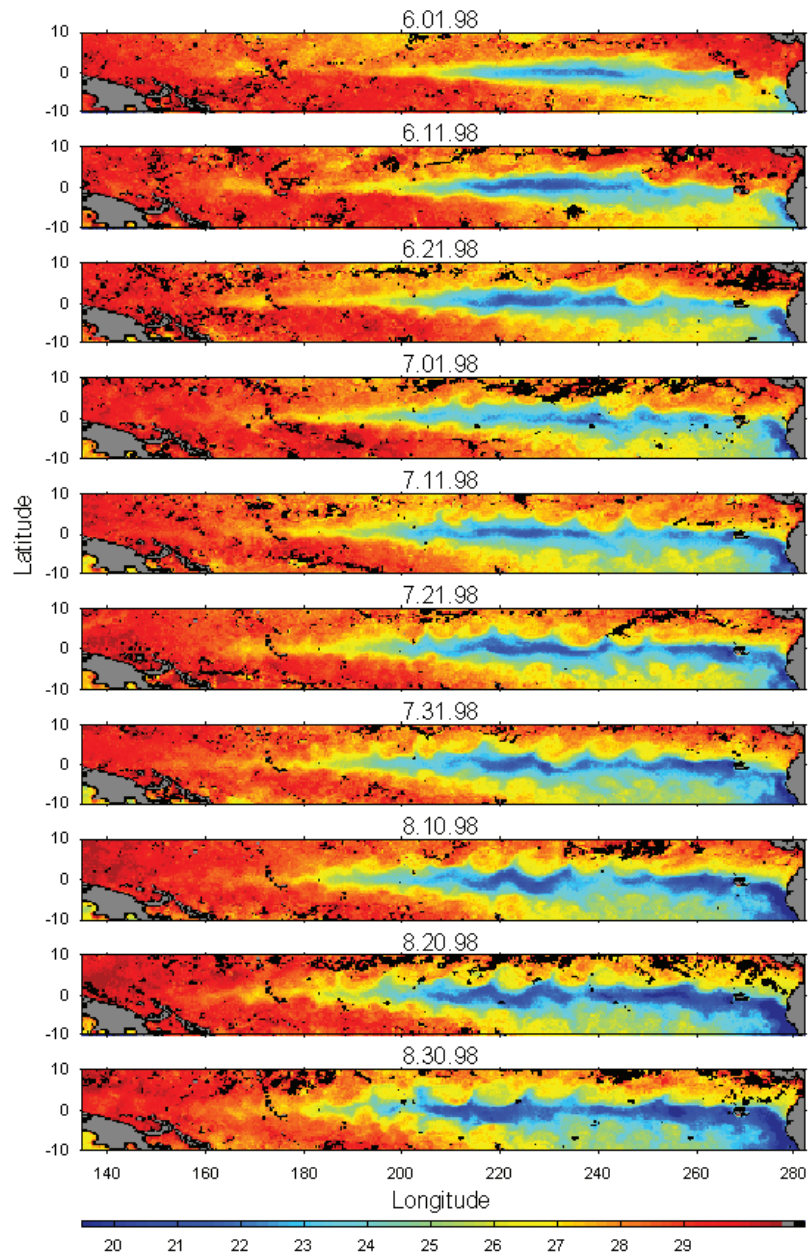


Figure 1.2: Tropical instability waves (TIW) seen in SST from the Tropical Rainfall Measuring Mission (TRMM) Microwave Imager (TMI). TMI imagery courtesy of Remote Sensing Systems (<http://www.ssmi.com/>). Cold area, called cold tongue, forms each year around June. Soon after it forms, its south and north boundaries (between the cold water (blue) and warm water (red)) are subjected to cusp shape deformation which propagate to the west with a wavelength of about 1000 km and a period of about 15~45 days. These oscillations are associated with the Tropical Instability Waves.

Nonlinear models by *McCreary and Yu* (1992) and *Yu et al.* (1995) produced two waves with distinct periods (wave 1 with periods about 20 days and wave 2 with periods about 40-50 days (*Yu et al.*, 1995)). These two waves have almost identical phase speeds, which suggests they may arise from the same critical latitude (*Proehl*, 1996). The nonlinear 2-1/2-layer model by *Donohue and Wimbush* (1998) also generated a 15-day wave with a phase speed about 0.88 ms^{-1} and a strong meridional signal centered on the equator and a 30-day wave with a phase speed about 0.42 ms^{-1} and sea level maxima near $6^\circ N$. They argued that the 15-day wave arose from the barotropic instability of the cyclonic shear of south flank of the north South Equatorial Current (SEC) while the 30-day waves arose from both the barotropic instability of the anticyclonic shear of the north flank of SEC and the baroclinic conversion near the core of SEC. With observational data and a projected linearized model, *Lyman et al.* (2007) were able to identify the 33-day waves as unstable first meridional mode Rossby waves; however, the fast 17-day waves did not show up as unstable waves when the authors ran the linearized model with five vertical modes and gradually increased the shear of the mean equatorial currents. So how these 17-20 day Yanai-like waves with relative fast propagation speed are generated still remains unclear.

1.7 Outline

In Chapter II, we will derive a new asymptotic approximation of linear Kelvin wave on the sphere valid in the limit $\sqrt{s^2 + \epsilon} \gg 1$.

In Chapter III, we apply perturbation theory to analyze traveling waves of small amplitude. We then describe the numerical methods that will be employed. Our perturbative and numerical analysis will explicitly treat only low zonal wavenumbers, $s = 1$ and $s = 2$. However, the methodologies are completely general. We concentrate on *small* zonal wavenumbers because as illustrated in *Boyd and Zhou* (2008b), Kelvin

waves of moderate and large s are *equatorial* rather than *global* modes and are therefore well-modeled by the equatorial beta-plane studies of previous work *Boyd* (1998, 2006). The spatial structure of the corner wave is analyzed. Variations of the phase speed and height of the corner wave are described and comparisons with observations are then discussed followed by a summary.

In Chapter IV, we first study how a background jet modifies the linear Kelvin waves, like spatial structures and phase speeds. Then we calculate the nonlinear traveling Kelvin waves following the same numerical methods employed in Chapter III.

In Chapter V, we focus on the TIWs arising from the barotropic instability and investigate how the nonlinearity changes their strength, periods, etc. Especially, we explain how the two distinct types of waves with different propagating speeds arise. We then evaluate the effect of external forcings on these two types of waves.

Final conclusion comes in Chapter VI. Since we already give detailed summary or conclusion in each separate chapter, we only briefly summarize the main results. Also we talk about limitations of our theory and possible future work in this chapter.

CHAPTER II

Uniform Asymptotics for the Linear Kelvin Wave in Spherical Geometry

In this chapter, we will derive a new asymptotic approximation of the linear Kelvin wave on the sphere valid in the limit $\sqrt{s^2 + \epsilon} \gg 1$.

2.1 A New Asymptotic Approximation

2.1.1 Derivation

The linear tidal equations can be written, as in *Longuet-Higgins* (1968),

$$\sigma U - \mu \tilde{V} - s\phi = 0 \quad (2.1)$$

$$\mu U - \sigma \tilde{V} + (1 - \mu^2)\phi_\mu = 0 \quad (2.2)$$

$$sU - (1 - \mu^2)\tilde{V}_\mu - \epsilon \sigma (1 - \mu^2)\phi = 0 \quad (2.3)$$

where $\mu = \cos(\theta)$, θ is colatitude, λ is longitude, ϕ is the height and σ the nondimensional frequency. All variables have been nondimensionalized using a as the length scale, 2Ω as the time scale and H as the depth scale. U and \tilde{V} are the nondimensional “Margules-Robert” velocities:

$$U = \frac{1}{2\Omega} \frac{d\lambda}{dt} \sqrt{1 - \mu^2}; \quad \tilde{V} = -i \frac{1}{2\Omega} \frac{d\theta}{dt} \sqrt{1 - \mu^2} \quad (2.4)$$

The factor of $i = \sqrt{-1}$ accounts for a quarter-of-a-wavelength phase differences between the north-south velocity and the other fields; the minus sign ensures that V is positive for a northward flow, as is the usual meteorological convention (but opposite to the velocity as defined using a physicist's longitude-colatitude spherical coordinates since θ increases from zero at the north pole to π at the south pole).

It is convenient to define a new pressure/height unknown so that for the Kelvin wave, U will approximately equal the new unknown h where

$$h = (s/\sigma)\phi \quad \leftrightarrow \quad \phi = (\sigma/s)h \quad (2.5)$$

Solving the longitudinal momentum equation for U in terms of the other variables reduces the set to two equations in two unknowns:

$$\begin{aligned} \left\{ \frac{s}{\sigma^2}\mu^2 - s \right\} \tilde{V} + \frac{s}{\sigma}\mu h + (1 - \mu^2) h_\mu &= 0 \\ \mu\tilde{V}/\sigma - (1 - \mu^2)\tilde{V}_\mu/s + \left\{ 1 - \epsilon \frac{\sigma^2}{s^2}(1 - \mu^2) \right\} h &= 0 \end{aligned} \quad (2.6)$$

Fig. 2.1 shows how this pair of equations is simplified to yet another set (2.12) which is solved exactly below.

The first approximating principle is that when either s or ϵ is large, the Kelvin mode will be confined very close to the equator. Equatorial confinement was demonstrated for large ϵ by Longuet-Higgins; Fig. 2.2 shows that even for $\epsilon = 0$, the Kelvin wave becomes more and more confined to low latitude as the zonal wavenumber s increases. It follows that in the region where the wave has significant amplitude, the neighborhood of $\mu = 0$, it will be a good approximation to replace $(1 - \mu^2)$ by one.

The second approximating principle is that for all ϵ , the frequency σ is close to its beta-plane value $s/\sqrt{\epsilon}$ with a relative error which falls rapidly with increasing s or ϵ . To be precise, Longuet-Higgins has demonstrated numerically that $\sigma/(s/\sqrt{\epsilon})$ varies monotonically between its $\epsilon = 0$ limit ($\sqrt{1 + 1/s}$) and $\epsilon = \infty$ limits (one), implying

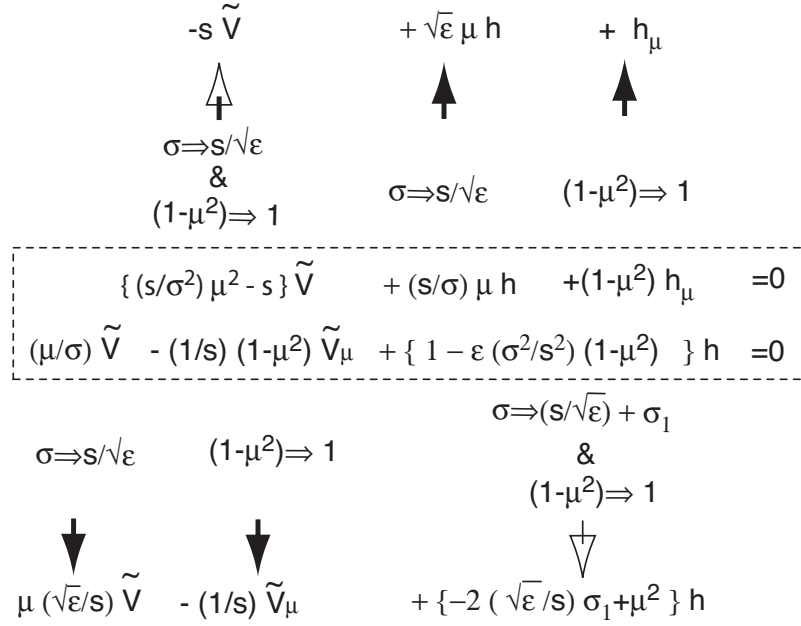


Figure 2.1: Schematic of the approximation of the exact pair of equations (middle inside the dotted rectangle) by the terms at the top and bottom of the diagram; this simplified pair of equations is then solved exactly.

that

$$\sigma = \frac{s}{\sqrt{\epsilon}} \{1 + \zeta\}, \quad \zeta \leq \sqrt{1 + 1/s} - 1 \leq 1/(2s) \quad (2.7)$$

For fixed s and large ϵ , Longuet-Higgins showed that $\zeta \sim 1/(4\epsilon)$. It follows that for either large s or ϵ , it is a good approximation to replace σ by $s/\sqrt{\epsilon}$.

There are subtleties in the two terms which require both approximations simultaneously (marked by hollow arrows). In the upper left of the diagram, the frequency approximation σ suggests

$$(s/\sigma^2)\mu^2 - s \approx -s \left(1 - \frac{\epsilon}{s^2}\mu^2\right) \quad (2.8)$$

When $\epsilon \leq s^2$, the μ^2 term can be neglected compared to the one in the parentheses. The subtlety is that when $\epsilon \rightarrow \infty$ for fixed s , the usual rules of the equatorial beta-plane apply, and in this limit, the scale of μ is $O(\epsilon^{-1/4})$ so that the term in μ^2 is

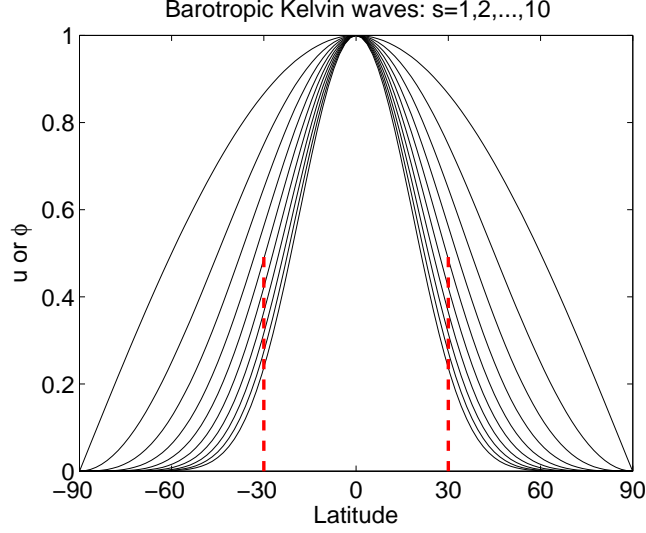


Figure 2.2: The latitudinal structure of u or ϕ (which are identical) for the lowest ten zonal wavenumbers s for $\epsilon = 0$ [barotropic waves]. $u = (1 - \mu^2)^{s/2}$. The widest curve is $s = 1$ and the waves become more and more narrow as s increases. The dotted curves are guidelines that show that the half-width of the wave is within the tropics ($|\text{latitude}| \leq 30^\circ$) for $s \geq 5$.

emphatically *not small* compared to one. However, in this same limit, \tilde{V} tends to zero as $O(\epsilon^{-3/4})$ relative to h as shown by Longuet-Higgins (1968). Therefore, the replacement $\{(s/\sigma^2)\mu^2 - s\}\tilde{V} \approx -s\tilde{V}$ yields small errors relative to the other terms in the equation for s or ϵ or both large.

In the last term in the second equation (bottom right of the figure), the factor

$$1 - \epsilon \frac{\sigma^2}{s^2}(1 - \mu^2) = \left\{ 1 - \epsilon \frac{\sigma^2}{s^2} \right\} + \epsilon \frac{\sigma^2}{s^2} \mu^2 \quad (2.9)$$

consists of a (μ -independent) constant plus a term quadratic in μ^2 , which we might naively think could be neglected. However, when σ is equal to its limiting value as $\epsilon \rightarrow \infty$, the constant in the braces is *zero*. It follows that, no matter how large ϵ is, it is never a good approximation to neglect the μ^2 part of this factor. However, in the limit $\epsilon \rightarrow \infty$, \tilde{V} diminishes rapidly compared to h , and μ^2 will be small in the equatorial region where the wave has most of its amplitude. It follows that although

$1 - \epsilon\sigma^2/s^2$ is small compared to one, this term is not negligible. Therefore, writing

$$\sigma = s/\sqrt{\epsilon} + \sigma_1(\epsilon, s) \quad (2.10)$$

we shall treat this factor with near-cancellations as

$$1 - \epsilon \frac{\sigma^2}{s^2} (1 - \mu^2) \approx -2 \frac{\sqrt{\epsilon}}{s} \sigma_1 + \mu^2 \quad (2.11)$$

Everywhere else in (2.6), $1 - \mu^2 \rightarrow 1$ and $\sigma \rightarrow s/\sqrt{\epsilon}$, yielding the *approximate* equations

$$\begin{aligned} -s\tilde{V} + \sqrt{\epsilon}\mu h + h_\mu &= 0 \\ \mu \frac{\sqrt{\epsilon}}{s} \tilde{V} - \tilde{V}_\mu/s + \left\{ -2 \frac{\sqrt{\epsilon}}{s} \sigma_1 + \mu^2 \right\} h &= 0 \end{aligned} \quad (2.12)$$

The *exact* solution of this *simplified* pair of equations is

$$h = \exp\left(-\frac{1}{2}\sqrt{\epsilon + s^2}\mu^2\right) \quad (2.13)$$

$$\tilde{V} = \left\{ \frac{\sqrt{\epsilon}}{s} - \sqrt{1 + \frac{\epsilon}{s^2}} \right\} \mu \exp\left(-\frac{1}{2}\sqrt{\epsilon + s^2}\mu^2\right) \quad (2.14)$$

$$\sigma_1 = -\frac{1}{2s} + \frac{1}{2\sqrt{\epsilon}} \sqrt{1 + \frac{\epsilon}{s^2}} \quad (2.15)$$

There is one further refinement that is helpful for small zonal wavenumber s . All of the unknowns U , \tilde{V} and ϕ have expansions in spherical harmonics, and all spherical harmonics of a given wavenumber have a common factor of $(1 - \mu^2)^{s/2}$ which forces all these fields to have a root of order $s/2$ at each pole. (This property is true of all scalars in spherical geometry when expanded in a longitudinal Fourier series as discussed in Boyd (2001).) For small s and ϵ , the Gaussian factors of μ in (2.13) and

(2.14) do not enforce these zeros. It is therefore desirable to make the replacement

$$\exp\left(-\frac{1}{2}\sqrt{\epsilon + s^2}\mu^2\right) \approx (1 - \mu^2)^{s/2} \exp\left(-\frac{1}{2}\left\{\sqrt{\epsilon + s^2} - s\right\}\mu^2\right) \quad (2.16)$$

Because $(1 - \mu^2)^{s/2} = \exp((s/2)\log(1 - \mu^2)) \approx \exp(-(s/2)\mu^2)$ for small μ , these two expressions in (2.16) are indistinguishable when either s or ϵ or both are large, but separation of the $s/2$ order zeros at the poles yields a better approximation when s and ϵ are small.

2.1.2 Results

Converting back to the original variables gives the final asymptotic approximation, uniformly accurate when either s or ϵ or both are large:

$$\phi = (1 - \mu^2)^{s/2} \exp\left(-\frac{1}{2}\left\{\sqrt{\epsilon + s^2} - s\right\}\mu^2\right) \quad (2.17)$$

$$\tilde{V} = \frac{s}{\sigma} \left\{ \frac{\sqrt{\epsilon}}{s} - \sqrt{1 + \frac{\epsilon}{s^2}} \right\} \mu (1 - \mu^2)^{s/2} \exp\left(-\frac{1}{2}\left\{\sqrt{\epsilon + s^2} - s\right\}\mu^2\right) \quad (2.18)$$

$$U = \frac{s}{\sigma} \phi + \frac{\mu}{\sigma} \tilde{V} \quad (2.19)$$

$$\sigma = s/\sqrt{\epsilon} - \frac{1}{2s} + \frac{1}{2\sqrt{\epsilon}}\sqrt{1 + \frac{\epsilon}{s^2}} \quad (2.20)$$

For *fixed* s and large ϵ , this frequency approximation simplifies to the formula derived nearly forty years ago by Longuet-Higgins (1968), $\sigma = s/\sqrt{\epsilon} \left\{ 1 + \frac{1}{4\sqrt{\epsilon}} \right\}$.

The price for the simplicity of these approximations is that their derivation is not based on systematic power series expansions, but rather more on the sort of mathematical banging-on-pipes that engineers do without apology (“if the dam holds, hurrah!”) and that physicists dignify with the fine-sounding German word *ansatz*. In this instance, no apologies are necessary because the full parameter space is only two-dimensional (Fig. 1.1) and we have a highly accurate numerical method to com-

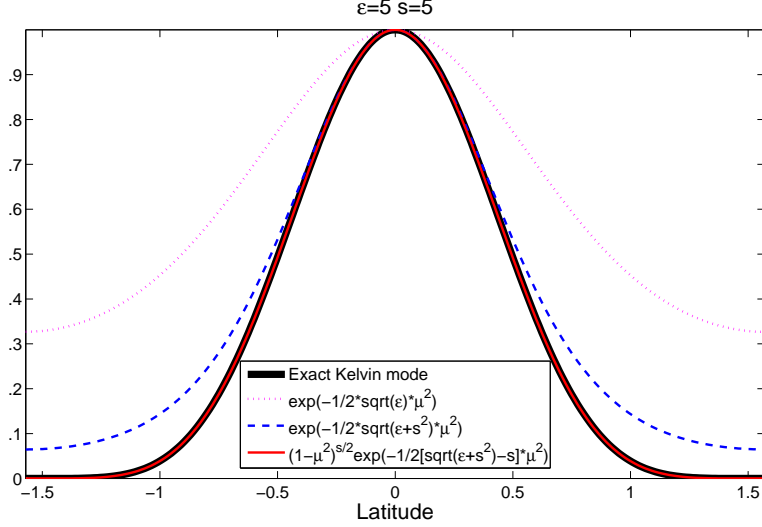


Figure 2.3: The thick black curve is the exact Kelvin mode for $s = 5$ and $\epsilon = 5$. The red curve is the improved new asymptotic approximation, $\phi \approx (1 - \mu^2)^{s/2} \exp(-1/2) \{ \sqrt{\epsilon + s^2} - s \} \mu^2$ which is graphically indistinguishable from the Kelvin wave. The dashed curve is the new asymptotic approximation without the $(1 - \mu^2)$ factor, $\phi \approx \exp(-1/2) \sqrt{\epsilon + s^2} \mu^2$. The dotted curve is the classical equatorial beta-plane approximation, $\phi \approx \exp(-1/2) \sqrt{\epsilon} \mu^2$.

pute “exact” solutions to compare with the approximations throughout the whole of parameter space, and thus validate the approximations with a thoroughness that even a mathematician can accept.

2.2 Results and Numerical Plots of Errors

The maximum relative errors in the new approximation for the frequency σ for all $\epsilon \in [0, \infty]$ are 6.1 % [$s = 1$], 2.5 % [$s = 2$], 1.2 % [$s = 3$] and 0.70 % [$s = 4$] and in general $O(1/(8s^2))$. It is remarkable that an approximation derived for large s and/or ϵ is in fact rather accurate even for small s and ϵ .

Fig. 2.3 compares the exact Kelvin wave on the sphere, as computed numerically, with three different asymptotic approximations for a typical pair of parameter values ($\epsilon = 5, s = 5$). The equatorial beta-plane approximation (dots) is terrible. The

asymptotic approximation which is unconstrained to vanish at the poles is much better, but not too good at high latitudes. The asymptotic approximation which is proportional to $(1 - \mu^2)^{s/2}$, in contrast, is visually indistinguishable from the exact height field.

Fig. 2.4 shows the error in frequency σ [upper left] and of (u, v, ϕ) [in the L_∞ norm, that is, the maximum error for any latitude] for the new asymptotic approximation in the $\sqrt{\epsilon} - s$ plane. The frequency error is not one-signed, but rather has an accidental zero along a ray $s \approx 3\sqrt{\epsilon}$. This is not important, but the fact that the error is small everywhere is gratifying. The errors in the velocities and height are very small for small $\sqrt{\epsilon}$ because of the built-in factor of $(1 - \mu^2)^{s/2}$: u and ϕ are approximately equal to this factor for small ϵ . However, again the error is uniformly small everywhere in the two-dimensional parameter space.

2.3 Summary

We have derived a new asymptotic approximation for the Kelvin wave that fills the gap between the equatorial beta-plane (fixed zonal wavenumber s , Lamb's parameter $\epsilon \rightarrow \infty$) and the small ϵ , velocity-potential-is- $P_n^n(\mu) \exp(is\lambda)$ approximation. The new approximation was derived under the assumption that at least one of (s, ϵ) is large, but numerically, is *moderately* good even when both parameters are small.

The approximation shows that the degree of equatorial confinement is not controlled by ϵ alone, but rather by the parameter

$$\epsilon_{eff} = s^2 + \epsilon \tag{2.21}$$

Boyd (1985) showed that the same is true for Rossby waves. A Kelvin wave of moderate zonal wavenumber s will be confined to the tropics even for $\epsilon = 0$, a barotropic wave, as illustrated in Fig. 2.2.

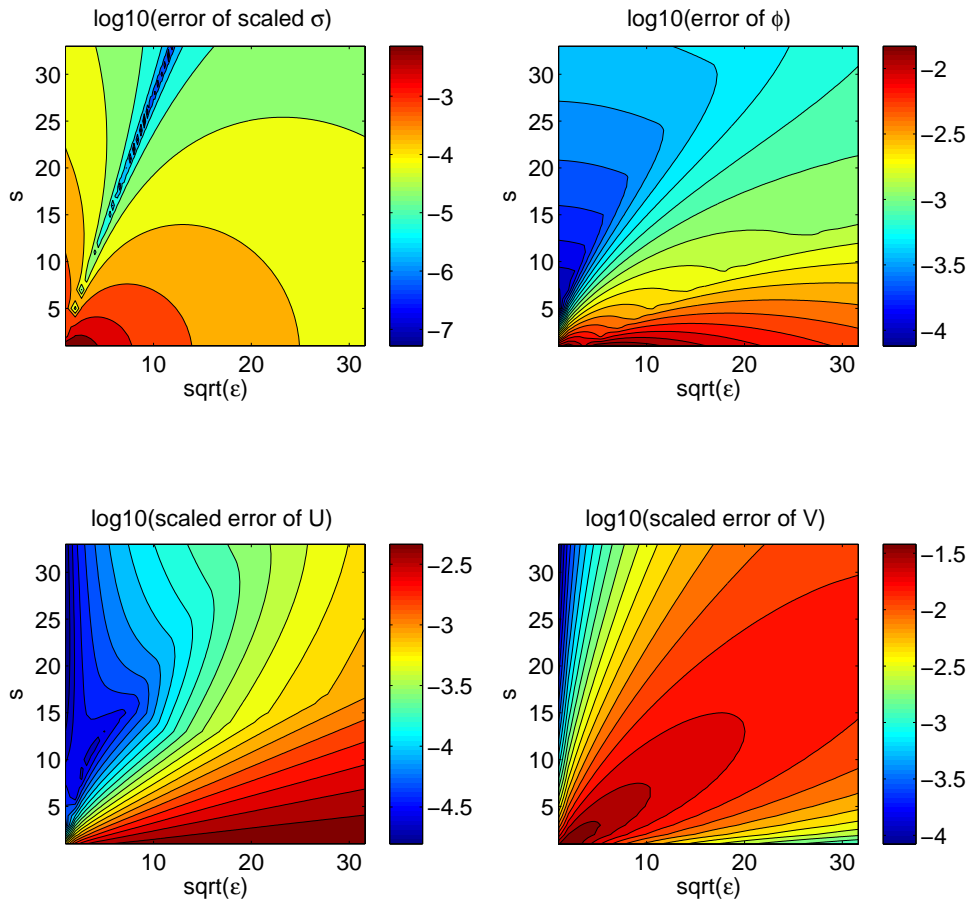


Figure 2.4: $\log_{10}(\text{errors})$ in the new asymptotic approximation to the Kelvin wave for the frequency (upper left) and the three unknowns (remaining three panels). The frequency error is the error in $\sigma/(s/\sqrt{\epsilon})$, which is close to one for all s and ϵ . The eigenfunctions are normalized by scaling the height to have a maximum of one, so the errors are both the absolute and relative errors in this variable. u and v were scaled by dividing the absolute errors by the global maximum of each velocity, and plotting these scaled variables.

CHAPTER III

Kelvin Waves in the Nonlinear Shallow Water Equations on the Sphere: Nonlinear Traveling Waves and the Corner Wave Bifurcation

In linear wave dynamics, assumption is made that the wave amplitude is small so that the wave-wave interaction terms could be dropped. However, in nonlinear wave dynamics the wave amplitude is no longer small so the wave-wave interaction terms need to be retained. So instead of living in a two dimensional parameter space of wavenumber s and Lamb's parameter ϵ like linear Kelvin waves, nonlinear Kelvin waves live in a three dimensional parameter space with the wave amplitude as the third dimension. If we fix wavenumber s , then we only need to consider two dimensions. When $\epsilon=0$ and wave amplitude is infinitesimal, we know that the Kelvin wave solution is just the linear Kelvin wave solution for $\epsilon=0$. So we could derive the asymptotic solution of nonlinear Kelvin waves when s and ϵ are both small by expanding the unknowns in a double power series in the wave amplitude and in the square root of Lamb's parameter ϵ , so called "perturbation method". The perturbation method fails when either wave amplitude or ϵ becomes large enough. And we will use numerical method to pursue the solution when the perturbation method fails.

3.1 Nonlinear Kelvin wave on sphere by perturbation theory

3.1.1 Introduction

In this section, we shall approximate the traveling wave solution of the nonlinear Kelvin wave on the sphere by a perturbation series. First, the nonlinear shallow water equations will be nondimensionalized. Second, we will simplify by shifting to the velocity variables introduced by Margules and changing the north-south coordinate. Finally, the traveling wave solution with period 2π will be perturbatively derived by expanding the unknowns in a double power series in the wave amplitude and in the square root of Lamb's parameter ϵ .

3.1.2 Nonlinear shallow Water Equations on the Sphere

The nonlinear shallow water equations in spherical coordinate over a flat sea bottom are

$$\frac{\partial u'}{\partial t'} + \frac{u'}{a \sin(\theta)} \frac{\partial u'}{\partial \lambda} - \frac{v'}{a} \frac{\partial u'}{\partial \theta} - \left(2\Omega \cos(\theta) + \frac{u' \cot(\theta)}{a} \right) v' + \frac{g}{a \sin(\theta)} \frac{\partial h'}{\partial \lambda} = 0 \quad (3.1)$$

$$\frac{\partial v'}{\partial t'} + \frac{u'}{a \sin(\theta)} \frac{\partial v'}{\partial \lambda} - \frac{v'}{a} \frac{\partial v'}{\partial \theta} + \left(2\Omega \cos(\theta) + \frac{u' \cot(\theta)}{a} \right) u' - \frac{g}{a} \frac{\partial h'}{\partial \theta} = 0 \quad (3.2)$$

$$\frac{\partial h'}{\partial t'} + \frac{u'}{a \sin(\theta)} \frac{\partial h'}{\partial \lambda} - \frac{v'}{a} \frac{\partial h'}{\partial \theta} + \frac{h'}{a \sin(\theta)} \left(\frac{\partial u'}{\partial \lambda} - \sin(\theta) \frac{\partial v'}{\partial \theta} - v' \cos(\theta) \right) = 0 \quad (3.3)$$

where θ is colatitude, λ is longitude, t' is the dimensional time, u' is the dimensional eastward velocity, v' is the dimensional northward velocity, h' is the total depth of the fluid, and a is the radius of the planet. (Note that following the usual geophysical convention, $v' = -a D\theta/Dt$ where D/Dt is the total derivative because colatitude θ is increasing southward.)

It is convenient to nondimensionalize the variables as follows:

$$t' = (1/[2\Omega])\sqrt{\epsilon} t \quad (3.4)$$

$$u' = 2\Omega a \frac{\hat{u}}{\sin(\theta)}, \quad v' = 2\Omega a \frac{\hat{v}}{\sin(\theta)}, \quad (3.5)$$

$$h = H (1 + \sqrt{\epsilon} \phi) \quad (3.6)$$

Note that \hat{u} and \hat{v} are the ‘‘Margules velocities’’, introduced in the early twentieth century by the Austrian meteorologist Max Margules because the $\sin(\theta)$ factors ensure that these modified velocities have the same behavior at the poles as scalar variables such as the height h .

It is common in tidal theory to rescale time by 2Ω , velocities by $2\Omega a$ and the deviation height field by ϵ . We have chosen different scales for time and ϕ for convenience in applying perturbation theory as explained in the next section. We employed the same scalings for the numerical studies to facilitate comparisons between perturbative and numerical results.

For notational simplicity, we omit the accents on the Margules velocities below.

In the meridional direction, we change the coordinate from θ to μ via

$$\cos(\theta) = \mu, \quad \sin(\theta) = \sqrt{1 - \mu^2}, \quad \frac{\partial}{\partial \theta} \rightarrow -\sqrt{1 - \mu^2} \frac{\partial}{\partial \mu} \quad (3.7)$$

We now specialize to traveling waves of the form $u(\lambda - ct, \mu)$ and similarly for the other variables where c is the nondimensional phase speed. The usual dimensional phase speed in units meters/second is

$$c_{dim} = a \frac{2\Omega}{\sqrt{\epsilon}} c \quad (3.8)$$

The eigenmodes of Laplace’s tidal equations, which are the linearization of the shallow water equations about a state of rest, are standing waves in latitude and propagate only east-west, and this is true of the nonlinear traveling waves as well. To explicitly collapse the number of coordinates from three (λ, μ, t) to two, it is convenient to define a new coordinate in a frame of reference that moves with the

wave:

$$x \equiv \lambda - ct \quad (3.9)$$

Then

$$\frac{\partial}{\partial t} \rightarrow -c \frac{\partial}{\partial x}, \quad \frac{\partial}{\partial \lambda} \rightarrow \frac{\partial}{\partial x} \quad (3.10)$$

After all these steps and defining $\delta \equiv \sqrt{\epsilon}$, the shallow water equations become, without approximation,

$$(c(1 - \mu^2) - \delta u) \frac{\partial u}{\partial x} - \delta(1 - \mu^2)v \frac{\partial u}{\partial \mu} - (1 - \mu^2) \frac{\partial \phi}{\partial x} + \delta \mu(1 - \mu^2)v = 0 \quad (3.11)$$

$$(c(1 - \mu^2) - \delta u) \frac{\partial v}{\partial x} - \delta(1 - \mu^2)v \frac{\partial v}{\partial \mu} - (1 - \mu^2)^2 \frac{\partial \phi}{\partial \mu} - \delta \mu \{u^2 + v^2 + (1 - \mu^2)u\} = 0 \quad (3.12)$$

$$(c(1 - \mu^2) - \delta u) \frac{\partial \phi}{\partial x} - \delta(1 - \mu^2)v \frac{\partial \phi}{\partial \mu} - (1 + \delta \phi) \left(\frac{\partial u}{\partial x} + (1 - \mu^2) \frac{\partial v}{\partial \mu} \right) = 0 \quad (3.13)$$

3.1.3 Traveling waves by perturbative double expansion

The traveling wave solution of (3.11)–(3.13) can be approximated by perturbation theory. As is standard in nonlinear wave theory, we assume the wave amplitude is small as measured by a placeholder variable A . Unfortunately, linearizing in A merely generates Laplace's tidal equations whose solutions, the Hough functions, cannot be found analytically except in the limits $\epsilon \rightarrow 0$ and $\epsilon \rightarrow \infty$. We therefore perform a double expansion on the further assumption that ϵ is sufficiently small. Then u, v, ϕ, c can be expressed as series of A and δ , which is $\sqrt{\epsilon}$.

$$u = \sum_{i=0}^n \sum_{j=1}^m u_{i,j} \delta^i A^j, \quad v = \sum_{i=0}^n \sum_{j=1}^m v_{i,j} \delta^i A^j, \quad \phi = \sum_{i=0}^n \sum_{j=1}^m \phi_{i,j} \delta^i A^j, \quad c = \sum_{i=0}^n \sum_{j=0}^m c_{i,j} \delta^i A^j \quad (3.14)$$

Substitute these expressions into (2.11)–(2.13) and collect the coefficients of $\delta^i A^j$ from each equation. Perturbation theory requires all these coefficients should be zero. The lowest order equations, coefficients of $\delta^0 A^1$, are simply the $\epsilon = 0$ limit of Laplace's

(linear) tidal equations,

$$c_{0,0}u_{0,1,x} - \phi_{0,1,x} = 0 \quad (3.15)$$

$$c_{0,0}v_{0,1,x} - (1 - \mu^2)\phi_{0,1,\mu} = 0 \quad (3.16)$$

$$u_{0,1,x} + (1 - \mu^2)v_{0,1,\mu} - c_{0,0}(1 - \mu^2)\phi_{0,1,x} = 0 \quad (3.17)$$

$\phi_{0,1}$ and $v_{0,1}$ can be quickly eliminated and the equations become one single equation of $u_{0,1}(x, \mu)$ and $c_{0,0}$. Further more, let $u_{0,1}(x, \mu) = U(\mu)\cos(sx)$ where s is the zonal wave number. We get

$$(1 - \mu^2)\frac{\partial^2 U(\mu)}{\partial \mu^2} - 2\mu\frac{\partial U(\mu)}{\partial \mu} + \left(c_{0,0}^2 s^2 - \frac{s^2}{1 - \mu^2}\right)U(\mu) = 0 \quad (3.18)$$

This is Legendre's equation. Since $c_{0,0}$ is unknown, it is an eigenvalue problem. The solutions bounded on the sphere are

$$U(\mu) = P_l^s(\mu), \quad l = s, s + 1, s + 2, \dots \&, \quad c_{0,0} = \frac{\sqrt{l(l+1)}}{s} \quad (3.19)$$

Note that the Legendre equation (3.18) also has a negative root for $c_{0,0}$ since the eigenvalue is the *square* of the phase speed; however, the reduction from three equations to one requires dividing by a factor that is *zero* for $c_{0,0} = -\sqrt{s(s+1)}/s$. Thus, the “anti-Kelvin” wave, as this spurious mode has been dubbed, is not a true eigenfunction of the original system of three linearized equations; the only true $l = s$ eigenmode has a positive (eastward) phase speed.

When $l = s$, the solution is the well known linear Kelvin wave on the sphere:

$$c_{0,0} = \frac{\sqrt{s(s+1)}}{s} \quad (3.20)$$

$$u_{0,1}(x, \mu) = P_s^s(\mu) \cos(sx) \quad (3.21)$$

$$v_{0,1}(x, \mu) = (1 - \mu^2) \frac{\partial P_s^s(\mu)}{\partial \mu} \frac{\sin(sx)}{s} \quad (3.22)$$

$$\phi_{0,1}(x, \mu) = c_{0,0} P_s^s(\mu) \cos(sx) \quad (3.23)$$

The higher order equations almost have the same form as equations (3.15), (3.16) and (3.17), except they have forcing terms from lower order solutions on the right hand side of these equations. After eliminating $\phi_{i,j}$ and $v_{i,j}$, there is always an inhomogeneous Legendre equation for $u_{i,j}$ with inhomogeneous part containing $c_{i,j-1}$. By employing the Fredholm solvability condition, which requires the inner product of the eigenfunction and inhomogeneous term be zero, we can get the eigenvalue $c_{i,j-1}$, and then get the particular solution for $u_{i,j}$. The homogenous solutions can always be absorbed to the lowest order solution because they have the same form of the lowest order solutions. A is a placeholder used to order the variables.

For the $s = 1$ case (i.e., a longitudinal period of 2π), the nonlinear Kelvin wave on the sphere is, to the lowest nonlinear order,

$$c = \sqrt{2} - \frac{1}{4}\delta + \frac{17\sqrt{2}}{320}\delta^2 - \frac{1}{160}\delta^3 + \frac{61\sqrt{2}}{40}\delta^2 A^2 - \frac{83}{40}\delta^3 A^2 \quad (3.24)$$

$$u = \sqrt{1 - \mu^2} \cos(x) A - \frac{\sqrt{2}}{2} (1 + \mu^2) \sqrt{1 - \mu^2} \cos(x) \delta A + \frac{27}{40} (1 + \mu^2) \sqrt{1 - \mu^2} \cos(x) \delta^2 A + 2\sqrt{2} (1 - \mu^2) \cos(2x) \delta A^2 \quad (3.25)$$

$$\begin{aligned}
v &= -\mu\sqrt{1-\mu^2}\sin(x)A + \mu\sqrt{2(1-\mu^2)}\sin(x)\delta A \\
&\quad + \frac{\mu}{20}\sqrt{1-\mu^2}(2\mu^2-29)\sin(x)\delta^2 A - 2\sqrt{2}\mu(1-\mu^2)\sin(2x)\delta A^2
\end{aligned} \tag{3.26}$$

$$\begin{aligned}
\phi &= \sqrt{2(1-\mu^2)}\cos(x)A - \frac{5}{4}\sqrt{1-\mu^2}\cos(x)\delta A \\
&\quad - \frac{\sqrt{2}}{320}(64\mu^2-273)\sqrt{1-\mu^2}\cos(x)\delta^2 A + \left(\frac{15}{4}(1-\mu^2)\cos(2x) - \frac{\mu^2}{4}\right)\delta A^2
\end{aligned} \tag{3.27}$$

The extension to $s > 1$ is straightforward.

3.2 Kepler mapping/Galerkin method/Newton continuation method

In this section, we shall calculate the same traveling wave solution derived in the previous section, but without the restriction to small wave amplitude and small Lamb’s parameter. We shall combine a change of coordinate (“Kepler mapping”) with a spectral Galerkin method and Newton continuation.

3.2.1 Kepler mapping

To improve the Fourier rate of convergence from second order to fourth order in the degree of the coefficients, we transformed the longitudinal coordinate from x to a new stretched coordinate z . The “Kepler mapping”, so named because inverting the transformation requires solving the Kepler equation of celestial mechanics, concentrates high resolution near the discontinuous corner at $x = 0$ while preserving the periodic behavior in longitude (Boyd, 2006). This creates a mild complication because we apply the numerical method to waves of different longitudinal periods $2\pi/s$ where s is the zonal wavenumber of the lowest nonzero longitudinal Fourier

component. The form of Kepler mapping has a slightly different form for different s :

$$x = z - \frac{\sin(sz)}{s} \quad (3.28)$$

$$\frac{\partial}{\partial x} \rightarrow \frac{1}{1 - \cos(sz)} \frac{\partial}{\partial z} \quad (3.29)$$

The mapping preserves spatial periodicity and $x = z$ at $z = n\pi/s, n = 0, \pm 1, \pm 2, \dots$

3.2.2 Galerkin method

The Galerkin method for discretizing a differential equation demands that when the truncated Fourier series for each unknown is substituted into the shallow water equations to obtain the so-called “residual” function, the leading terms of the Fourier series of the residual are zero. These constraints are obtained by evaluating the integral inner product of the basis functions with the residual function and demanding that this integral should be zero or equivalently, that each basis function is orthogonal to the residual function. The number of orthogonality conditions is equal to the number of undetermined coefficients in the Fourier series for the unknowns, thus deriving a consistent set of nonlinear algebraic equations for the Fourier coefficients of u , v and ϕ . A full discussion is given in *Boyd (2001)*.

To reduce the number of unknowns by a factor of four, we assume that u and ϕ are symmetric about the equator and $z = 0$, and v is antisymmetric about the equator $z = 0$. (Our success in computing solutions with the assumed symmetries is an *a posteriori* justification for these assumptions.) The domain of the entire globe is $[0, 2\pi]$ in longitude and $[0, \pi]$ in colatitude. But by employing the periodicity and parities of the Kelvin wave, we can reduce the domain by a factor of $2s$ in longitude and half it in latitude. So we only need to calculate the unknowns in the region of $[0, \frac{\pi}{s}]$ in x or z and $[0, \frac{\pi}{2}]$ in θ .

As explained in *Boyd (1984)*, the nonlinear traveling wave eigenproblem has a

unique solution only after specification of the longitudinally-averaged zonal flow, in this case, zero. By integrating geostrophic balance around a circle of latitude, one finds that a zero mean for u at each latitude implies that $\phi_{geostrophic}$ must have a zero mean and vice-versa. Integrating the *full* latitudinal momentum equation around a circle of latitude gives, denoting the zonal mean by an overline, $g \partial \bar{h} / \partial \theta = \overline{u \partial v / \partial \lambda} / \sin(\theta) - (1/2) \partial \bar{v}^2 / \partial \theta + \cot(\theta) \bar{u}^2$. As usual, however, such a cyclostrophically-balanced flow is negligible *Boyd* (1976); in our computations, the mean height field \bar{h} was always less than one part in ten thousand relative to the maximum of the wave.

Also by employing the parities of the unknowns, we can halve the number of basis functions used in both directions. In z , the basis functions of u and ϕ are

$$\psi_{sym,0}^{(z)} = 1$$

$$\psi_{sym,1}^{(z)} = \cos(sz) + \frac{1}{2} \tag{3.30}$$

$$\psi_{sym,m}^{(z)} = \cos(smz), \quad m = 2, 3, \dots M \tag{3.31}$$

where the constant $\psi_{sym,0}^{(z)}$ is used only for ϕ and the basis functions of v are

$$\psi_{asym,m}^{(z)} = \sin(smz), \quad m = 1, 2, \dots M \tag{3.32}$$

The additive factor of $(1/2)$ in $\psi_{sym,1}^{(z)}$ ensures that all basis functions with $m > 0$ *individually* have a zero longitudinal mean, despite the change of coordinate from longitude to the Kepler coordinate s , so that the Kelvin wave will not be accompanied by a zonal mean flow; note that $\int_0^\pi \cos(sz(x)) dx = -\pi/2$, (*Boyd*, 2006).

In colatitude, the basis functions of u and ϕ are

$$\psi_{sym,n}^{(\theta)} = \cos((2n - 2)\theta) \sin(\theta)^s, \quad n = 1, 2, \dots N \tag{3.33}$$

and the basis functions of v are

$$\psi_{asym,n}^{(\theta)} = \cos((2n - 1)\theta) \sin(\theta)^s, \quad n = 1, 2, \dots, N \quad (3.34)$$

The reason for the \sin^s factor is explained in *Orszag* (1974), *Boyd* (1978a) and Chapter 18, Sec. 8, of *Boyd* (2001); suffice it to say that the rate of convergence is greatly improved in spherical geometry by multiplying the cosines by $\sin^s(\theta)$.

Finally, we expand u , ϕ and v as

$$u = \sum_{m=1}^M \sum_{n=1}^N a_{mn}^u \psi_{sym,m}^{(z)} \psi_{sym,n}^{(\theta)} \quad (3.35)$$

$$\phi = \sum_{m=0}^M \sum_{n=1}^N a_{mn}^\phi \psi_{sym,m}^{(z)} \psi_{sym,n}^{(\theta)} \quad (3.36)$$

$$v = \sum_{m=1}^M \sum_{n=1}^N a_{mn}^v \psi_{asym,m}^{(z)} \psi_{asym,n}^{(\theta)} \quad (3.37)$$

where a_{mn}^u , a_{mn}^ϕ and a_{mn}^v are the coefficients u , ϕ and v , whose sizes are $M \times N$, $M \times (N + 1)$ and $M \times N$.

The number of points used in z should be no fewer than the number of basis function used in z . So it requires $M_{pts} \geq M$. Similarly, $N_{pts} \geq N$.

To apply the Galerkin method, first substitute the (truncated) Fourier series into the nonlinear shallow water equations. The resulting ‘‘residual functions’’ are just the Left-Hand Sides (L. H. S.) of (3.11) to (3.13). The residual functions depend on the spectral coefficients $\{a_{mn}^u, a_{mn}^v, a_{mn}^\phi\}$ and the phase speed c . We then demand that the residual should be orthogonal to a set of test functions when integrated over the domain. In ‘‘mean weighted residual’’ methods, the test functions can be very general; Galerkin’s method is the special case in which the test functions are the basis functions. Thus, for Eq. (3.11) and (3.13), the test functions are $\psi_{asym}^{(z)}$ in z and $\psi_{sym}^{(\theta)}$ in θ . For Eq. (3.12) the test functions are $\psi_{sym}^{(z)}$ in z , $\psi_{asym}^{(\theta)}$ in θ ;

The Galerkin residual is

$$r_{1,mn} = \int \int LHS(3.11) \times \psi_{sym,m}^{(z)}(\theta) \times \psi_{asym,n}^{(z)}(z) dzd\theta \quad (3.38)$$

$$r_{2,mn} = \int \int LHS(3.12) \times \psi_{asym,m}^{(\theta)}(\theta) \times \psi_{sym,n}^{(z)}(z) dzd\theta \quad (3.39)$$

$$r_{3,mn} = \int \int LHS(3.13) \times \psi_{sym,m}^{(\theta)}(\theta) \times \psi_{asym,n}^{(z)}(z) dzd\theta \quad (3.40)$$

where $m = 1 \dots M, n = 1 \dots N$. The sizes of \vec{r}_1, \vec{r}_2 and \vec{r}_3 are $M \times N, M \times (N + 1)$ and $M \times N$, so there are in total $3MN + M$ residual elements.

The integrals are numerically approximated using M_{pts} quadrature points in z ,

$$z = \frac{(2i - 1)\pi}{2M_{pts}s}, \quad i = 1, 2, \dots, M_{pts} \quad (3.41)$$

so $z \in (0, \frac{\pi}{s})$, which is also the range of the unmapped coordinate x . We use N_{pts} points in colatitude,

$$\theta = \frac{(2j - 1)}{4N_{pts}}\pi, \quad j = 1, 2 \dots N_{pts} \quad (3.42)$$

Because the integrands are periodic in both z and θ , the trapezoidal rule converges exponentially fast in M_{pts} and N_{pts} except for the corner wave. Because of parity symmetry, the range of the quadrature points may be halved, just like the number of basis functions, in each coordinate. So the span is only half of the one hemisphere.

3.2.3 Newton continuation method

The $3MN + M + 1$ unknowns are the scalar c plus three vectors of lengths $MN, M(N + 1)$ and MN : a^u, a^ϕ and a^v . However, there are only $3MN + M$ values of \vec{r}_1, \vec{r}_2 and \vec{r}_3 . So in addition, we require that value of ϕ at $x = 0$, latitude = 0, or ϕ_{00} for short, is fixed during the iteration. This gives us an additional residual r_4 .

We can reshape the coefficient matrices a^u, a^ϕ and a^v to three vectors. Stacking

these and c together to form a $(3MN + M + 1) \times 1$ vector $\vec{a}_{(3MN+M+1) \times 1}$. Similarly, we can form a vector $\vec{r}_{(3MN+M+1) \times 1}$ from \vec{r}_1 , \vec{r}_2 and \vec{r}_3 and r_4 .

The algebraic system $\vec{r}(\vec{a}) = \vec{0}$ is solved by a Newton/continuation method. The Newton iteration is to iterate the following until the difference between successive iterates is below a (tiny) user-chosen error tolerance:

$$\vec{a}^{(n+1)} = \vec{a}^{(n)} - \vec{J}^{-1}(\vec{r}^{(n)}) \quad (3.43)$$

where \vec{J} is the Jacobian matrix

$$J_{ij} = \frac{\partial r_i}{\partial a_j}, \quad i = 1 \dots 3MN + M + 1, \quad j = 1 \dots 3MN + M + 1. \quad (3.44)$$

and n is the iterative number. Unfortunately, all iterative methods require a “first guess” or “initialization”.

Parameter continuation provides the required first guess. To trace a complete branch of solutions, we march from small amplitude (where the initialization is provided by perturbation theory as in the previous section) to large amplitude while keeping all other parameters fixed. We chose ϕ_{00} , which is the equatorial height at the crest of the wave, $\phi(x = 0, \theta = \pi/2)$, as the amplitude parameter (though other choices are possible). The continuation strategy is to march in small steps of the amplitude parameter. The computed solution for the k -th value of ϕ_{00} is used as the initialization for Newton’s iteration to compute the Fourier coefficients \vec{a} for the $(k + 1)$ -st value of ϕ_{00} .

As the amplitude of Kelvin wave increases, it evolves to the corner wave, so-called because it has a slope discontinuity at the crest *Boyd* (2005b). The branch of traveling waves ends abruptly at the corner wave: there are no solutions for larger amplitude. (Instead, all waves larger than the corner wave break.) The corner wave is a sort of anti-bifurcation point in the sense that no additional branches are born at the corner

wave, but rather the branch simply dies. So when the amplitude is a little greater than that of the corner wave, Newton's iteration will fail.

ϵ	0.01	0.1	0.5	1	3	5	15	30
$s = 1$	0.0007	0.002	0.0005	0.0008	0.007	0.001	0.004	0.009
$s = 2$	0.001	0.002	0.008	0.009	0.004	0.003	0.003	0.007

Table 3.1: Relative coarse-fine differences in the L_∞ norm

3.2.4 Resolution Check

Two different resolutions were used as a self-consistency check. The coarse solutions used $M = 20$ basis functions in longitude, $N = 10$ in latitude with $M_{pts} = 30$ [longitude] and $N_{pts} = 15$ [latitude]. All high resolution computations set $M = 30$, $N = 15$, $M_{pts} = 40$ and $N_{pts} = 20$. The difference between these two results for the corner waves are given in Table 3.1, which catalogues the L_∞ norm of the difference between the coarse and fine grid approximations, divided by ϕ_{00} , for various ϵ and s . We see that coarse resolution gives very decent results: the coarse-fine relative differences are all less than 0.9%.

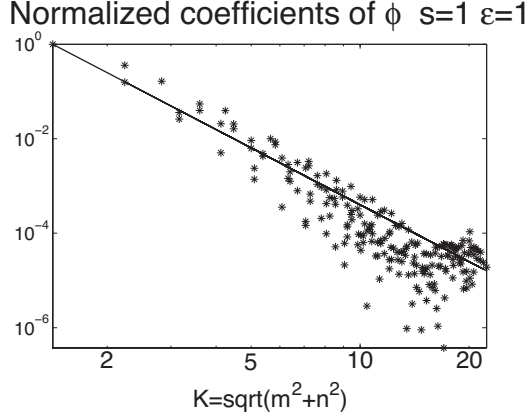


Figure 3.1: Normalized absolute values of Fourier coefficients of ϕ . ϕ is the solution of the corner wave of $s = 1$ and $\epsilon = 1$ case. m and n are coefficient degree in longitudinal and latitudinal directions respectively. The solid line has a slope proportional to K^{-4} , confirming the predicted fourth order rate of convergence when the Kepler change-of-coordinate is used. The rate of convergence is good enough to show that the solution of the corner wave is reliable.

3.3 Spatial Structure of the Corner Wave

We computed steadily-propagating Kelvin waves of $s = 1$ (longitudinal period of 2π) and $s = 2$ (longitudinal period π) for various Lamb's parameter ϵ using the numerical methods described in the previous section.

Figure 3.1 shows the normalized absolute values of Fourier coefficients of ϕ in the corner wave limit. The rate of convergence is about $O(K^{-4})$, where $K = \sqrt{m^2 + n^2}$ is the total degree of the Fourier basis function indexed by m and n . When the amplitude is less than its corner wave limit, the rate of convergence is exponential. At the corner wave limit, the rate slows to $O(K^{-4})$.

It would be helpful if the solution of the discretized partial differential system terminated at the corner wave, but alas, this is not true. The algebraic system has a solution even *beyond* the corner wave limit because the branches of the solution to a *finite* dimensional system of polynomial equations cannot simply stop. Instead, when ϕ_{00} is beyond the corner wave limit, the Fourier coefficients cease to converge so

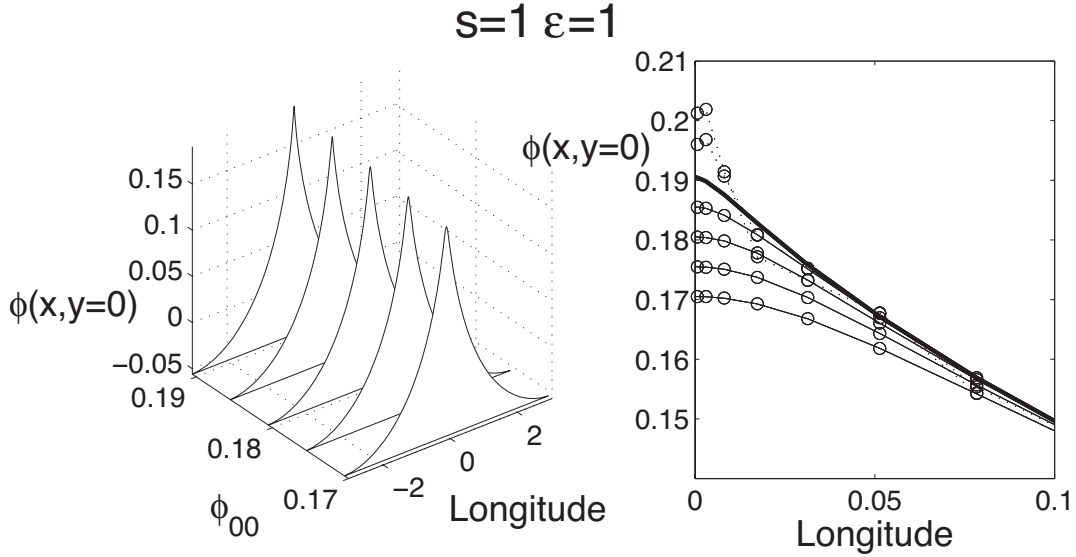


Figure 3.2: Traveling Kelvin wave solutions with $s = 1$ and $\epsilon = 1$. Left: equatorial section of ϕ for $\phi_{00} = 0.1705, 0.1755, 0.1805, 0.1855$ and 0.1905 , respectively. $\phi(x, \theta = \pi/2)$ steepens with the increasing ϕ_{00} . When $\phi_{00} = 0.1905$, $\phi(x, \pi/2)$ is the corner wave, discontinuous in its first derivative at the crest. Right: A zoom in plot of $\phi(x, \pi/2)$ with $\phi_{00} = 0.1755, 0.1805, 0.1855, 0.1905, 0.1955, 0.2005$. The heavy curve is for $\phi_{00} = 0.1905$. Note that this graph includes two values of ϕ_{00} larger than that of the corner wave (dashed); these are unphysical as indicated by their unphysical oscillations near $x = 0$. The interval in longitude is from 0 to 0.1, which is about 1.6% of the total width. (Note that the plot is in the physical longitudinal coordinate x ; the circles on each curve show the points of the grid, which is evenly spaced in z , but very heavily concentrated in x near $x = 0$.) This graph shows that the corner wave is easily distinguished by eye from near-corner waves with a zoom plot.

that the finite-dimensional Galerkin-discretized polynomial system no longer yields a good approximation to the solution of the differential equation, which is a system of infinite dimension. The subtleties of identifying the corner wave are discussed in detail in *Boyd (2006)*. However, we will discuss graphical clues to spurious solutions below.

Figure 3.2 shows traveling Kelvin wave at the equator for $s = 1$ and $\epsilon = 1$ of different amplitude ϕ_{00} . The right figure of Figure 3.2 is a zoom plot of the same five solutions illustrated in the left panel. All five solutions are very close to the corner

$$s=1 \quad \epsilon=1 \quad \phi_{00}=0.1905$$

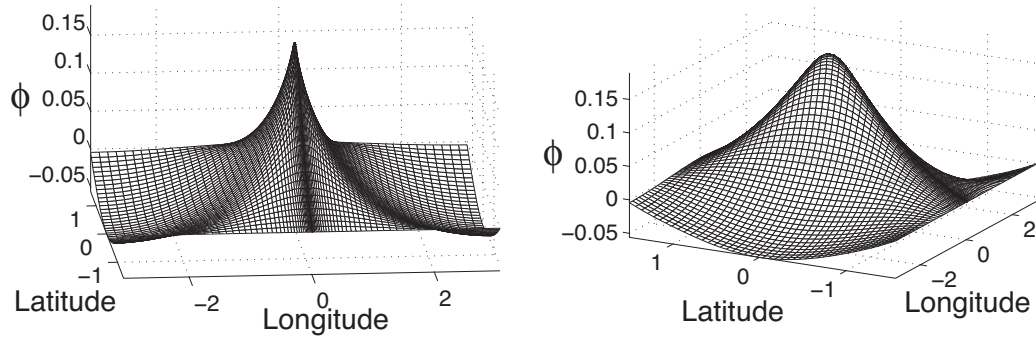


Figure 3.3: ϕ of the corner wave for $s = 1$ and $\epsilon = 1$ on sphere; left and right differ only in viewing angle. The peak value of ϕ_{00} is 0.1905. The comparison shows that only the longitudinal derivative is discontinuous at the peak.

wave, and seem to rise to a corner at $x = 0$ in the left figure. Graphical magnification by plotting the variable on a small x -interval shows that the slope discontinuities are only optical illusions for four of the five: the lower four solid curves have narrow regions of high curvature very close to the origin where these waves flatten out to zero slope at $x = 0$. In contrast, when $\phi_{00} = 0.1905$, the corner wave is almost linear all the way to $x = 0$. Thus, the corner wave is easily distinguished by eye from near-corner waves with a zoom plot *Boyd* (2003). The two dashed curves are physically spurious solutions whose amplitude is larger than that of the corner wave; these are genuine solutions of the system of polynomial equations generated by the Galerkin discretization, but these are not approximations to solutions of the shallow water equations. The coefficients of these spurious solutions converge slowly. These spurious solution vary when the number of basis function changes while the real physical solutions with amplitude smaller than $\phi_{00} = 0.1905$ do not change.

Surface mesh plots ϕ for the corner wave limit are shown in Figure 3.3. One question is: Are *both* components of the gradient of ϕ discontinuous at the peak, or only one? We visually answered this question by plotting ϕ twice from different viewing angles. The left diagram shows that the longitudinal derivative is (at least

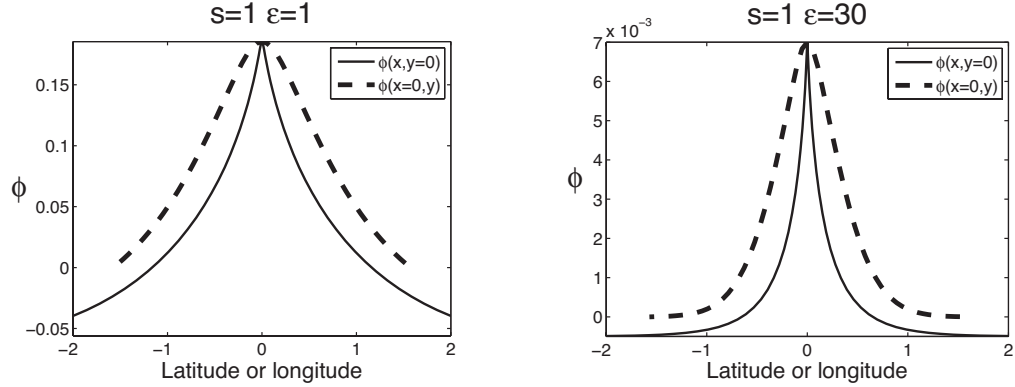


Figure 3.4: Profile of ϕ along the equator (solid) and the profile of ϕ at $x = 0$ as a function of latitude (dashed) for the corner wave for $s = 1$ for two different values of Lamb's parameter. [Left: $\epsilon = 1$. Right: $\epsilon = 30$.] The horizontal axis does doubly duty, being longitude for $\phi(x, \text{latitude} = 0)$ and latitude for $\phi(x = 0, \text{latitude})$. In both panels, the longitudinal derivative (solid) is clearly discontinuous at the crest whereas the north-south derivative shows not the slightest hint of non-smoothness.

visually) discontinuous. However, rotating the viewing angle by roughly a quarter-turn shows only a smooth, rounded crest: the north-south derivative shows no signs of discontinuity.

Figure 3.4 displays line graphs that, for two different values of ϵ , make the same point. In each, the solid curve is a longitudinal cross-section at the equator while the dashed curve shows $\phi(0, y)$. The x -derivative is discontinuous, but the latitudinal derivative is smooth.

Just as for infinitesimal amplitude Kelvin waves, u of the corner wave is graphically indistinguishable from ϕ and so is not plotted. The first derivative of the northward velocity v is everywhere continuous, so v is not plotted.

Figure 3.5 compares $\phi(x, y = 0)$, normalized by dividing by ϕ_{00} , for many different ϵ . As ϵ increases, the corner wave becomes narrower and narrower in longitude. This trend is also evident by comparing the left and right panels of Fig. 3.4. Dispersion and the height of the corner wave both diminish rapidly as ϵ increases; it is remarkable that the corner wave becomes narrower, more focused in longitude, in this same limit.

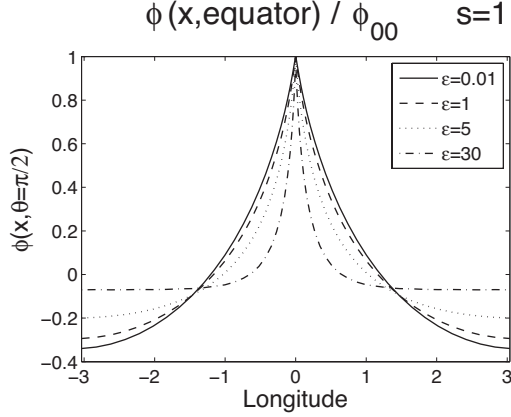


Figure 3.5: Normalized $\phi(x, \theta = \pi/2)$ [longitudinal section at the equator] of the corner wave solution of $s = 1$ and $\epsilon = 0.01, 1, 5, 30$. The profiles of $\phi(x, \theta = \pi/2)$ are scaled by their corresponding maxima, ϕ_{00} . The shape of ϕ at the equator becomes narrower and narrower as ϵ increases.

The latitudinal width, not shown, becomes narrower and narrower as captured by the equatorial beta-plane approximation, $\phi(x, \theta) \sim A(x) \exp(-\sqrt{\epsilon}(\theta - \pi/2)^2)$. However, the latitudinal width is controlled by *linear* dynamics whereas the longitudinal focusing is caused entirely by *nonlinearity*: when the amplitude is much smaller than the corner wave, the longitudinal structure of the Kelvin mode is approximately $\cos(s\lambda)$.

Another interesting question is how far does the slope discontinuity extend from the equator to the poles? To answer this question, we calculated $d\phi/dx$. Figure 3.6 shows ϕ_x at several latitudes, shown on the full longitudinal range at left and as a zoom plot on the right. A finite spectral series must always impose a truncation-dependent smoothing on a discontinuity. Even so, it is clear the slope rapidly diminishes away from the equator. It seems likely that the Kelvin wave is discontinuous only at the equator.

The graphs for $s = 2$ were so similar to those for $s = 1$ that they are omitted. However, the maximum equatorial height $\phi_{00}(\epsilon)$ and phase speed $c(\epsilon)$ for the corner wave are discussed for both $s = 1$ and $s = 2$ in the next section.

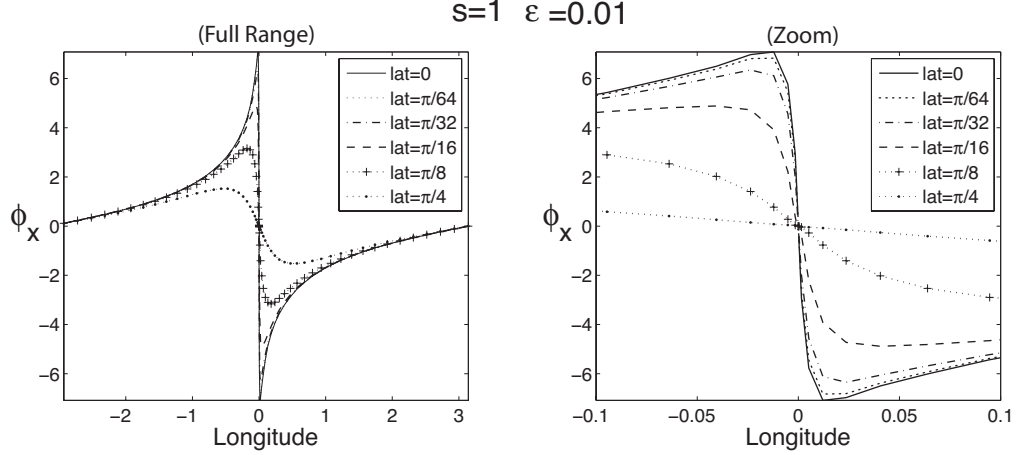


Figure 3.6: The derivative of ϕ of the corner wave solution of $s = 1$ and $\epsilon = 0.01$ case with respect to the longitude x . Left: ϕ_x at latitudes $0, \frac{\pi}{64}, \frac{\pi}{32}, \frac{\pi}{16}, \frac{\pi}{8}, \frac{\pi}{4}$, plotted on the full global domain. Right: same, but a zoom plot with a much smaller range.

ϵ	0.01	0.1	0.5	1	3	5	15	30
Phase speed c	1.4327	1.3792	1.3008	1.2551	1.1758	1.141	1.082	1.0572
ϕ_{00}	3.5	0.95	0.32	0.19	0.074	0.045	0.0145	0.0071
$(c^2 - 1)/(3\sqrt{\epsilon})$	3.5088	0.9510	0.3262	0.1918	0.0736	0.0450	0.0147	0.0072
$h_{00} \equiv \phi_{00}\sqrt{\epsilon}$	0.3500	0.3004	0.2263	0.1900	0.1282	0.1006	0.0562	0.0389

Table 3.2: Parameters in the corner wave limit for $s=1$ case

3.4 Variations of Phase Speed and Corner Height

The parameters of the corner wave for different ϵ are summarized in Table 3.2 [$s = 1$] and Table 3.3 [zonal wavenumber two]. From the table, we can see both ϕ_{00} and phase speed c decrease as ϵ increases. This is as expected: because the dispersion due to the earth's sphericity decreases rapidly with ϵ (as known from Longuet-Higgins' large ϵ asymptotic expansion of the linear phase speed), it is plausible that nonlinearity will overwhelm dispersion, giving breaking instead of traveling waves, at lower and lower values of the wave amplitude ϕ_{00} as $\epsilon \rightarrow \infty$.

ϵ	0.01	0.1	0.5	1	3	5	15	30
Phase speed	1.2349	1.2169	1.1883	1.1698	1.1327	1.1135	1.0739	1.0537
ϕ_{00}	1.75	0.5	0.192	0.12	0.053	0.036	0.0129	0.0067
$(c^2 - 1)/(3\sqrt{\epsilon})$	1.7499	0.5069	0.1942	0.1228	0.0545	0.0358	0.0132	0.0067
$h_{00} \equiv \phi_{00}\sqrt{\epsilon}$	0.1750	0.1581	0.1358	0.1200	0.0918	0.0805	0.0500	0.0367

Table 3.3: Parameters in the corner wave limit for s=2 case

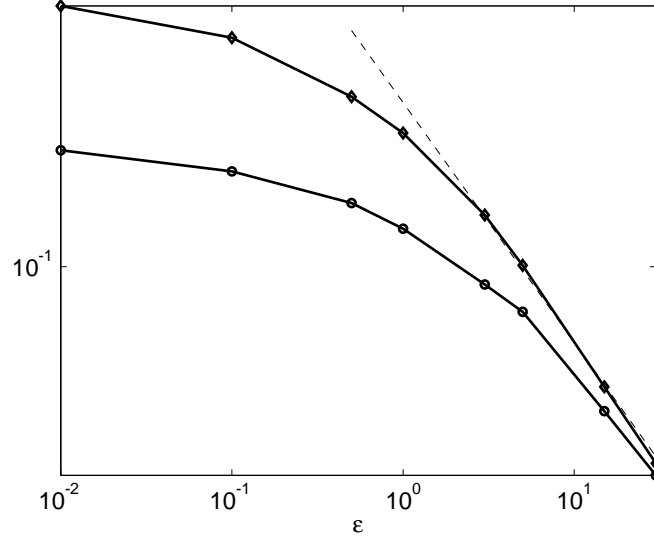


Figure 3.7: h_{00} of the corner waves of different ϵ for $s = 1$ [upper thick curve with diamonds] and $s = 2$ [lower thick curve with circles]. The dashed line on this log-log plot shows that h_{00} decays asymptotically proportional to $1/\sqrt{\epsilon}$ as $\epsilon \rightarrow \infty$.

The tables also list the quantity

$$h_{00} \equiv \sqrt{\epsilon} \phi_{00} \tag{3.45}$$

This gives the maximum perturbative height of the Kelvin corner wave relative to the mean depth H , that is, the maximum perturbative height is $h_{00} H$ in meters. We have listed this quantity because it decreases more slowly with increasing ϵ than does ϕ_{00} itself.

Fig. 7 compares the equatorial height of the corner wave versus ϵ for both $s = 1$

and $s = 2$. The results are very similar for the two wavenumbers. As ϵ increases, the dispersion due to the sphericity of the earth decays very rapidly. Consequently, the height h_{00} of the corner wave diminishes very rapidly, too. On a log-log plot, a power law asymptotes to a straight line; the dashed guideline here suggests that $h_{00} \approx 0.2/\sqrt{\epsilon}$ for both wavenumbers one and two. The graph suggests that the corner wave maximum height is independent of zonal wavenumber s in the equatorial beta-plane limit that $\epsilon \rightarrow \infty$.

The tables also show an interesting empirical relationship between the phase speed and maximum height of the corner wave:

$$\phi_{00} \approx \frac{c^2 - 1}{3\sqrt{\epsilon}} \quad (3.46)$$

By matching discontinuities in the x -derivatives of u and ϕ , we can derive the diagnostic relationship $(c - u_{00}\sqrt{\epsilon})^2 = 1 + h_{00}$ at the crest of the corner wave. (We thank a reviewer for suggesting this.) Unfortunately, it is not possible to extend this further: the rest of our study is based on perturbation series and computations.

3.5 Limitations of Theory

This chapter is a comprehensive study of the full parameter space for flow without mean currents, clouds or vertical propagation, aimed at illuminating the reality that Kelvin waves sometimes break and sometimes don't and have something-or-other as a boundary between these two regimes as seen in numerical models that do include mean flow. We have resisted making comparisons between our results and observations because of the limitations of our theory. Equatorially-trapped Kelvin waves are strongly affected by the strong mean currents in the tropical ocean: the alternating jets known as the South Equatorial Current, North Equatorial Current, North Equatorial Counter-Current, and the Equatorial Undercurrent. We have shown here that

the dispersion created by the earth's sphericity weakens and weakens as ϵ increases. For the large values of ϵ relevant to the tropical ocean, as catalogued in Table 1.1, spherical effects will be overwhelmed by the much stronger dispersion induced by these alternating jets.

This is hard within the shallow water model because of critical latitude effects *Boyd and Christidis* (1982); *Natarov and Boyd* (2001), which are known to weakly destabilize the Kelvin waves. The Equatorial Undercurrent, which has strong vertical shear and (as its name implies) does not extend to the surface, can only be incorporated into a three space-dimensional model, a task orders-of-magnitude more difficult than the two-dimensional travelling wave models considered here.

Mean flow, though not negligible in the troposphere, is relatively less important to atmospheric Kelvin waves than oceanic because the rather small values of ϵ relevant to the atmosphere imply much stronger dispersion due to the earth's sphericity. However, tropospheric Kelvin waves are both excited by cumulus convection and simultaneously organize and transport this convection. Parameterizing cumulus convection in general circulation models is still a major research frontier.

Another difficulty in atmospheric theory is that the air is not a vertically-confined layer like the sea, but rather a semi-infinite layer with free vertical propagation. This is a serious technical complication because as the atmospheric density decreases with height, the amplitude of vertically-propagating waves must increase. Eventually, all inviscid, vertically-propagating waves must break. The breaking of tropospheric gravity waves is a major source of damping for larger scale motions in the middle atmosphere. Kelvin waves are also dissipated by rather strong radiative damping in the mesosphere. Thus, there is competition between growth (due to decreasing density) and decay (due to damping). Water waves experience a similar energy growth when propagating into water of decreasing depth. (Similarly, ocean equatorial Kelvin waves propagate through variable depth because of the deepening of the main thermocline

to the west in the Pacific Ocean *Long and Chang* (1990).) *Grimshaw* (1970, 1971, 1979) showed that the soliton slowly adjusts to the changing depth while shedding a shelf to conserve total mass and energy. Thirty-seven years later, he and his collaborators have progressed to a model with both a gradual slope and dissipation (El Ga, Grimshaw and Kamchatnov (2007)); however, a two-dimensional model without Coriolis force is much simpler than the shallow water equations on a rotating sphere, and parameterized gravity wave breaking and radiative dissipation are more complicated than the Chezy bottom friction of their article.

Mean currents strongly modulate the propagation of Kelvin waves. Indeed, this is the heart of the Lindzen-Holton theory of the Quasi-Biennial Oscillation (QBO) in the tropical lower stratosphere (Andrews *et al.*, 1987): Kelvin and Yanai waves in turn force the mean flow to reverse sign, but the QBO strongly modulates the upward penetration of both wave species so that they switch roles with each QBO cycle. Existing theories use parameterizations of wave-breaking and other drastic simplifications; the length scales are so short that it is only recently that General Circulation Models (GCMs), metaphorically the supercomputer-hogging aircraft carriers of climate research, have been able to even crudely capture the QBO. Kelvin waves also are a major driving force in the Semiannual Wind Oscillation in the tropical upper stratosphere and are in turn controlled by the ever-changing mean current *Boyd* (1978b,c). There is thus a large gap between the idealizations of our computations and the real ocean and atmosphere, but this is not uncommon in geophysical fluid dynamics (e. g., Lorenz and Krishnamurthy, 1987, Boyd 1994, 1995).

3.6 Summary and Conclusions

The computations confirm the results of simplified models and equatorial beta-plane computations: the traveling waves of the Kelvin mode terminate in a corner wave of finite height. The amplitude of the corner wave diminishes very rapidly with

ϵ when the mean flow is neglected. In the real ocean or atmosphere, our results for large ϵ are quantitatively suspect because the very weak dispersion due to spherical geometry would likely be overwhelmed by the stronger dispersion due to the mean zonal currents.

As ϵ increases, the longitudinal profile of the corner wave becomes very narrow whereas the corner waves for small ϵ span the whole equator.

In two space dimensions, slope discontinuities may take the form of a *cone* (with discontinuities in both x and y derivatives at the peak), a *crease* with a *curve* or *line* of discontinuous slope extending away from the equator into both hemispheres, or a *point* singularity in which only one derivative is discontinuous, and that only at a single point. All previous studies of corner waves have been limited to one horizontal dimension and therefore furnish no guidance. Although it is impossible to prove theorems through inexact numerical computations, our graphs strongly suggest that the third possibility is true of the Kelvin corner wave: the height and velocity fields are singular only at the peak, and only through a discontinuity in the direction of propagation, longitude.

Although we performed detailed computations only for zonal wavenumbers $s = 1$ and $s = 2$, there was so little qualitative difference that it appears that these conclusions are independent of zonal wavenumber s at least for small s . As illustrated in *Boyd and Zhou* (2008b), Kelvin waves of moderate and large s are *equatorially-trapped*. Therefore, short Kelvin waves are well-described by the equatorial beta-plane theory and computations in *Boyd* (1998, 2006).

Our computations cannot exclude the possibility that there may be nonlinear Kelvin branches which are not contiguous with small-amplitude, linear Kelvin waves. This is not a difficulty peculiar to Kelvin waves, but rather is a generic worry when computing the roots of any system of nonlinear algebraic or transcendental equations, whether resulting from the discretization of traveling waves or not; the peril of the

“missed solution branch” is ubiquitous. However, no such additional branches have been detected in numerous initial-value experiments: all Kelvin modes bigger than the corresponding corner wave break.

CHAPTER IV

Kelvin Waves in the Presence of a Jet on the Equatorial β -plane

In this chapter, we extend our calculation of nonlinear traveling Kelvin waves to the equatorial beta-plane in the presence of a jet. As mentioned in the first chapter, such nonlinear traveling wave solutions do not exist on the equatorial beta-plane due to the lack of dispersive mean flow terms. By adding a background jet, we introduce the necessary dispersion terms.

4.1 Model

4.1.1 The equatorial beta-plane approximation

Near the equator, the approximations

$$\sin\varphi \approx \varphi, \cos\varphi \approx 1 \tag{4.1}$$

can be used where φ is latitude. This is called “the equatorial beta-plane approximation”. Half of the earth lies at latitude less than 30° and the maximum percentage error of this approximation within $[30^\circ S, 30^\circ N]$ is only 14% (*Gill*, 1982). In this approximation, the Coriolis parameter f is given by

$$f = \beta y \tag{4.2}$$

where y is the distance northward from the equator. And β is given by

$$\beta = 2\Omega/r = 2.3 \times 10^{-11} m^{-1} s^{-1} \quad (4.3)$$

4.1.2 Nonlinear Shallow Water Equations on the Equatorial β -Plane

Applying the equatorial beta-plane approximation, the nonlinear dimensional shallow-water equations over a flat bottom can be written as

$$u_t + uu_x + vu_y - y\beta v + gh_x = 0 \quad (4.4)$$

$$v_t + uv_x + vv_y + y\beta u + gh_y = 0 \quad (4.5)$$

$$h_t + uh_x + vh_y + h(u_x + v_y) = 0 \quad (4.6)$$

where u and v are the eastward and northward velocities, h is the total depth, g is the gravitational constant, and β is Rossby parameter at the equator. This is also called the ‘one-and-a-half-layer’ model because it describes a two-layer fluid in the hydrostatic approximation when the lower layer is infinitely deep. This model is also widely used to describe the baroclinic modes in both atmospheric and oceanic dynamics when h is the equivalent depth of these modes.

It is convenient to nondimensionalize using

$$L = \sqrt{\frac{c}{\beta}} \text{ (Horizontal length scale)} \quad (4.7)$$

$$T = \sqrt{\frac{1}{c\beta}} \text{ (Time scale)} \quad (4.8)$$

$$H = H_0 \text{ (Vertical length scale)} \quad (4.9)$$

where $c = \sqrt{gH_0}$.

Then the dimensionless variables are

$$u' = \frac{1}{L/T}u, v' = \frac{1}{L/T}v, h' = \frac{1}{H}h, x' = \frac{1}{L}x, y' = \frac{1}{L}y, t' = \frac{1}{T}t \quad (4.10)$$

The same length and time scales are commonly employed in equatorial oceanography.

By writing h' as $h' = 1 + \phi$ and omitting the tildes of dimensionless variables, we get the nondimensionalized equations,

$$u_t + uu_x + vu_y - yv + \phi_x = 0 \quad (4.11)$$

$$v_t + uv_x + vv_y + yu + \phi_y = 0 \quad (4.12)$$

$$\phi_t + u\phi_x + v\phi_y + (1 + \phi)(u_x + v_y) = 0 \quad (4.13)$$

We then shift the zonal coordinate so that it moves with the wave we are interested in. The wave will appear stationary in the new coordinate system. Suppose the wave has a wave speed of c in the original coordinate system of x , y and t . Now we introduce new coordinate system of \tilde{x} , \tilde{y} and \tilde{t} , where $\tilde{x} = x - ct$, $\tilde{y} = y$ and $\tilde{t} = t$. Then the derivative operators in the original coordinate become

$$\frac{\partial}{\partial t})_{x,y,t} \rightarrow \frac{\partial}{\partial \tilde{t}})_{\tilde{x},\tilde{y},\tilde{t}} - c \frac{\partial}{\partial \tilde{x}})_{\tilde{x},\tilde{y},\tilde{t}} \quad (4.14)$$

$$\frac{\partial}{\partial x})_{x,y,t} \rightarrow \frac{\partial}{\partial \tilde{x}})_{\tilde{x},\tilde{y},\tilde{t}} \quad (4.15)$$

$$\frac{\partial}{\partial y})_{x,y,t} \rightarrow \frac{\partial}{\partial \tilde{y}})_{\tilde{x},\tilde{y},\tilde{t}} \quad (4.16)$$

in the new coordinate system. The subscripts denote which coordinate system is used. Since the wave with a phase speed of c in the original coordinate appears stationary in the new coordinate system, we can simply drop the derivatives with respect to \tilde{t} .

So

$$\left(\frac{\partial}{\partial t}\right)_{x,y,t} \rightarrow -c \left(\frac{\partial}{\partial \tilde{x}}\right)_{\tilde{x},\tilde{y},\tilde{t}} \quad (4.17)$$

$$(4.18)$$

Further, we write u and ϕ as $u = \bar{U} + u_a$, $\phi = \bar{\Phi} + \phi_a$ where $\bar{\Phi}$ is the zonal mean of ϕ , $\bar{\Phi}$ and \bar{U} satisfy the geostrophic balance, $\bar{U} = -\frac{1}{y}\bar{\Phi}_y$. ϕ_a and u_a are the ageostrophic parts. By omitting the accents of \tilde{x} , \tilde{y} and \tilde{t} and the subscripts of ϕ_a and u_a , equations 4.11 to 4.13 become

$$(\bar{U} - c)u_x + v\bar{U}_y - yv + \phi_x + \delta(uu_x + vv_y) = 0 \quad (4.19)$$

$$(\bar{U} - c)v_x + yu + \phi_y + \delta(uv_x + vv_y) = 0 \quad (4.20)$$

$$(\bar{U} - c)\phi_x + v\bar{\Phi}_y + (1 + \bar{\Phi})(u_x + v_y) + \delta\{u\phi_x + v\phi_y + \phi(u_x + v_y)\} = 0 \quad (4.21)$$

δ is a flag parameter, which is equal to either 0 or 1. When $\delta = 0$, the equations are linearized. All possible modes existing with the background mean can be obtained by solving this set of linearized equations as a linearized eigenvalue problem with c as the eigenvalue. The details about how to solve the linearized eigenvalue value problem are given in Appendix A (the eigenvalue in Appendix A is phase speed ω or kc instead of c ; k is the wavenumber).

When $\delta = 1$, the equations are fully nonlinear. Nonlinear traveling wave solution can be obtained through a combination of mapping/Galerkin method/Newton continuation method.

4.1.3 The background jet

The zonal mean $\bar{\Phi}$ has the form of $\frac{U_0}{6}e^{-3y^2}$, and $\bar{U}=U_0e^{-3y^2}$. So the jet is symmetric with respect to the equator. A similar jet profile has been used by *McPhaden and Knox* (1979) and *Philander* (1979) in their linear Kelvin wave analyses. In the equatorial ocean, the vertical displacement associated with waves tends to be greatest near the thermocline. So of the system of currents in the equatorial region, the Equatorial Undercurrent(EUC) should affect Kelvin wave because its strongest flow is located near the thermocline. So an eastward jet profile used here crudely mimics the profile of the EUC. And in the atmosphere, a westward jet crudely mimics the profile of the easterly jet. The accurate profile is not necessary since our study is highly conceptual and the gross characteristics of the results of this study are not sensitive to the detailed profiles.

In the equatorial ocean, unit dimensionless U_0 equals about 2.0 m/s in dimensional unit for the 1st baroclinic mode with an equivalent depth $H_0 \sim 0.4 m$; in the atmosphere, unit dimensionless U_0 equals to about 20 m/s in dimensional unit for the 1st baroclinic mode with an equivalent depth $H_0 \sim 40 m$.

One thing to note is that for nonlinear traveling waves, the zonal mean of the ageostrophic part of zonal velocity is not necessarily 0. In equation 4.19, nonlinear terms, uv_x and vv_y will produce nonzero zonal means which must be balanced by either yu or ϕ_y . Since we prescribe the zonal mean $\bar{\Phi}$, the zonal mean of ϕ as well as ϕ_y must be zero. So the zonal mean of u has to be nonzero. However, the zonal mean of u is relatively small comparing with \bar{U} . For example, for the corner Kelvin wave with $U_0 = -0.5$ and $k = 1$, the amplitude of the zonal mean of u is only $\sim 1\%$ of that of \bar{U} . Thus the final total zonal mean of $(\bar{U} + u_a)$ differs slightly from \bar{U} .

4.1.4 Mapping in longitude and latitude

4.1.4.1 Mapping in latitude

On the equatorial β -plane, $y \in (-\infty, \infty)$ for mathematical convenience even though the β -plane approximation is only valid when y is not too far from the equator¹. Numerically speaking, evenly spaced grids in y would be a poor choice since most wave activity is concentrated near the equator due to the equatorial wave guide effect. To improve the resolution in y direction we change the coordinate from y to ζ via $\zeta = \tanh(y/L)$ where L is a user-choosable parameter. When L is smaller, more discretization points will be concentrated near $y = 0$. A value of 1.5 will be used for L in the following sections if not otherwise specified. The range of the new coordinate ζ is from $[-1,1]$.

4.1.4.2 Kepler mapping in longitude

Mapping in longitude is not necessary when the wave amplitude is small. However, when the wave amplitude is close to the corner wave limit, the change of coordinate with Kepler mapping becomes crucial. By transforming the longitudinal coordinate from x to a new stretched coordinate z , we can improve the Fourier rate of convergence from second order to fourth order in the degree of the coefficients. The “Kepler mapping”, so named because inverting the transformation requires solving the Kepler equation of celestial mechanics, concentrates high resolution near the discontinuous corner at $x = 0$ while preserving the periodic behavior in longitude (Boyd, 2006). We apply the numerical method to waves of different longitudinal periods $2\pi/k$ where k is the zonal wavenumber of the lowest nonzero longitudinal Fourier

¹In the absence of mean currents, the linearized wave equations have eigenmodes whose latitudinal factors are parabolic cylinder functions. When $y \in (-\infty, \infty)$, the parabolic cylinder functions simplify to Hermite functions. Because Hermite functions are the product of $\exp(-y^2/2)$ with a polynomial, they are much more treatable than parabolic cylinder functions.

component. The form of Kepler mapping has a slightly different form for different k :

$$x = z - \frac{\sin(kz)}{k} \quad (4.22)$$

$$\frac{\partial}{\partial x} \rightarrow \frac{1}{1 - \cos(kz)} \frac{\partial}{\partial z} \quad (4.23)$$

The mapping preserves spatial periodicity and $x = z$ at $z = n\pi/k, n = 0, \pm 1, \pm 2, \dots$

4.1.5 Galerkin method

The Galerkin method for discretizing a differential equation demands that when the truncated Fourier series for each unknown is substituted into the shallow water equations to obtain the so-called “residual” function, the leading terms of the Fourier series of the residual are zero. These constraints are obtained by evaluating the integral inner product of the basis functions with the residual function and demanding that this integral should be zero or equivalently, that each basis function is orthogonal to the residual function. The number of orthogonality conditions is equal to the number of undetermined coefficients in the Fourier series for the unknowns, thus deriving a consistent set of nonlinear algebraic equations for the Fourier coefficients of u , v and ϕ . A full discussion is given in *Boyd (2001)*.

To reduce the number of unknowns by a factor of four, we assume that u and ϕ are symmetric about the equator and $x = 0$, and v is antisymmetric about the equator $x = 0$. (Our success in computing solutions with the assumed symmetries is an *a posteriori* justification for these assumptions.) The domain of waves of wavenumber k within one wavelength is $[-\pi/k, \pi/k]$ in longitude and $[-1, 1]$ in latitude. But by employing the periodicity and parities of the Kelvin wave, we can halve the domain in both longitude and latitude. So we only need to calculate the unknowns in the region of $[0, \pi/k]$ in x or z and $[0, 1]$ in ζ .

Also by employing the parities of the unknowns, we can halve the number of basis

functions used in both directions. In z , the basis functions of u and ϕ are

$$\psi_{sym,0}^{(z)} = 1$$

$$\psi_{sym,1}^{(z)} = \cos(kz) + \frac{1}{2} \quad (4.24)$$

$$\psi_{sym,m}^{(z)} = \cos(kmz), \quad m = 2, 3, \dots M \quad (4.25)$$

where the constant $\psi_{sym,0}^{(z)}$ is used only for u and the basis functions of v are

$$\psi_{asym,m}^{(z)} = \sin(kmz), \quad m = 1, 2, \dots M \quad (4.26)$$

The additive factor of $(1/2)$ in $\psi_{sym,1}^{(z)}$ ensures that all basis functions with $m > 0$ *individually* have a zero longitudinal mean, despite the change of coordinate from longitude to the Kepler coordinate z ; note that $\int_0^\pi \cos(kz(x))dx = -\pi/2$, (Boyd, 2006).

In latitude, we use the Chebyshev polynomials as the basis. $T_n(\zeta)$ is a polynomial of degree n . It may be calculated directly via the three-term recurrence relation, but a more efficient definition is

$$T_n(\zeta) = \cos(nt) \quad (4.27)$$

$$t = \arccos(\zeta) \leftrightarrow \zeta = \cos(t) \quad (4.28)$$

This further changes the coordinate from ζ to t . The range of t for the full domain is $[-\pi, \pi]$. As the wave activities vanish far away from the equator, we can define the spectral basis functions to be linear combinations of the Chebyshev polynomials which each vanish at $t = \pm\pi$. The basis functions of u and ϕ are

$$\psi_{sym,n}^{(t)} = \cos(2nt) - 1, \quad n = 1, 2, \dots N \quad (4.29)$$

and the basis functions of v are

$$\psi_{asym,n}^{(t)} = \cos((2n + 1)t) - \cos(t), \quad n = 1, 2, \dots, N \quad (4.30)$$

These basis functions match the latitudinal parities of u , v and ϕ . Finally, we expand u , ϕ and v as

$$u = \sum_{m=0}^M \sum_{n=1}^N a_{mn}^u \psi_{sym,m}^{(z)} \psi_{sym,n}^{(\theta)} \quad (4.31)$$

$$\phi = \sum_{m=1}^M \sum_{n=1}^N a_{mn}^\phi \psi_{sym,m}^{(z)} \psi_{sym,n}^{(\theta)} \quad (4.32)$$

$$v = \sum_{m=1}^M \sum_{n=1}^N a_{mn}^v \psi_{asym,m}^{(z)} \psi_{asym,n}^{(\theta)} \quad (4.33)$$

where a_{mn}^u , a_{mn}^ϕ and a_{mn}^v are the coefficients u , ϕ and v , whose sizes are $M \times (N + 1)$, $M \times N$, and $M \times N$.

The number of points used in z should be no fewer than the number of basis function used in z . So it requires $M_{pts} \geq M$. Similarly, $N_{pts} \geq N$.

To apply the Galerkin method, first substitute the (truncated) Fourier series into the nonlinear shallow water equations. The resulting ‘‘residual functions’’ are just the Left-Hand Sides (L. H. S.) of (4.19) to (4.21). The residual functions depend on the spectral coefficients $\{a_{mn}^u, a_{mn}^v, a_{mn}^\phi\}$ and the phase speed c . We then demand that the residual should be orthogonal to a set of test functions when integrated over the domain. In ‘‘mean weighted residual’’ methods, the test functions can be very general; Galerkin’s method is the special case in which the test functions are the basis functions. Thus, for Eq. (4.19) and (4.21), the test functions are $\psi_{asym}^{(z)}$ in z and $\psi_{sym}^{(t)}$ in t . For Eq. (4.20) the test functions are $\psi_{sym}^{(z)}$ in z , $\psi_{asym}^{(t)}$ in t ;

The Galerkin residual is

$$r_{1,mn} = \int \int LHS(4.19) \times \psi_{sym,m}^{(z)}(\theta) \times \psi_{asym,n}^{(z)}(z) dzd\theta \quad (4.34)$$

$$r_{2,mn} = \int \int LHS(4.20) \times \psi_{asym,m}^{(\theta)}(\theta) \times \psi_{sym,n}^{(z)}(z) dzd\theta \quad (4.35)$$

$$r_{3,mn} = \int \int LHS(4.21) \times \psi_{sym,m}^{(\theta)}(\theta) \times \psi_{asym,n}^{(z)}(z) dzd\theta \quad (4.36)$$

where $n = 1 \dots N$ for all three equations, $m = 1 \dots M$ for 4.34 and 4.36, and $m = 0 \dots M$ for 4.35. The sizes of \vec{r}_1 , \vec{r}_2 and \vec{r}_3 are $M \times N$, $M \times (N + 1)$ and $M \times N$, so there are in total $3MN + M$ residual elements.

The integrals are numerically approximated using M_{pts} quadrature points in z ,

$$z = \frac{(2i - 1)\pi}{2M_{pts}k}, \quad i = 1, 2, \dots, M_{pts} \quad (4.37)$$

so $z \in (0, \frac{\pi}{k})$, which is also the range of the unmapped coordinate x . We use N_{pts} points in colatitude,

$$t = \frac{(2j - 1)}{4N_{pts}}\pi, \quad j = 1, 2 \dots N_{pts} \quad (4.38)$$

Because the integrands are periodic in both z and t , the trapezoidal rule converges exponentially fast in M_{pts} and N_{pts} except for the corner wave. Because of parity symmetry, the range of the quadrature points may be halved, just like the number of basis functions, in each coordinate. As required by Galerkin method, $M_{pts} \geq M$, $N_{pts} \geq N$, we use $M = N = 50$ and $M_{pts} = N_{pts} = 150$.

4.1.6 Newton continuation method

The $3MN + M + 1$ unknowns are the scalar c plus three vectors of lengths MN , $M(N + 1)$ and MN : a^u , a^ϕ and a^v . However, there are only $3MN + M$ values of \vec{r}_1 , \vec{r}_2 and \vec{r}_3 . So in addition, we require that value of ϕ at $x = 0$, latitude = 0, or ϕ_{00} for

short, is fixed during the iteration. This gives us an additional residual r_4 .

We can reshape the coefficient matrices a^u, a^ϕ and a^v to three vectors. Stacking these and c together to form a $(3MN + M + 1) \times 1$ vector $\vec{a}_{(3MN+M+1) \times 1}$. Similarly, we can form a vector $\vec{r}_{(3MN+M+1) \times 1}$ from \vec{r}_1, \vec{r}_2 and \vec{r}_3 and r_4 .

The algebraic system $\vec{r}(\vec{a}) = \vec{0}$ is solved by a Newton/continuation method. The Newton iteration is to iterate the following until the difference between successive iterates is below a (tiny) user-chosen error tolerance:

$$\vec{a}^{(n+1)} = \vec{a}^{(n)} - \vec{J}^{-1}(\vec{r}^{(n)}) \quad (4.39)$$

where \vec{J} is the Jacobian matrix

$$J_{ij} = \frac{\partial r_i}{\partial a_j}, \quad i = 1 \dots 3MN + M + 1, \quad j = 1 \dots 3MN + M + 1. \quad (4.40)$$

and n is the iterative number. Unfortunately, all iterative methods require a “first guess” or “initialization”.

Parameter continuation provides the required first guess. To trace a complete branch of solutions, we march from small amplitude (where the initialization is provided by linearized Kelvin waves as in Appendix A) to large amplitude while keeping all other parameters fixed. We chose ϕ_{00} , which is the equatorial height at the crest of the wave, $\phi(x = 0, t = \pi/2)$, as the amplitude parameter (though other choices are possible). The continuation strategy is to march in small steps of the amplitude parameter. The computed solution for the k -th value of ϕ_{00} is used as the initialization for Newton’s iteration to compute the Fourier coefficients \vec{a} for the $(k + 1)$ -st value of ϕ_{00} .

For a westward jet, as the amplitude of Kelvin wave increases, it evolves to the corner wave, so-called because it has a slope discontinuity at the crest (*Boyd, 2005b; Boyd and Zhou, 2008a*). The branch of traveling waves ends abruptly at the corner

wave: there are no solutions for larger amplitude. (Instead, all waves larger than the corner wave break.) The corner wave is a sort of anti-bifurcation point in the sense that no additional branches are born at the corner wave, but rather the branch simply dies. So when the amplitude is a little greater than that of the corner wave, Newton's iteration will fail.

For an eastward jet, when the amplitude of Kelvin wave increases, the branch resonates with waves of some higher wavenumbers and it loses its identity as the Kelvin wave of wavenumber k . The resonance with waves of higher wavenumbers makes the Galerkin method fail as the required number of basis function increases rapidly with amplitude and make the numerical calculation formidable.

4.2 Modified linear Kelvin waves in the presence of a jet

4.2.1 Wave structure

The infinitesimal Kelvin wave with a resting background has the simple solution: $u = \phi = e^{-y^2/2}\cos(kx)$, $v = 0$, $c = 1$ for all different wavenumber k . However, in the presence of a jet, both the structures and phase speeds of the modified linear Kelvin waves differ significantly from this simple solution for different U_0 and wavenumber k . Details about how to obtain the normal modes in the presence of a jet are given in Appendix A.

Figure 4.1 shows the modified Kelvin waves of wavenumber $k = 1, 4$ with a westward jet ($U_0 = -0.25$) and an eastward jet ($U_0 = 0.25$). The gross characteristics of these modified Kelvin waves, except for the one with $k = 4$ and $U_0 = 0.25$, still resemble the Kelvin waves with a resting background. The most obvious difference is that v is no longer zero and has opposite directions when the direction of the jet is opposite. For the case of $k = 4$ and $U_0 = 0.25$, ϕ has two maximums off the equator instead of one at the equator which makes it visually different from the Kelvin wave linearized about state of rest. More quantitative details are given in Figure 4.2 and 4.3.

These modified Kelvin waves have the solutions in the form of $\phi = \tilde{\phi}(y)\cos(kx + \theta)$, $u = \tilde{u}(y)\cos(kx + \theta)$, and $v = \tilde{v}(y)\sin(kx + \theta)$ where θ is an arbitrary constant phase. $\tilde{\phi}(y)$ and $\tilde{u}(y)$ are symmetric with respect to the equator and $\tilde{v}(y)$ is antisymmetric with respect to the equator. Results of $\tilde{\phi}(y)$, $\tilde{u}(y)$ and $\tilde{v}(y)$ on the north hemisphere for various U_0 and wavenumber k are given in Figure 4.2 and 4.3. $\tilde{\phi}(y)$, $\tilde{u}(y)$ and $\tilde{v}(y)$ have been divided by the maximum value of $\tilde{u}(y)$. The simple solution of $\tilde{\phi}(y)$ and $\tilde{u}(y)$ when the background is at rest, $e^{-y^2/2}$, and the profile of the jet are also shown in the graphs.

The modified Kelvin waves have very different responses to the direction of the

jet. For the westward jet shown in Figure 4.2, 1) $\tilde{\phi}(y)$ always has only one maximum at the equator while $\tilde{u}(y)$ tends to develop two maxima off the equator as the strength of the jet increases or k decreases; 2) the wave narrows as the wavelength shortens and resides inside the jet for large k (e.g,4). However, for the eastward jet shown in Figure 4.3, 1) both $\tilde{\phi}(y)$ and $\tilde{u}(y)$ could develop two maxima off the equator as the strength of the jet increases or the wavenumber increases; 2) the wave gradually moves away from the equator as the wavelength shortens and almost resides outside the jet for large k (e.g,4). The appearance of two ϕ centers off the equator for large k makes them substantially different from the traditional Kelvin wave concept and look more like inertial gravity waves. We still call them modified Kelvin waves since they are the continuation of the Kelvin mode as we increase k gradually. One common phenomenon for either westward or eastward jets is that $\tilde{v}(y)$ increases when either the strength of the jet or k increases.

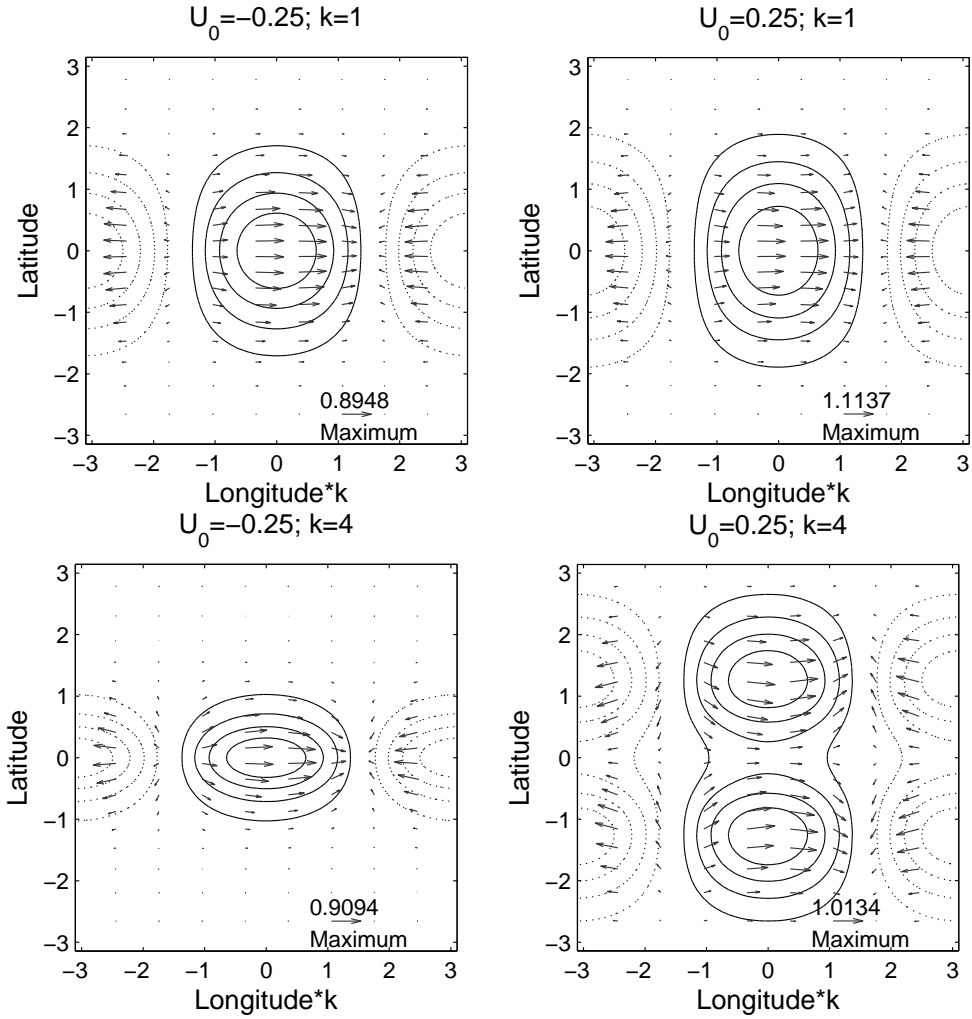


Figure 4.1: Surface height ϕ (contours) and $u-v$ velocity fields (vectors) of the modified linear Kelvin waves with $k = 1, 4$ and $U_0 = \pm 0.25$. Values of ϕ, u, v have been normalized by $\phi(x=0, y=0)$. Solid contour lines are positive ϕ with a contour interval of 0.2 units. Dotted lines are negative ϕ and the zero contour is omitted. The maximum velocity vectors in each panel are specified in the bottom right corner. The x axis is the product of the nondimensionalized longitude and the wavenumber k .

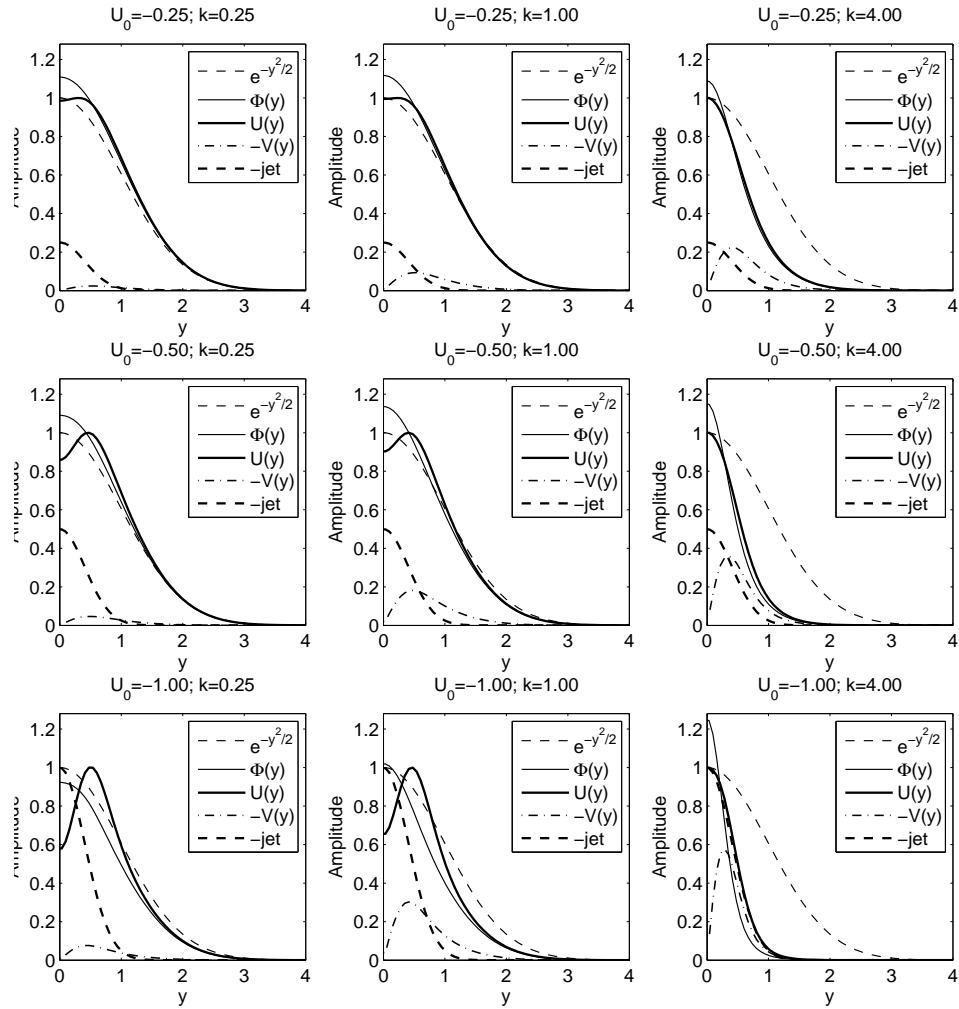


Figure 4.2: Eigenfunctions corresponding to the modified Kelvin waves in the presence of a westward jet for $U_0 = -0.25$ (top panel), $U_0 = -0.5$ (middle panel) and $U_0 = -1.0$ (bottom panel), $k = 0.25$ (left column), and for $k = 1$ (middle column), $k = 4$ (right column).

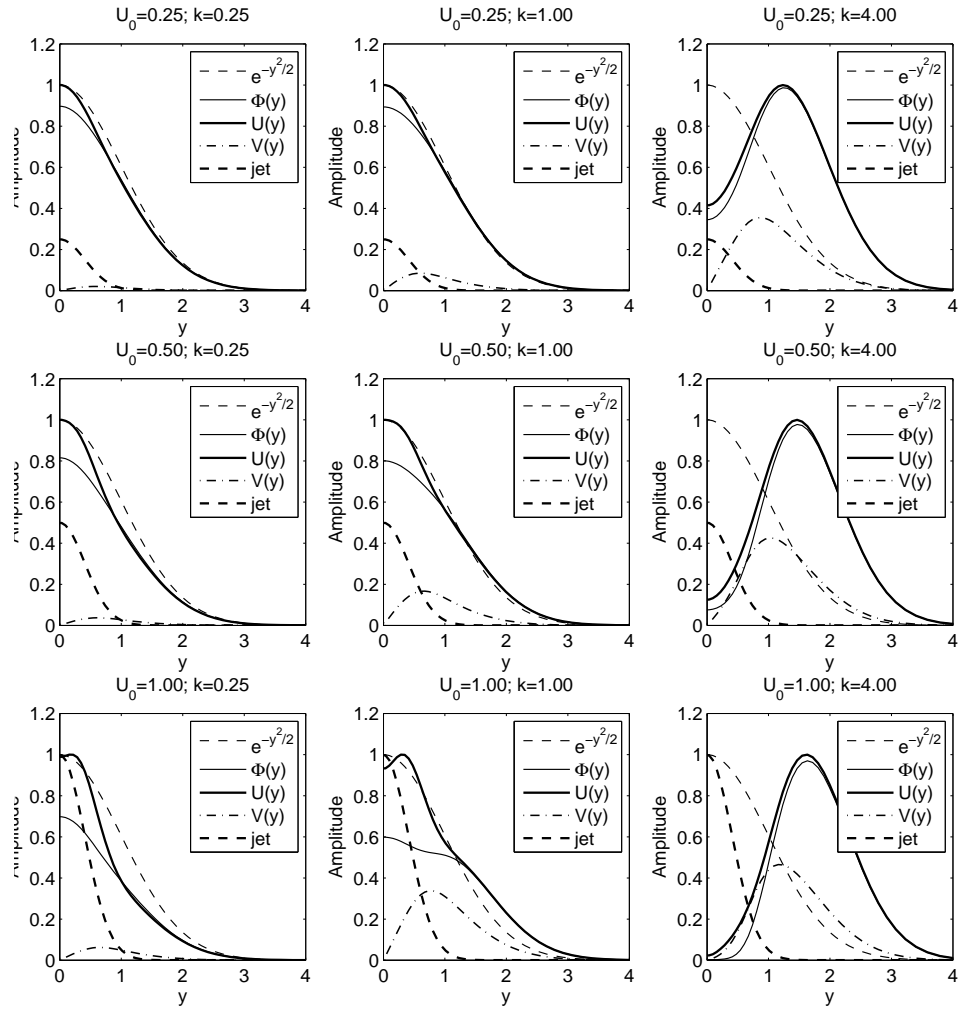


Figure 4.3: Eigenfunctions corresponding to the modified Kelvin waves in the presence of a eastward jet for $U_0 = 0.25$ (top panel), $U_0 = 0.5$ (middle panel) and $U_0 = 1.0$ (bottom panel), $k = 0.1$ (left column), and for $k = 1$ (middle column), $k = 4$ (right column).

4.2.2 Phase speed

Figure 4.4 shows how the phase speeds vary as the U_0 and k changes. Despite the opposite responses of the wave structures to the direction of the jet when k increases, the phase speeds share the same trend that for both eastward and westward jets; short Kelvin waves always travel slower to the east than long ones for the same U_0 . The reason is that for the eastward jet, short Kelvin waves shift their centers outside of the jet, thus the background advection to the east is reduced; while for the westward jet, short Kelvin waves are more concentrated inside the jet, thus the background advection to the west is enhanced.

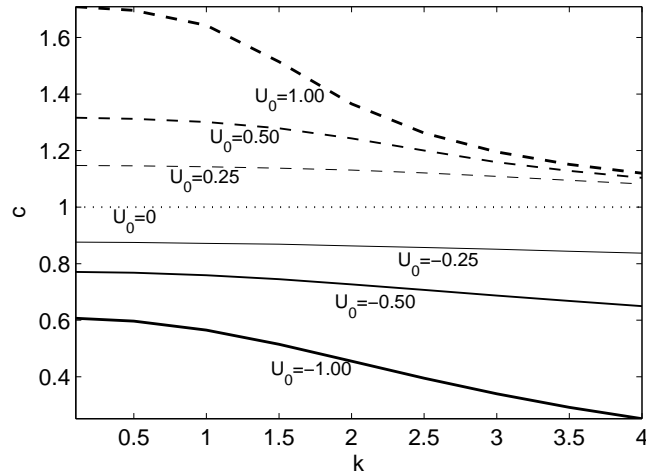


Figure 4.4: Phase speeds of free Kelvin modes for various wavenumber k and U_0

4.3 Nonlinear Traveling Kelvin waves

We use 50 basis functions in both latitude and longitude. For each U_0 , Newtonian iteration/continuation starts from small value of ϕ_{00} (the value of ϕ at $x=0, y=0$) using the modified linear Kelvin waves described in previous section as the initial guess and gradually marches to larger ϕ_{00} until the Newtonian iteration fails to converge either due to the singularity of the corner waves or resonance with waves with higher wavenumber k .

4.3.1 Results of westward jets

4.3.1.1 Spatial structure

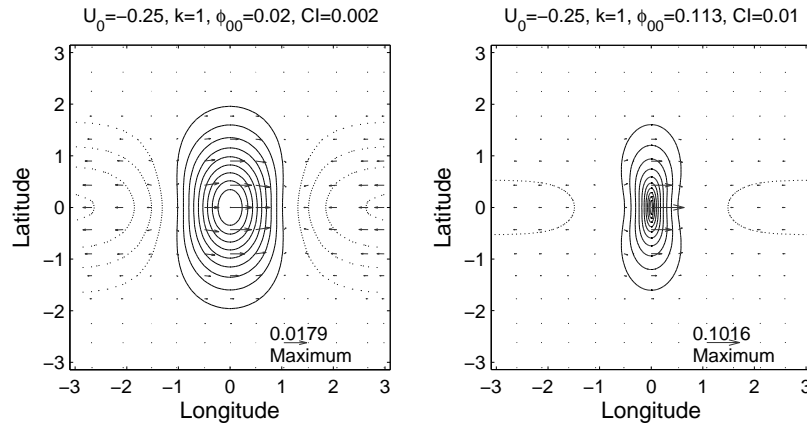


Figure 4.5: Surface height ϕ (contours) and $u - v$ velocity fields (vectors) of the nonlinear traveling Kelvin waves with amplitude $\phi_{00}=0.02$ (left) and 0.113 (right) for $k = 1$ and $U_0 = -0.25$. When $\phi_{00}=0.113$, it is the corner wave. Solid contour lines are positive ϕ . Dotted lines are negative ϕ and the zero contour is omitted. Contour intervals are 0.002 for left graph and 0.01 for the right graph. The maximum velocity vectors in each panel are specified in the bottom right corner.

Figure 4.5 gives the nonlinear traveling Kelvin waves of two different amplitudes, $\phi_{00}=0.02$ and 0.113 where ϕ_{00} is the value of the surface height ϕ at $x = 0, y = 0$.

Comparing with the linear Kelvin wave with the same U_0 and k in Figure 4.1, the change in longitude is obvious. Unlike sinusoidal waves, they have smaller area of positive ϕ and larger area of negative ϕ which makes them more isolated, even spike-like for large amplitudes.

Figure 4.6 shows how the equatorial sections of ϕ , u and v along $y = 1$ evolve as the wave amplitude increases. When ϕ_{00} is small, $\phi(x, y = 0)$ and $u(x, y = 0)$ look like sinusoidal waves. As ϕ_{00} increases, they steepen and become more isolated pulse-like oscillations, and eventually evolve to sharp corner shapes when $\phi_{00} = 0.113$. The corner wave limit is easily determined in a zoom in plot of either $\phi(x, y = 0)$ or $u(x, y = 0)$. At the the corner wave limit with $\phi_{00} = 0.113$, $\phi(x, y = 0)$ shows a clear corner even though the range of the x axis is only about 0.25% of the total one wavelength. $\phi(x, y = 0)$ becomes smooth rapidly as ϕ_{00} drops below the corner wave limit. Above the corner wave limit, a spurious unphysical solution is obtained. We would be happy if the solution of the discretized partial differential system terminated at the corner wave. However, the algebraic system has a solution even ‘beyond’ the corner wave limit because the branching of the solution in a ‘finite’ dimensional system of polynomial equations cannot simply stop. Instead, when ϕ_{00} is beyond the corner wave limit, the Fourier coefficients cease to converge to a solution of the differential equation, so that the finite-dimensional Galerkin-discretized polynomial system no longer yields a good approximation of the solution of the differential equation (Boyd (2006)). Longitudinal sections of v also steepen as ϕ_{00} increases. However, these are everywhere smooth at the corner limit.

Another interesting question is how far the slope discontinuity of the ϕ or u in x direction extends from the equator. To answer this question, we show longitudinal sections of both ϕ and its first derivatives in longitude along different latitudes in Figure 4.7. While $\phi(x, y = 0)$ clearly shows a corner like shape at $x = 0$, $\phi(x, y = 0.006)$ has already become very smooth. One may argue that the tip of $\phi(x, y = 0)$ is

also smooth, not discontinuous. This is because a finite spectral series must always impose a truncation-dependent smoothing on a discontinuity. From ϕ_x , we see a shock like jump at the equator. A little farther away from the equator, the slope rapidly diminishes. It seems likely that the Kelvin wave is discontinuous only at the equator.

In latitude, the Kelvin waves also steepen as the amplitude increase. Figure 4.8 shows how the normalized latitudinal sections of ϕ along $x = 0$ steepen from the linear case to the corner wave case. But $\phi(x = 0, y)$ does not show any slope discontinuity in latitude at the corner wave limit.

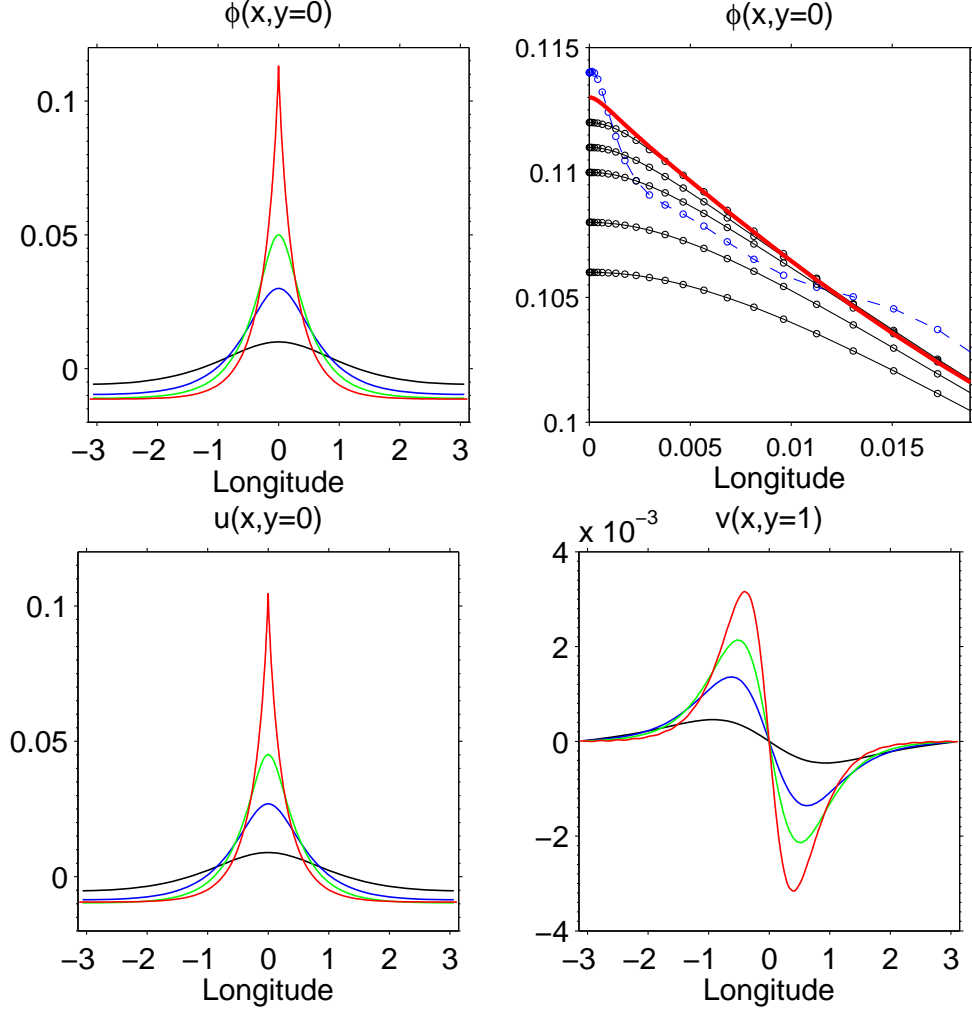


Figure 4.6: Traveling Kelvin wave solutions with $U_0 = -0.25$ and $k=1$. (Upper left) Equatorial section of ϕ for $\phi_{00}=0.01, 0.03, 0.05,$ and 0.113 , respectively; $\phi(x, y = 0)$ steepens with the increasing ϕ_{00} . When $\phi_{00}=0.113$, $\phi(x, y = 0)$ is the corner wave, discontinuous in its first derivative at the crest. (Upper right) A zoom in plot of $\phi(x, y = 0)$ with $\phi_{00}=0.106, 0.108, 0.11, 0.111, 0.112, 0.113, 0.114$. The heavy curve is for $\phi_{00}=0.113$. Note that this graph includes one dotted curve with the value of ϕ_{00} (0.114) larger than that of the corner wave; this is unphysical as indicated by its unphysical oscillations near $x=0$. The interval in longitude is from 0 to 0.016, which is about 0.25% of the total one wavelength. (Note that the plot is in the physical longitudinal coordinate x ; the circles on each curve show the points of the grid, which is evenly spaced in z but very heavily concentrated in x near $x=0$.) This graph shows that the corner wave is easily distinguished by the eye from near-corner waves in a zoom in plot. (Lower left) Equatorial section of u for $\phi_{00}=0.01, 0.03, 0.05,$ and 0.113 , respectively. $u(x, y = 0)$ exhibits the same behavior as $\phi(x, y = 0)$ and is also discontinuous for $\phi_{00}=0.113$. (Lower right) v along $y = 1$ for $\phi_{00}=0.01, 0.03, 0.05,$ and 0.113 , respectively. $v(x, y = 1)$ is continuous for all ϕ_{00} .

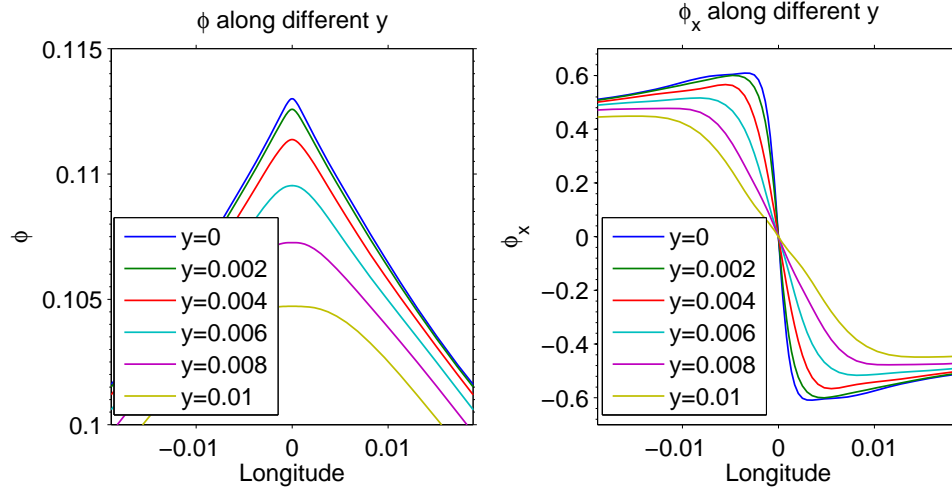


Figure 4.7: Longitudinal sections of ϕ (left) and ϕ_x (right) along different latitudes at the corner wave limit for $U_0 = -0.25$ and $k = 1$.

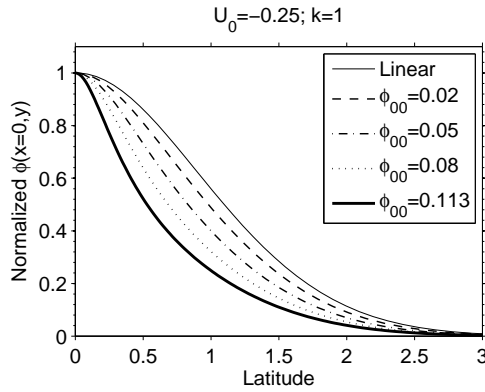


Figure 4.8: Latitudinal sections of ϕ along $x=0$ divided by ϕ_{00} of the modified linear Kelvin wave and nonlinear traveling Kelvin waves for $\phi_{00}=0.02, 0.05, 0.08,$ and 0.113 with $U_0 = -0.25$ and $k=1$. $\phi(x = 0, y)$ steepens with the increasing ϕ_{00} . At the corner wave limit when $\phi_{00}=0.113$, $\phi(x = 0, y)$ is still continuous in latitude.

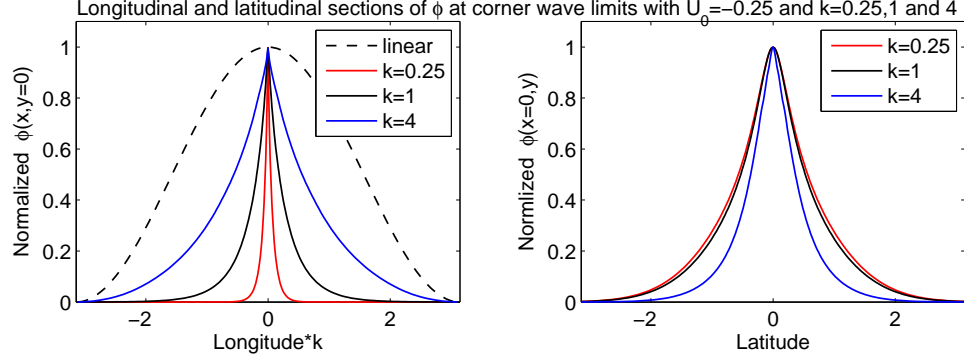


Figure 4.9: (left) Longitudinal sections of ϕ , $\phi(x, y = 0)$, at the corner wave limit along the equator with $U_0 = -0.25$ and $k = 0.25, 1$ and 4 . The x axis is the product of longitude and the wavenumber k . $\phi(x, y = 0)$ has been normalized in a way such that the base is 0 and tip is 1. The dashed line is the normalized $\cos(x)$. (right) Latitudinal sections of ϕ , $\phi(x = 0, y)$, at the corner wave limit along $x = 0$ with $U_0 = -0.25$ and $k = 0.25, 1$ and 4 . $\phi(x = 0, y)$ has been normalized by ϕ_{00} .

Figure 4.9 gives the normalized $\phi(x, y = 0)$ and $\phi(x = 0, y)$ of the corner waves with $U_0 = -0.25$ and $k = 0.25, 1$ and 4 . The x axis of the left graph is the product of the longitude and wavenumber k . So the range of one wavelength is $[-\pi, \pi]$ for all different k . The amplitudes, ϕ_{00} , of the corner waves are 0.118, 0.113 and 0.080 for $k = 0.25, 1$ and 4 . Initially, the normalized $\phi(x, y = 0)$ of the linear Kelvin waves with different k all have the same shape as the dashed line. But when they reach their corner wave limits, they differ substantially. The change of the shape of ϕ in longitude due to the nonlinearity is much larger for the long wave than for the short wave. For $k = 0.25$, the normalized $\phi(x, y = 0)$ narrows from the dashed line of the linear wave to the red line of the corner wave. The corner wave in this case is much more isolated in longitude and becomes more like a soliton. While for $k = 4$, the normalized $\phi(x, y = 0)$ only narrows from the dashed line to blue line. In latitude, $\phi(x = 0, y)$ of all different k are all narrower than their linear cases. The changes for different k are roughly equal.

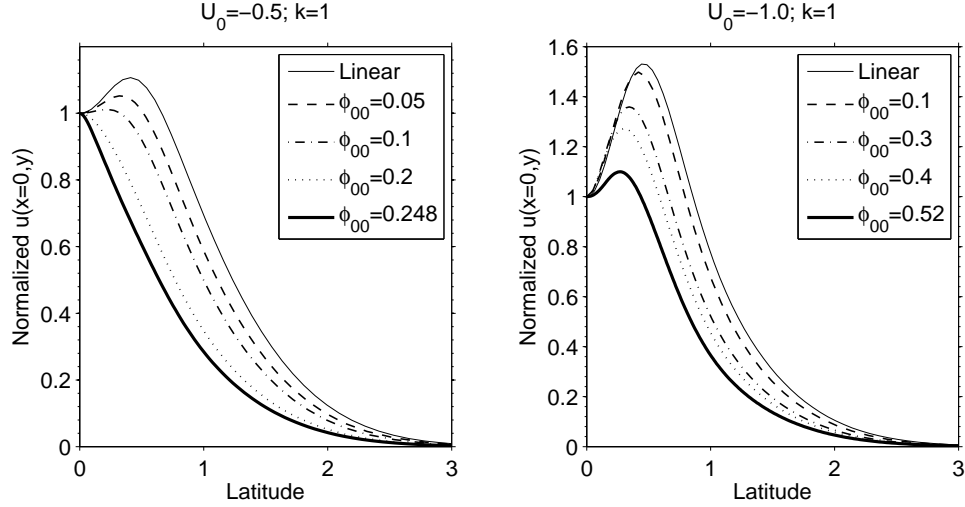


Figure 4.10: Latitudinal sections of u along $x=0$ divided by $u(x = 0, y = 0)$ for $U_0 = -0.5$ (left) and $U_0 = -1.0$ (right) and $k=1$. The curves correspond to normalized $u(x = 0, y)$ of the modified linear Kelvin wave(thin solid line) to the corner Kelvin wave(thick solid line) from right to left.

As we increase the strength of the westward jet from $U_0 = -0.25$ to $U_0 = -1.0$, the behavior of ϕ and u in longitude when the wave amplitude ϕ_{00} increases does not change. They just steepen until corners form. In latitude, ϕ also narrows and is still continuous. The extra complication comes from u . From the linear analysis we see that ϕ just narrows in latitude as the strength of the jet increases. However, u gradually develops two maxima off the equator. Figure 4.10 shows the normalized latitudinal sections of u along $x = 0$. For $U_0 = -0.5$, $u(x = 0, y)$ narrows as the ϕ_{00} increases. As u increases faster on the equator than at the areas off the equator, eventually the two maxima are reduced to only one maximum on the equator. However, for $U_0 = -1.0$, even though $u(x = 0, y)$ also narrows as the ϕ_{00} increases, two maxima remain off the equator since the initial maxima off the equator are much larger than u on the equator.

4.3.1.2 Amplitude and phase speed

	Linear wave speed	Corner wave speed	Corner wave amplitude ϕ_{00}
$U_0 = -0.25; k = 0.25$	0.875	0.900	0.118
$U_0 = -0.25; k = 1$	0.872	0.890	0.113
$U_0 = -0.25; k = 4$	0.837	0.846	0.080
$U_0 = -0.50; k = 1$	0.759	0.795	0.248
$U_0 = -1.00; k = 1$	0.565	0.645	0.520

Table 4.1: Phase speeds of modified linear Kelvin waves, phase speeds and ϕ_{00} of nonlinear traveling Kelvin waves at corner wave limits for various U_0 and wavenumber k .

Table 4.1 summarizes the phase speeds and amplitudes of linear and corner waves for various U_0 and k . The corner wave amplitude, ϕ_{00} , is largely determined by the amplitude of U_0 . This makes sense since these steadily traveling corner waves are the results of balance between the dispersion and nonlinearity. For example, the dispersive terms in equation 4.13 have the same order as $\bar{U}\phi_x$ and the nonlinear terms have the same order as $u\phi_x$ or ϕu_x . We could expect the ϕ of the corner wave is proportional to the amplitude of \bar{U} . For the same U_0 , short corner waves have smaller amplitudes and this is consistent with the results of corner Kelvin waves found on the sphere by *Boyd and Zhou* (2008a). The corner wave speeds are larger than the linear phase speed. However, the absolute increase are not substantial (all less than 0.1) and they are also highly related to U_0 or ϕ_{00} . For $U_0 = -0.25$ and $k = 1$, the increase is only 0.018, about 2% of 0.872. And for $U_0 = -1.0$, the increase is 0.08, about 14% of 0.565. Another factor to consider is, for these westward jets the corner waves are narrower in latitude than their linear waves; thus the advection to the west is larger for the corner waves. So the increase of the phase speed due to nonlinearity alone should be a little bit larger than the present increase.

4.3.2 Results of eastward jets

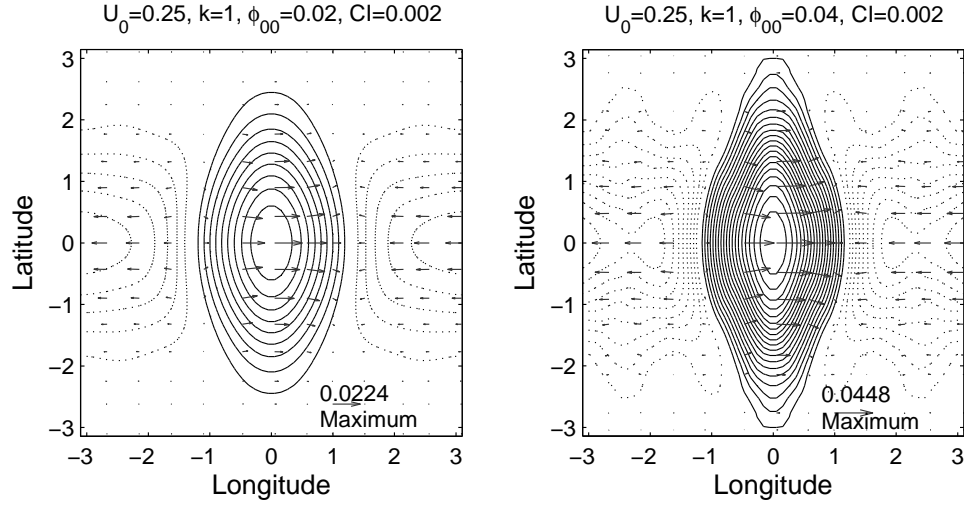


Figure 4.11: Surface height ϕ (contours) and $u - v$ velocity fields (vectors) of the nonlinear traveling Kelvin waves with amplitude $\phi_{00}=0.02$ (left) and 0.04 (right) for $k = 1$ and $U_0 = 0.25$. Solid contour lines are positive ϕ . Dotted lines are negative ϕ and the zero contour is omitted. Contour interval is 0.002 . The maximum velocity vectors in each panel are specified in the bottom right corner.

Figure 4.11 gives the nonlinear traveling Kelvin waves of two different amplitudes, $\phi_{00}=0.02$ and 0.04 for an eastward jet $U_0 = 0.25$. Compared to the linear Kelvin wave with the same U_0 and k in Figure 4.1, just like the nonlinear traveling Kelvin waves with a westward jet, they also steepen in longitude as the wave amplitude increases. But in latitude, they expand as the wave amplitude increases. Figure 4.12 shows how $\phi(x = 0, y)$ expands in latitude with the increasing ϕ_{00} . The phase speed is also increased from 1.147 of the linear case to 1.153 of the nonlinear traveling wave with $\phi_{00}=0.04$.

Our calculation of the traveling wave stops at $\phi_{00}=0.04$. One can easily notice the high wavenumber oscillations in the ϕ field (also in u and v) in Figure 4.11 (right) as the wave amplitude ϕ_{00} increases from 0.02 to 0.04 . As explained in *Boyd (2007)*, calculation of nonlinear traveling waves by discretizing the appropriate partial differ-

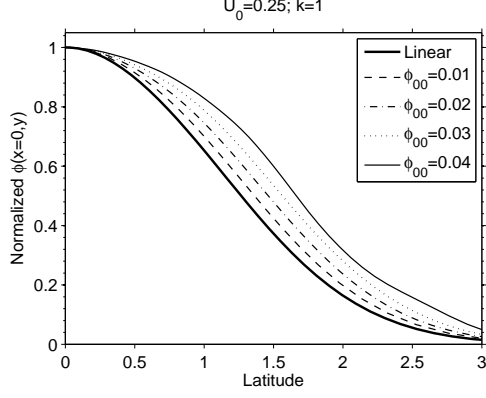


Figure 4.12: Latitudinal sections of ϕ along $x=0$ divided by ϕ_{00} of the modified linear Kelvin wave and nonlinear traveling Kelvin waves for $\phi_{00}=0.01, 0.02, 0.03,$ and 0.04 with $U_0 = 0.25$ and $k = 1$. Unlike the westward jets' cases, $\phi(x = 0, y)$ expands in latitude with the increasing ϕ_{00} .

ential equations and then employing Newtonian iteration/continuation can encounter a bunch of difficulties. The most relevant one here is resonance and mode-switching bifurcation. Because of the coincidence of phase speeds resonance, a solution could evolve from one mode to another mode as the amplitude increases. The traveling wave with $\phi_{00}=0.02$ does not show any high wavenumber oscillation in any field of ϕ, u and v . But at $\phi_{00}=0.04$, high wavenumber oscillations show up. We tested different resolutions, basis functions and mapping techniques and the solution of $\phi_{00}=0.04$ does not change. This suggests that until $\phi_{00}=0.04$, the calculation is stable and a solution does evolve gradually. But beyond $\phi_{00}=0.04$, the calculation fails to converge as even higher wavenumber oscillations appear. Figure 4.13 shows the phase speeds of the modified linear Kelvin waves and first 3 odd n symmetric eastward inertial gravity waves (EIGW) for $U_0=-0.25$ (left) and $U_0=0.25$ (right). We do not have to worry about the odd n antisymmetric EIGW modes since we already applied the symmetry when choosing the basis functions for u, v and ϕ . For the westward jet $U_0=-0.25$, there is no coincidence of phase speed between the Kelvin waves and the EIGW and we successfully track a solution until the corner wave limit. For the eastward jet $U_0=0.25$, such coincidence “resonance” exists. The Kelvin wave can resonate with

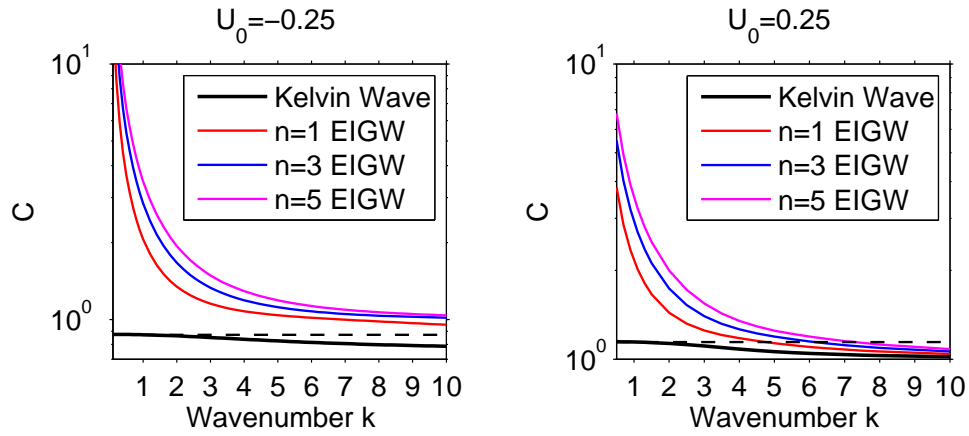


Figure 4.13: Phase speeds of the modified linear Kelvin waves and first 3 symmetric eastward inertial gravity waves (EIGW) for $U_0 = -0.25$ (left) and $U_0 = 0.25$ (right). The horizontal dashed horizontal line is a guide line showing the phase speed of the Kelvin wave with $k = 1$.

other high wavenumber EIGW modes (including $n > 3$ EIGW modes) which cause the calculation to fail.

4.4 Conclusion and Discussion

We show that the Kelvin waves linearized about jets, have much more complicated structures than the Kelvin wave with a resting background. For westward jets, the wave narrows in latitude as the wavenumber k increases; for eastward jets, they tend to shift away from the equator as k increases. As a result, phase speeds decrease as wavenumber increases regardless of whether the jet is eastward or westward.

For sufficiently small amplitude, there are nonlinear Kelvin traveling waves (cnoidal waves). As the amplitude increases, the waves narrow in longitude just like the traveling Kelvin wave on sphere *Boyd and Zhou (2008a)*. Even though we were not able to deduce a KdV equation from the shallow-water equation because of the complexity in the presence of a jet, these steadily translating Kelvin waves exhibit the property of solitary waves of the KdV equation. For the westward jets, the traveling waves terminate in a so-called corner wave with a discontinuous first derivative. All waves larger than the corner wave evolve to fronts and break. The singularity is a point singularity in which only the longitudinal derivative is discontinuous, which is the same as the singularity of corner Kelvin waves on the sphere without mean currents. For an eastward jet, calculation of nonlinear Kelvin waves with large amplitude is numerically impossible due to the resonance with waves of higher wavenumbers.

In latitude, the waves narrow for a westward jet but widen for an eastward jet as ϕ_{00} increases. A similar phenomenon has been reported by *Choi (2003)* in long solitary surface gravity waves of finite amplitude in uniform shear flow. The solitary wave in uniform shear flow is wider when propagating upstream (opposite to the direction of surface drift), while it is narrower when propagating downstream. In our case, this opposite reaction in latitude could largely be explained through the linear dynamics. In the linear analysis, we show that for the westward jets, the waves narrow in latitude as the wavenumber k increases while for the eastward jets, the waves shift away from the equator as k increases. So, for example, if we decompose the $k = 1$ nonlinear

Kelvin waves into the set of the linearized eigenmodes, the dominant eigenmode will be the $k = 1$ modified linear Kelvin wave. The rest will project onto the higher k Kelvin modes plus other possible Rossby and inertial gravity modes. However, the higher k Kelvin mode should dominate.

Phase speeds also increase to the east as the amplitude increases. However, the phase speeds are largely determined by the linear Kelvin wave dynamics, the increment is relatively small. In *Boyd and Zhou (2008a)*, we derived the first correction to the phase speed due to the amplitude of nonlinear Kelvin waves on sphere is second order in amplitude. We did not derive the equivalent expression here due to the mathematical difficulty when a jet is involved, but we would expect similar results. As the amplitude of the nonlinear Kelvin waves are generally less than 1 in nondimensionalized units, the correction is relatively small.

CHAPTER V

Nonlinear Shallow Water Tropical Instability Waves on the Equatorial β -plane: Genesis of Two Distinct Types of Waves

In this chapter, we will focus on the TIWs arising from the barotropic instability and investigate how the nonlinearity changes their strength, periods, etc. Especially, we explain how the two distinct types of waves with different propagating speeds arise. We then evaluate the effect of external forcings on these two types of waves.

5.1 Model

The nonlinear shallow-water equations over a flat bottom on equatorial beta plane are

$$u_t + uu_x + vu_y - y\beta v + gh_x = 0 \quad (5.1)$$

$$v_t + uv_x + vv_y + y\beta u + gh_y = 0 \quad (5.2)$$

$$h_t + uh_x + vh_y + h(u_x + v_y) = 0 \quad (5.3)$$

where u and v are the eastward and northward velocities, h is the total depth, g is the gravitational constant, and β is Rossby parameter at the equator. This is also called the ‘one-and-a-half-layer’ model because it describes two-layer fluid in the hydrostatic approximation when the lower layer is infinitely deep. In this study results are not

sensitive to a realistic range of h in the equatorial ocean from 0.2 m to 0.8 m. A value of 0.5 m, approximately equal to the equivalent depth of the 1st baroclinic mode, is used. Numerical schemes follow *Boyd* (1998). The spatial derivatives in both latitude and longitude are approximated by centered eighth-order differences. For the temporal derivatives, we use the 4th order Runge-Kutta for the first two steps since it is self starting and the 3rd order Adams-Bashforth after. 6th order dissipation is used with a hyperviscosity coefficient chosen in a way such that the e -folding time of the shortest $2\Delta x$ wave is 0.1 day. The domain size is $[20^\circ S, 20^\circ N]$ in latitude, and 300° in longitude. In latitude, due to the equatorial wave guide effect, there is no substantial wave activity on north and south boundaries. So we simply keep using the initial values on these boundaries during the integration. In longitude, we first used heavy damping near the boundaries, so-called “sponge layers” by simply multiplying the deviation of u, v and h from the initial zonal mean with an coefficient which is zero at the boundary but exponentially growing to one only 3° inside the boundary. Since the domain in longitude is large and the initial disturbance is very small, the late developed wave additivity is highly periodic in the central region of the domain except at the two ends in longitude. So we also tried a smaller domain in longitude and periodic condition in longitude. The findings of this chapter remain unchanged. The spatial resolution is 5 km and the time step is 4 minutes.

5.2 Nonlinear Evolution

5.2.1 Free nonlinear evolution

The nonlinear evolution of TIWs is initialized with a small random perturbation to the initial mean state shown in Figure 5.1. This mean state is based on Figure 4 in *Hansen and Paul* (1984) which was based on measurements made by 20 satellite-tracked surface drifters in the region $10^\circ S - 10^\circ N, 130 - 140^\circ W$, from June 6 to

October 27 in 1979. The evolution of the waves originating near the center of the 300° longitude band is analyzed.

Before day 175, in the latitudinal range from 6°S to 8°N, TIWs with a wavelength of 995 km, a period of 29 days, growing exponentially with an e -folding time of 11.4 days, and similar wave pattern as that on day 175 in Figure 5.1 dominate the whole domain. These results are consistent with the stability analysis following *Philander* (1978). Details about how to obtain the unstable modes are given in Appendix A. As shown in Figure 5.1, after day 175, the TIWs rapidly grow into fully nonlinear vortices and further growth stops around day 200. Three related things happen during this period. First, the vortex shown in the total h field begins to rotate, changing its oval shape on day 175 to disk shape on day 200. Second, the rotation decouples the components of TIWs at different latitudes. The wave near the equator detaches from the wave near 5°N and propagates faster to the west. Third, the rotation also stabilizes the zonal mean substantially. Wavelengths of these waves do not change during the process. On day 225, the vortex rotates back to an oval shape and the zonal mean is restored partially. However, this process is irreversible. The wave near the equator keeps moving faster to the west. And the wave near 5°N continue to surrender its energy to the fast wave near the equator after day 225 and reaches some quasi-equilibrium after day 350. On day 450 the fast wave near the equator has relative stronger amplitude than the wave near 5°N. Figure 5.2 shows how v along the equator and 5°N in a selected region near the center in longitude varies with time. Before day 175, the period is 29 days and the phase speed is 0.4 ms^{-1} at both latitudes; after day 200, the period is 20 days and phase speed is 0.58 ms^{-1} at the equator, and the period is about 36 days and the phase speed is 0.31 ms^{-1} at 5°N. Close look indicates that the 20-day wave dominates [4°S, 2°N] and the 36-day wave dominates [3°N, 8°N]. Figure 5.2 (right) also shows that the 36-day wave keeps losing its energy to the 20-day wave till day 350.

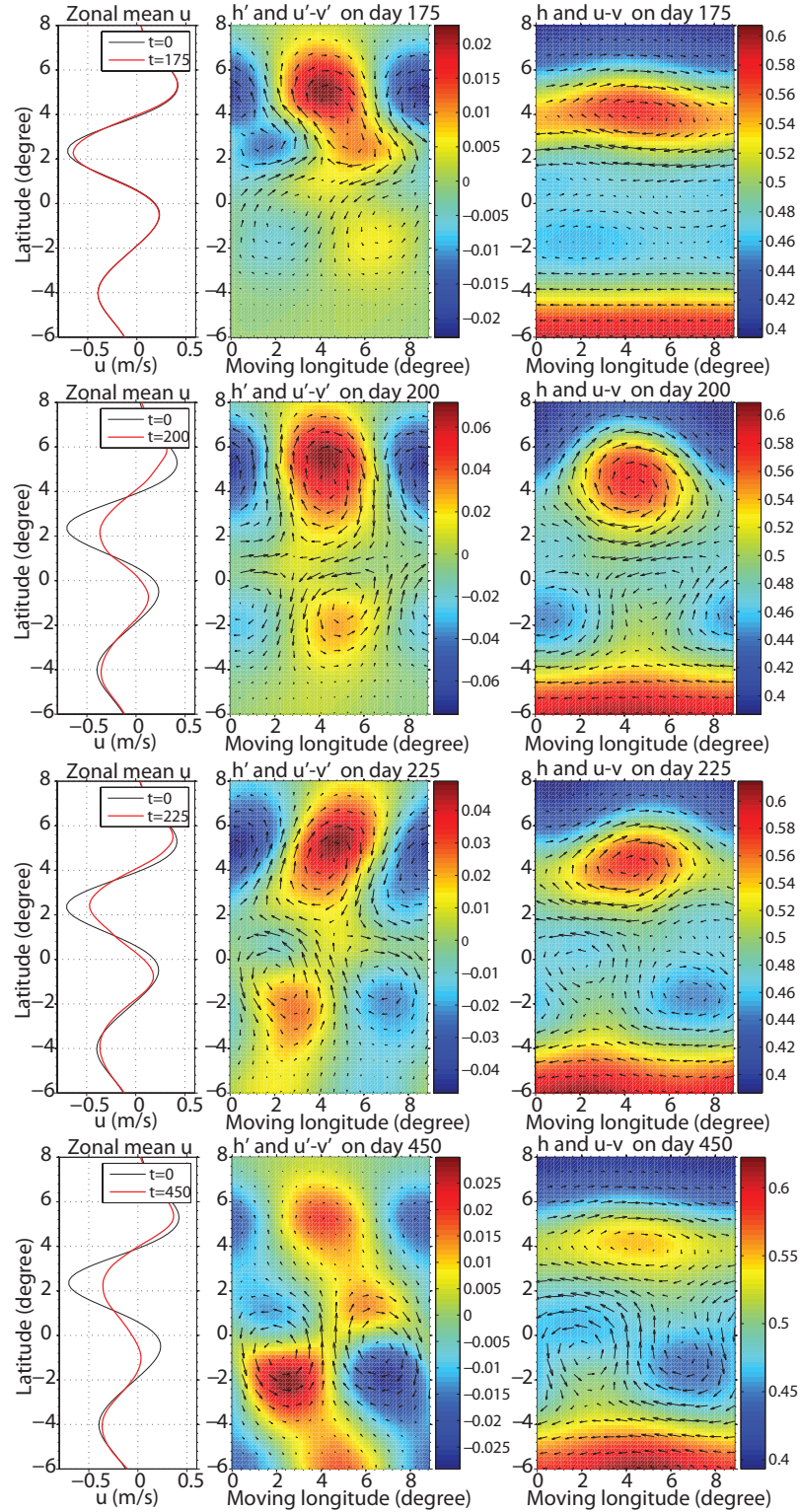


Figure 5.1: Zonal mean velocity (left column), zonal deviation h' and $u' - v'$ (middle column), and h and $u - v$ (right column) on a moving coordinate following a positive h' center near $5^\circ N$ on day 175 (top panel), 200 (2nd panel), 225 (3rd panel) and 450 (bottom panel).

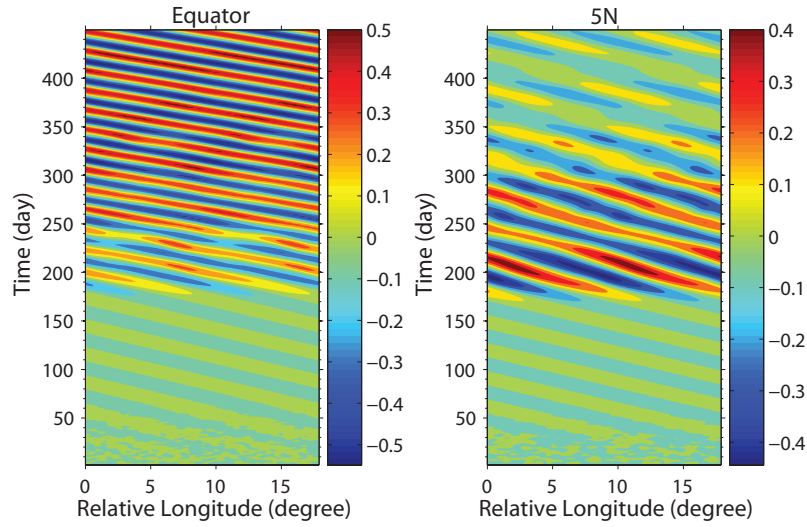


Figure 5.2: Time-longitude plots of v along the equator and $5^\circ N$. Before the most unstable wave reaches to its fully nonlinear stage around day 200, the periods are 29 days at both the equator and $5^\circ N$. After day 250, the periods are 20 days at the equator and about 36 days at $5^\circ N$.

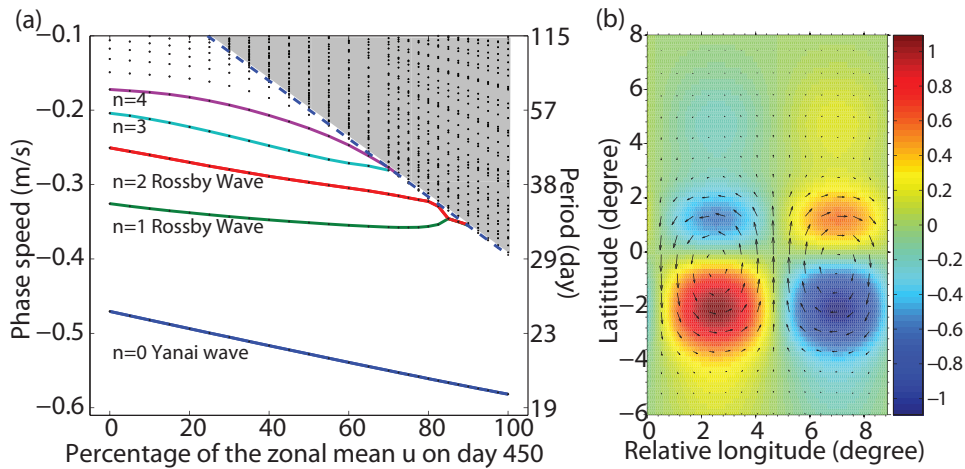


Figure 5.3: (a) Phase speed and periods of the free modes with a wavelength of 995 km when increasing the background zonal mean from 0 to 100% of the zonal mean on day 450. Blue dashed line denotes where the phase speed equals to the minimum value of the zonal mean. Neutral modes in the shaded area are continuous. (b) The free Yanai wave with a wavelength of 995 km wave, linearized about the zonal mean on day 450.

The genesis of these two types of waves with distinct phase speeds could be explained through the linear dynamics. Recall that zonal wavenumber $k=1$ is a dimensional wavelength of 995 km while its second harmonic ($k=2$) is a wavelength of 498 km. Even though the TIWs around day 200 are fully nonlinear, Fourier analysis indicates the $k=1$ waves are still dominant, about 10 times larger than the second harmonics on day 200 at $2^\circ S$ (center of the fast 20-day wave) and $5^\circ N$ (center of the 36-day wave). The stabilized zonal mean on day 200 does not support the original 29-day unstable mode anymore. The whole large perturbation field must be decomposed to a new set of free modes existing with the new stabilized zonal mean. Since the zonal mean on day 200 closely resembles the zonal mean on day 450, we use the latter as an example. As shown in Figure 5.3(a), the only discrete neutral Rossby-like waves now is a 20-day Yanai wave and all other neutral Rossby-like waves are continuous. It also has a 41-day discrete unstable growing mode centered $5^\circ N$ with an e -folding time of 36 days and several other slower growing discrete modes. As the zonal deviation of the fast wave from $4^\circ S$ to $2^\circ N$ on day 450 and the Yanai mode in Figure 5.3(b) have the same wavelength, period and similar wave pattern, we identify this fast 20-day wave as the neutral Yanai wave. While the near 36-day waves centered $5^\circ N$ vary with time and involve both continuous neutral modes and discrete unstable modes which makes it impossible to identify them with any particular mode.

5.2.2 Sensitivity of the late emerging Yanai wave to the zonal mean

Although the initial zonal mean used in the previous subsection is representative of a very large collection of data in one year, substantial variations of strength and structure are known to occur from year to year. Here we just simply rescale the magnitude of the zonal mean to a wider range to represent such interannual variations.

The magnitude U_{max} of our “typical” zonal mean is 0.7 m s^{-1} . If we rescale U_{max} up to 1.0 m s^{-1} (decreasing the e -folding time of the most unstable mode from 11.4

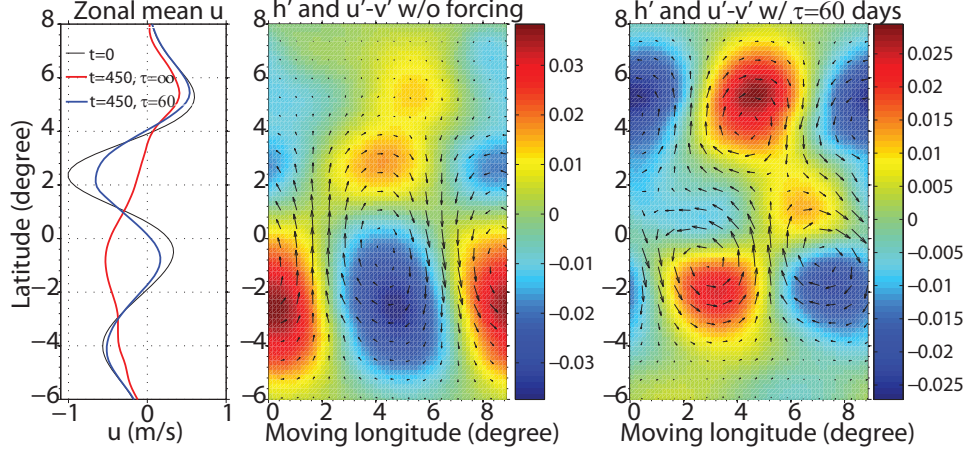


Figure 5.4: (left) Zonal mean velocity without nudging terms ($\tau = \infty$) and with forcing terms ($\tau=60$ days) for $U_{max} = 1.0 \text{ m s}^{-1}$; (middle) Zonal deviation h' and $u' - v'$ on day 450 without nudging terms; (right) Zonal deviation h' and $u' - v'$ on day 450 with nudging terms ($\tau=60$ days).

days to 7.3 days), then the late emerging 15-day Yanai wave will dominate from $6^\circ S$ to $6^\circ N$ as shown in Figure 5.4 (middle). The initial 25-day TIW near $5^\circ N$ do not have any remnant near $5^\circ N$. Figure 5.4 (left) also shows that the structure of the zonal mean on day 450 without forcing terms differs from the initial structure significantly. However, if we rescale U_{max} down to 0.5 m s^{-1} (increasing the e -folding time of the most unstable mode from 11.4 days to 18.3 days), then the late emerging Yanai wave with a period of 22 days will have such weak strength that the period can only be obtained from the Fourier analysis (figures are not shown here). The initial 32-day wave with modified wave structure near the equator still dominates from $6^\circ S$ to $8^\circ N$.

5.2.3 Forced nonlinear evolution

The sensitivity of the strength of the late emerging Yanai wave is largely due to the lack of external forcing terms in our nonlinear shallow-water model. Here we use Newtonian relaxation to represent the external forces, like wind stresses, by adding nudging terms $(\bar{u} - u)/\tau$, $(\bar{v} - v)/\tau$ and $(\bar{h} - h)/\tau$ to the the right hand sides of equation 4.4, 4.5 and 4.6 respectively. They act to nudge the flow back towards the

Relaxation time τ	$5^\circ N$	Yanai
w/o nudging	36	20
90 days	34	21.5
60 days	33	22
30 days	32	suppressed

Table 5.1: Periods of TIWs centered about $5^\circ N$ and late emerging Yanai waves near the equator for $U_{max} = 0.7 \text{ ms}^{-1}$ after the nonlinear adjustment with various relaxation times. The period of TIWs during the linear stage is 29 days over the domain.

initial mean state \bar{u} , $\bar{v}(=0)$ and \bar{h} with a relaxation time of τ .

Figure 5.4 (right) shows the zonal deviation h' , $u' - v'$ on day 450 with a relaxation time of 60 days for an increased U_{max} of 1.0 ms^{-1} . Comparing with the result without nudging terms on day 450 shown in Figure 5.4 (middle), the wave near $5^\circ N$ now has large amplitude and dominates from $3^\circ N$ to $8^\circ N$. The Yanai wave is restricted to $4^\circ S$ to $2^\circ N$. The stabilized zonal mean is also nudged close to the initial mean as shown in Figure 5.4 (left).

Table 5.1 gives the periods of TIWs centered about $5^\circ N$ and late emerging Yanai waves near the equator for $U_{max}=0.7 \text{ ms}^{-1}$ with various relaxation times, measured after the nonlinear adjustment. Nudging terms tend to bring the periods of the waves near $5^\circ N$ towards the initial period in the linear stage. For a relaxation time less than 30 days, the Yanai wave is suppressed. If we increase U_{max} , then we need to decrease τ to suppress the late emerging Yanai waves.

5.3 Summary and Discussion

In this chapter, we investigated how the nonlinearity could change the behavior of the TIWs and provide a new mechanism to explain the coexistence of two different types of two different types of TIWs. The neutral Yanai waves are shown to emerge as the initial TIWs grow into full nonlinear vortices and stabilize the zonal mean

significantly. The strength and structure of these Yanai waves are highly dependent on the instability of the initial mean states if no forcing terms are present. Such sensitivity could largely be eliminated by adding climatological nudging terms to the equations.

CHAPTER VI

Conclusion and Discussion

6.1 Linear Kelvin waves

We have derived a new asymptotic approximation for the Kelvin wave that fills the gap between the equatorial beta-plane (fixed zonal wavenumber s , Lamb's parameter $\epsilon \rightarrow \infty$) and the small ϵ , velocity-potential-is- $P_n^n(\mu) \exp(is\lambda)$ approximation. The new approximation was derived under the assumption that at least one of (s, ϵ) is large, but it turns to be surprisingly accurate outside its formal range of validity in the region where both s and ϵ are small. The approximation shows that the degree of equatorial confinement is not controlled by ϵ alone, but rather by the parameter

$$\epsilon_{eff} = s^2 + \epsilon \tag{6.1}$$

Boyd (1985) showed that the same is true for Rossby waves. A Kelvin wave of moderate zonal wavenumber s will be confined to the tropics even for $\epsilon = 0$, a barotropic wave, as illustrated in Fig. 2.2.

We also solved the Kelvin waves linearized about various jets. The waves have much more complicated structures than the Kelvin wave with a resting background. These results are consistent with previous studies (*McPhaden and Knox, 1979; Philander, 1979*). For westward jets, the wave narrows in latitude as the wavenumber k increases; for eastward jets, they tend to shift away from the equator as k increases.

As a result, phase speeds decrease as wavenumber increase regardless of whether the jet is eastward or westward.

6.2 Nonlinear Kelvin waves

We first derived the analytic solution for the nonlinear Kelvin wave on sphere when the amplitude and ϵ are small by perturbative method. When the amplitude or ϵ increase, we computed the nonlinear traveling Kelvin waves by numerical calculations. On the equatorial beta-plane in the presence of a jet, we also computed the nonlinear traveling Kelvin waves by numerical calculations.

For sufficiently small amplitude, there are nonlinear Kelvin traveling waves (cnoidal waves). As the amplitude increases, the waves narrow in longitude and terminates in a so-called corner wave with a discontinuous first derivative. All waves larger than the corner wave evolve to fronts and break. The singularity is a point singularity in which only the longitudinal derivative is discontinuous.

In latitude, the waves narrow for the Kelvin waves on the sphere with a resting background or the Kelvin waves on the equatorial beta-plane in the presence of a westward jet as the wave amplitude increases. However the waves widen for the Kelvin waves on the equatorial beta-plane in the presence of an eastward jet. This opposite reaction to the direction of the jet can be explained by projecting the nonlinear solution to the set of the linearized eigenmodes.

Phase speeds also increase to the east as the amplitude increases. However, the phase speeds are largely determined by the linear Kelvin wave dynamics, the increment is relatively small, about several to ten percentage. In *Boyd and Zhou (2008a)*, we derived the first correction to the phase speed due to the amplitude of nonlinear Kelvin waves on sphere is second order in amplitude. As the amplitude of the nonlinear Kelvin waves are generally less than 1 in nondimensionalized units, the correction is relatively small. However, *Fedorov and Melville (2000)* suggest that nonlinear ef-

fects can increase phase speeds by 10%~30% in regions where the thermocline is shallow or shoaling. In our study the phase speed is the phase speed of the steadily traveling wave while in their study it is the phase speed of the Kelvin waves which have evolved to a front. Plus they also included shoaling effect. This may explain why the nonlinearity has a stronger effect than ours.

6.3 Nonlinear tropical instability waves

In this study, we investigated how the nonlinearity could change the behavior of the TIWs and provide a new mechanism to explain the coexistence of two different types of TIWs. The neutral Yanai waves are shown to emerge as the initial TIWs grow into full nonlinear vortices and stabilize the zonal mean significantly. The strength and structure of these Yanai waves are highly dependent on the instability of the initial mean states if no forcing terms are present. Such sensitivity could largely be eliminated by adding climatological nudging terms to the equations.

One limitation of this study is the shallow-water model is only suitable for TIWs arising mainly from barotropic instability. For TIWs arising mainly from baroclinic or frontal instability, multiple-layer models are needed to examine their nonlinear adjustment processes. However, we expect it is still possible for neutral Yanai modes to emerge if the nonlinear TIWs could stabilize the zonal mean significantly, regardless of whether the TIWs arise from barotropic or baroclinic instability. It would be desirable to test this theory with a 3D ocean model in the future work.

APPENDIX

APPENDIX A

Eigenvalue Problem of Normal Modes on the Equatorial β -plane

On the equatorial β -plane, the linearized shallow-water equations about a zonally averaged mean state $\bar{U}(y)$ and $\bar{\Phi}(y)$ which satisfy the geostrophic balance $\bar{U}(y) = -\bar{\Phi}(y)/y$ are

$$u_t + \bar{U}u_x + v\bar{U}_y - yv + \phi_x = 0 \quad (\text{A.1})$$

$$v_t + \bar{U}v_x + yu + \phi_y = 0 \quad (\text{A.2})$$

$$\phi_t + \bar{U}\phi_x + v\bar{\Phi}_y + (1 + \bar{\Phi})(u_x + v_y) = 0 \quad (\text{A.3})$$

Expand u, v, ϕ as $u = u_0(y)e^{i(kx-\omega t)}$, $v = -iv_0(y)e^{i(kx-\omega t)}$, $\phi = \phi_0(y)e^{i(kx-\omega t)}$, then we get

$$k\bar{U}u_0 - (\bar{U}_y + y)v_0 + k\phi_0 = \omega u_0 \quad (\text{A.4})$$

$$k\bar{U}v_0 + yu_0 + \phi_{0y} = \omega v_0 \quad (\text{A.5})$$

$$k\bar{U}\phi_0 - \bar{\Phi}_y v_0 + (1 + \bar{\Phi})(k\bar{U} - v_{0y}) = \omega\phi_0 \quad (\text{A.6})$$

$\bar{U}, \bar{U}_y, \bar{\Phi}$ and $\bar{\Phi}_y$ are known functions of y ; while $u_0, v_0, \phi_0, v_{0y}, \phi_{0y}$ are unknown functions which vanish at infinity. ω is the unknown eigenvalue to be determined.

We can solve this eigenvalue problem by pseudospectral discretization method.

The first step is to change the coordinate from y to ζ via $\zeta = \tanh(y/L)$ where L is a user-choosable parameter. When L is smaller, more discretization points will be concentrated near $y = 0$. Now the range of the new coordinate ζ is $[-1, 1]$. The new boundary condition becomes

$$u_0(-1) = u_0(1) = 0, v_0(-1) = v_0(1) = 0, \phi_0(-1) = \phi_0(1) = 0 \quad (\text{A.7})$$

We use the Chebyshev polynomials as the basis. $T_n(\zeta)$ is a polynomial of degree n . It may be calculated directly via the three-term recurrence relation, but a more efficient definition is

$$T_n(\zeta) = \cos(nt) \quad (\text{A.8})$$

$$t = \arccos(\zeta) \leftrightarrow \zeta = \cos(t) \quad (\text{A.9})$$

To impose the boundary condition, we can define the spectral basis functions $\psi_j(\zeta)$ to be linear combinations of the Chebyshev polynomials which each vanish at $\zeta = \pm 1$ such as

$$\psi^{2n}(\zeta) = T_{2n}(\zeta) - 1, \psi^{2n+1}(\zeta) = T_{2n+1}(\zeta) - \zeta, n = 1, 2, 3, \dots \quad (\text{A.10})$$

The fact that $\psi^j(\pm 1) = 0$ for each j follows from the trigonometric definition of the Chebyshev polynomials, which implies $T_n(\pm 1) = (\pm 1)^n$.

Let N denote the number of basis functions used for each of the three unknowns. Discretize collocation points evenly space in t , $t = \frac{2i-1}{2N}\pi$ where $i=1, 2, 3, \dots, N$. Demanding that three shallow water equations be satisfied for this discrete set of N collocation points then converts the set of three differential equations into a generalized matrix eigenvalue problem.

So expand u_0, v_0, ϕ_0 as

$$u_0(\zeta(y)) = \sum_{j=2}^{N+1} a_j \times \psi^j(\zeta(y)) \quad (\text{A.11})$$

$$v_0(\zeta(y)) = \sum_{j=2}^{N+1} a_{(j+N)} \times \psi^j(\zeta(y)) \quad (\text{A.12})$$

$$\phi_0(\zeta(y)) = \sum_{j=2}^{N+1} a_{(j+2N)} \times \psi^j(\zeta(y)) \quad (\text{A.13})$$

where $\psi^j(\zeta) = \cos(jt) - 1$ for even j and $\psi^j(\zeta) = \cos(jt) - \cos(t)$ for odd j .

With the using following relationship

$$\frac{\partial}{\partial y} \leftrightarrow -\frac{\sin(t)}{L} \frac{\partial}{\partial t} \quad (\text{A.14})$$

we can easily get the summation forms for v_{0y} and ϕ_{0y} as

$$u_{0y}(\zeta(y)) = \sum_{j=2}^{N+1} a_j \times \psi_y^j(\zeta(y)) \quad (\text{A.15})$$

$$v_{0y}(\zeta(y)) = \sum_{j=2}^{N+1} a_{(j+N)} \times \psi_y^j(\zeta(y)) \quad (\text{A.16})$$

$$\phi_{0y}(\zeta(y)) = \sum_{j=2}^{N+1} a_{(j+2N)} \times \psi_y^j(\zeta(y)) \quad (\text{A.17})$$

where $\psi_y^j(\zeta) = -\frac{\sin(t)}{L}(-j \sin(jt))$ for even j and $\psi_y^j(\zeta) = -\frac{\sin(t)}{L}(-j \sin(jt) + \sin(t))$ for odd j .

Collect the coefficients of \vec{a} of the three equations we can get the following matrix form eigenvalue problem

$$\vec{A}_{3N \times 3N} \vec{a}_{3N \times 1} = \omega \vec{B}_{3N \times 1} \quad (\text{A.18})$$

The first N rows of $\vec{A}_{i,j}$ and \vec{B}_i are obtained from the x momentum equation.

$$\vec{A}_{i,j} = k\bar{U}(y_i)\psi^{j+1}(y_i) \quad (\text{A.19})$$

$$\vec{A}_{i,j+N} = (-\bar{U}_y(y_i) + y_i)\psi^{j+1}(y_i) \quad (\text{A.20})$$

$$\vec{A}_{i,j+2N} = k\psi^{j+1}(y_i) \quad (\text{A.21})$$

$$\vec{B}_i = \psi^{j+1}(y_i) \quad (\text{A.22})$$

where i is the collocation points index, from 1 to N ; j is the index of the basis functions, also from 1 to N .

The second N rows of $\vec{A}_{i,j}$ and \vec{B}_i are obtained from the y momentum equation.

$$\vec{A}_{i+N,j} = y_i\psi^{j+1}(y_i) \quad (\text{A.23})$$

$$\vec{A}_{i+N,j+N} = k\bar{U}(y_i)\psi^{j+1}(y_i) \quad (\text{A.24})$$

$$\vec{A}_{i+N,j+2N} = \psi^{j+1}(y_i) \quad (\text{A.25})$$

$$\vec{B}_{i+N} = \psi^{j+1}(y_i) \quad (\text{A.26})$$

The third N rows of $\vec{A}_{i,j}$ and \vec{B}_i are obtained from the continuation equation.

$$\vec{A}_{i+2N,j} = k(1 + \bar{\Phi}(y_i))\psi^{j+1}(y_i) \quad (\text{A.27})$$

$$\vec{A}_{i+2N,j+N} = -(1 + \bar{\Phi}(y_i))\psi_y^{j+1}(y_i) - \bar{\Phi}_y(y_i)\psi^{j+1}(y_i) \quad (\text{A.28})$$

$$\vec{A}_{i+2N,j+2N} = k\bar{U}(y_i)\psi^{j+1}(y_i) \quad (\text{A.29})$$

$$\vec{B}_{i+2N} = \psi^{j+1}(y_i) \quad (\text{A.30})$$

With the definition of \vec{A} and \vec{B} , the eigenvalues of ω and eigenvectors of \vec{a} are readily solved by many scientific softwares, like Matlab. Attention should be paid when identifying these eigenmodes when the background mean is not zero. One useful technique is increasing the background mean gradually from zero to full strength and

track the change of ω .

BIBLIOGRAPHY

BIBLIOGRAPHY

- Andrews, D. G., J. R. Holton, and C. B. Leovy (1987), *Middle Atmospheric Dynamics, Advances in Geophysics*, vol. 40, Academic Press, New York.
- Boyd, J. P. (1976), The noninteraction of waves with the zonally averaged flow on a spherical earth and the interrelationships of eddy fluxes of heat, energy, and momentum, *J. Atmos. Sci.*, *33*, 2285–2291.
- Boyd, J. P. (1978a), The choice of spectral functions on a sphere for boundary and eigenvalue problems: A comparison of chebyshev, fourier and associated legendre expansions, *Monthly Weather Review*, *106*, 1184–1191.
- Boyd, J. P. (1978b), The effects of latitudinal shear on equatorial waves, part i: Theory and methods, *Journal of the Atmospheric Sciences*, *35*, 2236–2258.
- Boyd, J. P. (1978c), The effects of latitudinal shear on equatorial waves, part ii: Applications to the atmosphere, *Journal of the Atmospheric Sciences*, *35*, 2259–2267.
- Boyd, J. P. (1980), The nonlinear equatorial kelvin wave, *J. Phys. Oceanogr.*, *10*, 1–11.
- Boyd, J. P. (1984), Equatorial solitary waves, part iv: Kelvin solitons in a shear flow, *Dyn. Atmos. Oceans*, *8*, 173–184.
- Boyd, J. P. (1985), Barotropic equatorial waves: The non-uniformity of the equatorial beta-plane, *J. Atmos. Sci.*, *42*, 1965–1967.
- Boyd, J. P. (1991), Nonlinear equatorial waves, in *Nonlinear Topics of Ocean Physics: Fermi Summer School, Course LIX*, edited by A. R. Osborne, pp. 51–97, North-Holland, Amsterdam.
- Boyd, J. P. (1994), The slow manifold of a five mode model, *Journal of the Atmospheric Sciences*, *51*, 1057–1064.
- Boyd, J. P. (1995), Eight definitions of the slow manifold: Seiches, pseudoseiches and exponential smallness, *Dynamics of Atmospheres and Oceans*, *22*, 49–75.
- Boyd, J. P. (1998), High order models for the nonlinear shallow water wave equations on the equatorial beta-plane with application to kelvin wave frontogenesis, *Dynamics of Atmospheres and Oceans*, *28*, 69–91.

- Boyd, J. P. (1998), High order models for the nonlinear shallow water wave equations on the equatorial beta-plane with application to Kelvin wave frontogenesis, *Dyn. Atmos. Oceans*, 28(2), 69–91.
- Boyd, J. P. (2001), *Chebyshev and Fourier Spectral Methods*, Dover, New York, 680 pp.
- Boyd, J. P. (2003), A legendre pseudospectral method for computing travelling waves with corners (slope discontinuities) in one space dimension with application to Whitham’s equation family, *J. Comput. Phys.*, 189(5), 98–110.
- Boyd, J. P. (2005a), Ostrovsky and Hunter’s generic wave equation for weakly dispersive short waves: analytical and numerical study of the parabolic and paraboloidal travelling waves (corner and near-corner waves), *Eur. J. Appl. Math.*, 16(1), 65–81.
- Boyd, J. P. (2005b), The Cnoidal Wave/Corner Wave/Breaking Wave Scenario: a one-sided infinite-dimension bifurcation, *Math. Comput. Simulation*, 69(3–4), 235–242.
- Boyd, J. P. (2005c), Near-corner waves of the Camassa-Holm equation, *Phys. Lett. A*, 336, 342–348.
- Boyd, J. P. (2005d), The short-wave limit of linear equatorial Kelvin waves in a shear flow, *J. Phys. Oceanogr.*, 35(6), 1138–1142.
- Boyd, J. P. (2006), Fourier pseudospectral method with Kepler mapping for travelling waves with discontinuous slope: Application to corner waves of the Ostrovsky-Hunter equation and equatorial Kelvin waves in the four-mode approximation, *Appl. Math. Comput.*, 177(1), 289–299.
- Boyd, J. P. (2007), Why Newton’s method is hard for travelling waves: Small denominators, KAM theory, Arnold’s linear Fourier problem, non-uniqueness, constraints and erratic failure, *Math. Comput. Simulation*, 74(2-3), 72–81, doi: 10.1016/j.matcom.2006.10.001, 4th IMACS International Conference on Nonlinear Evolution Equations and Wave Phenomena, Athens, GREECE, APR 11-14, 2005.
- Boyd, J. P., and Z. D. Christidis (1982), Low wavenumber instability on the equatorial beta-plane, *Geophys. Res. Lett.*, 9, 769–772.
- Boyd, J. P., and C. Zhou (2008a), Kelvin waves in the nonlinear shallow water equations on the sphere: Nonlinear travelling waves and the corner wave bifurcation, *J. Fluid Mech.*, 617, 185–205.
- Boyd, J. P., and C. Zhou (2008b), Uniform asymptotics for the linear Kelvin wave in spherical geometry, *J. Atmos. Sci.*, 65(2), 655–660.
- Chapman, S., and R. S. Lindzen (1970), *Atmospheric Tides*, D. Reidel, Dordrecht, Holland, 200 pp.

- Chen, G. Y., and J. P. Boyd (2002), Nonlinear wave packets of equatorial Kelvin waves, *Geophys. Astrophys. Fluid Dyn.*, *96*(5), 357–379.
- Choi, W. (2003), Strongly nonlinear long gravity waves in uniform shear flows, *Physical Review E*, *68*(2, Part 2), doi:10.1103/PhysRevE.68.026305.
- Donohue, K., and M. Wimbush (1998), Model results of flow instabilities in the tropical Pacific Ocean, *Journal Of Geophysical Research-Oceans*, *103*(C10), 21,401–21,412.
- El, G. A., R. H. J. Grimshaw, and A. M. Kamchatnov (2007), Evolution of solitary waves and undular bores in shallow-water flows over a gradual slope with bottom friction, *Journal of the Atmospheric Sciences*, *585*, 213–244.
- Fedorov, A. V., and W. K. Melville (2000), Kelvin fronts on the equatorial thermocline, *J. Phys. Oceanogr.*, *30*(7), 1692–1705.
- Flament, P., S. Kennan, R. Knox, P. Niiler, and R. Bernstein (1996), The three-dimensional structure of an upper ocean vortex in the tropical Pacific Ocean, *NATURE*, *383*(6601), 610–613.
- Gill, A. E. (1982), *Atmosphere-Ocean Dynamics, International Geophysics*, vol. 30, Academic, Boston.
- Greatbatch, R. J. (1985), Kelvin wave fronts, Rossby solitary waves and nonlinear spinup of the equatorial oceans, *J. Geophys. Res.*, *90*, 9097–9107.
- Grimshaw, R. (1970), Solitary wave in water of variable depth, *J. Fluid Mech.*, *42*, 639–.
- Grimshaw, R. (1971), Solitary wave in water of variable depth. 2, *J. Fluid Mech.*, *46*, 611–.
- Grimshaw, R. (1979), Slowly varying solitary waves. 1. Korteweg-deVries, *Proc. R. Soc. London A*, *368*(1734), 359–375.
- Grimshaw, R. H. J., L. A. Ostrovsky, V. I. Shrira, and Y. A. Stepanyants (1998), Long nonlinear surface and internal gravity waves in a rotating ocean, *Surveys in Geophysics*, *19*, 289–338.
- Halpern, D., R. Knox, and D. Luther (1988), Observations of 20-day period meridional current oscillations in the upper ocean along the Pacific equator, *Journal Of Physical Oceanography*, *18*(11), 1514–1534.
- Hansen, D., and C. Paul (1984), Genesis and effects of long waves in the equatorial Pacific, *Journal of Geophysical Research-Oceans*, *89*(NC6), 431–440.
- Hough, S. S. (1897), On the application of harmonic analysis to the dynamic theory of the tides, I. On Laplace’s “oscillations of the first species” and on the dynamics of ocean currents, *Phil. Trans. Roy. Soc. A*, *189*, 201–257.

- Hough, S. S. (1898), On the application of harmonic analysis to the dynamic theory of the tides, II. On the general integration of Laplace's tidal equations, *Phil. Trans. Roy. Soc. A*, *191*, 139–185.
- Kennan, S., and P. Flament (2000), Observations of a tropical instability vortex, *Journal of Physical Oceanography*, *30*(9), 2277–2301.
- Le Sommer, J., G. M. Reznik, and V. Zeitlin (2004), Nonlinear geostrophic adjustment of long-wave disturbances in the shallow-water model on the equatorial beta-plane, *J. Fluid Mech.*, *515*, 135–170.
- Legeckis, R. (1977), Long waves in eastern equatorial pacific ocean - view from a geostationary satellite, *Science*, *197*(4309), 1179–1181.
- Lindzen, R. S. (1970), The application of terrestrial atmospheric tidal theory to Venus and Mars, *J. Atmos. Sci.*, *27*(4), 536–549.
- Long, B., and P. Chang (1990), Propagation of an equatorial Kelvin wave in a varying thermocline, *J. Phys. Oceanogr.*, *20*, 1826–1841.
- Longuet-Higgins, M. S. (1968), The eigenfunctions of Laplace's tidal equation over a sphere, *Phil. Trans. Royal Society of London, Series A*, *262*, 511–607.
- Longuet-Higgins, M. S., and M. J. H. Fox (1996), Asymptotic theory for the almost-highest wave, *J. Fluid Mech.*, *317*, 1–19.
- Lorenz, E. N., and V. Krishnamurthy (1987), On the nonexistence of a slow manifold, *Journal of the Atmospheric Sciences*, *44*, 2940–2950.
- Lyman, J., D. Chelton, R. deSzoeki, and R. Samelson (2005), Tropical instability waves as a resonance between equatorial Rossby waves, *JOURNAL OF PHYSICAL OCEANOGRAPHY*, *35*(2), 232–254.
- Lyman, J. M., G. C. Johnson, and W. S. Kessler (2007), Distinct 17-and 33-day tropical instability waves in subsurface observations, *Journal of Physical Oceanography*, *37*(4), 855–872, doi:10.1175/JPO3023.1.
- Majda, A. (2003), *Introduction to PDEs and Waves for the Atmosphere and Ocean*, *Courant Lecture Notes*, vol. 9, American Mathematical Society, Providence, Rhode Island.
- Majda, A. J., R. R. Rosales, E. G. Tabak, and C. V. Turner (1999), Interaction of large-scale equatorial waves and dispersion of Kelvin waves through topographic resonances, *J. Atmos. Sci.*, *56*(24), 4118–4133.
- Marshall, H. G., and J. P. Boyd (1987), Solitons in a continuously stratified equatorial ocean, *J. Phys. Oceanogr.*, *17*, 1016–1031.
- McCreary, J., and Z. Yu (1992), Equatorial dynamics in a 2-1/2-layer model, *Progress In Oceanography*, *29*(1), 61–132.

- McPhaden, M., and R. Knox (1979), Equatorial kelvin and inertia-gravity waves in zonal shear-flow, *Journal Of Physical Oceanography*, 9(2), 263–277.
- Milewski, P. A., and E. G. Tabak (1999), A reduced model for nonlinear dispersive waves in a rotating environment, *Geophys. Astrophys. Fluid Dynamics*, 90, 139–159.
- Miller, L., D. WATTS, and M. WIMBUSH (1985), Oscillations of dynamic topography in the eastern equatorial pacific, *Journal Of Physical Oceanography*, 15(12), 1759–1770.
- Moore, D. W., and S. G. H. Philander (1977), Modelling of the tropical oceanic circulation, in *The Sea*, edited by E. D. Goldberg, no. 6 in The Sea, pp. 319–361, Wiley, New York.
- Natarov, A., and J. P. Boyd (2001), Beyond-all-orders instability in the equatorial Kelvin wave, *Dyn. Atmos. Oceans*, 33(3), 181–200.
- Orszag, S. A. (1974), Fourier series on spheres, *Monthly Weather Review*, 102, 56–75.
- Ostrovsky, L. A. (1978), Nonlinear internal waves in a rotation ocean, *Oceanology*, 18, 181–191.
- Pedlosky, J. (1987), *Geophysical Fluid Dynamics*, 2d ed., Springer-Verlag, New York.
- Philander, S. G. H. (1978), Instabilities of zonal equatorial currents, 2, *J. Geophys. Res.*, 83, 3679–3682.
- Philander, S. G. H. (1979), Equatorial waves in the presence of the equatorial undercurrent, *Journal of Physical Oceanography*, 9(2), 254–262.
- Proehl, J. A. (1996), Linear stability of equatorial zonal flows, *Journal of Physical Oceanography*, 26(4), 601–621.
- Qiao, L., and R. Weisberg (1995), Tropical instability wave kinematics - observations from the tropical instability wave experiment, *Journal Of Geophysical Research-Oceans*, 100(C5), 8677–8693.
- Ripa, P. (1982), Nonlinear wave-wave interactions in a one-layer reduced-gravity model on the equatorial beta-plane, *J. Phys. Oceanogr.*, 12, 97–111.
- Ripa, P. (1985), Nonlinear effects in the propagation of Kelvin pulses across the Pacific Ocean, in *Advances in Nonlinear Waves*, edited by L. Debnath, pp. 43–56, Pitman, New York.
- Shinoda, T., G. N. Kiladis, and P. E. Roundy (2009), Statistical representation of equatorial waves and tropical instability waves in the pacific ocean, *Atmospheric Research*, 94(1), 37 – 44, doi:DOI: 10.1016/j.atmosres.2008.06.002, ocean-Atmosphere Coupling.

- Shrira, V. I. (1981), Propagation of long nonlinear waves in a layer of rotating fluid, *Ivestiya Atm. Oceanic Phys.*, 17(1), 76–81.
- Shrira, V. I. (1986), On long strongly nonlinear waves in a rotating ocean, *Ivestiya Atm. Oceanic Phys.*, 22(4), 298–305.
- Stokes, G. G. (1847), On the theory of oscillatory waves, *Camb. Trans.*, 8, 441–473, also published in vol. 1 of *Mathematical and Physical Papers* (Cambridge University Press, Cambridge, 1880), pgs. 197–229.
- Thomson, S. (1880), On gravitational oscillations of rotating water, *Phil. Mag.*, 10, 109–116, reprinted in Vol. 4 of Kelvin’s collected papers, pgs. 141–148.
- Williams, G. P. (1996), Jovian dynamics. Part I. Vortex stability, structure and genesis, *J. Atmos. Sci.*, 53(18), 2685–2734.
- Williams, G. P., and R. J. Wilson (1988), The stability and genesis of Rossby vortices, *J. Atmos. Sci.*, 45, 207–249.
- Yu, Z., J. McCreary, and J. Proehl (1995), Meridional asymmetry and energetics of tropical instability waves, *Journal of Physical Oceanography*, 25(12), 2997–3007.
- Zurek, R. W. (1976), Diurnal tide in Martian atmosphere, *J. Atmos. Sci.*, 33(2), 321–337.